

# **Eine auf VTK basierende Analyse-Software zur Untersuchung der Orbita und des Mittelgesichts**

Dissertation  
zur Erlangung des akademischen Grades  
Dr. rer. med.  
an der Medizinischen Fakultät  
der Universität Leipzig

**eingereicht von:**

Dipl. Inf. (FH) Daniel Kruber

**Geburtsdatum und -ort:**

13.01.1980 in Merseburg

**angefertigt in der:**

Klinik und Poliklinik für Mund-, Kiefer- und Plastische Gesichtschirurgie;  
Universitätsklinikum Leipzig AöR

**Betreuer:**

Prof. Dr. med. Dr. med. dent. Thomas Hierl  
Prof. Dr. med. Dr. med. dent. Alexander Hemprich

**Beschluss über die Verleihung des Doktorgrads vom:**

16.04.2019

# Inhaltsverzeichnis

<b>1</b>	<b>Einführung</b>	<b>1</b>
1.1	VTK – Visualization Toolkit . . . . .	2
1.2	FAT – Facial Analysis Tool . . . . .	4
1.2.1	Importfunktionen . . . . .	4
1.2.2	Analyse-Funktion in FAT . . . . .	6
1.2.3	Konstruktionselemente in FAT . . . . .	23
<b>2</b>	<b>FAT-Anwendungen</b>	
	<b>Vergleich und Analyse komplexer Flächen</b>	<b>24</b>
2.1	CAD-CAM–Assisted Esthetic Facial Surgery . . . . .	24
2.2	Positioning of Bone Segments During Navigated Surgery . . . . .	36
2.3	Morphologic comparison of preformed orbital meshes . . . . .	44
2.4	Template-Based Orbital Wall Fracture Treatment Using Statistical Shape Analysis . . . . .	51
2.5	Preforming of Polydioxanone sheets for orbital wall fractures – a technical note . . . . .	62
2.6	Calculation of resected orbital wall areas in the treatment of endocrine orbitopathy . . . . .	67
2.7	Three-dimensional changes of scleral show after surgical treat- ment of endocrine orbitopathy . . . . .	75
2.8	Weitere Einsatzgebiete . . . . .	83

## Inhaltsverzeichnis

---

<b>3</b>	<b>Ausblick</b>	<b>85</b>
<b>4</b>	<b>Zusammenfassung der Arbeit</b>	<b>87</b>
	<b>Literaturverzeichnis</b>	<b>89</b>
	<b>Darstellung des eigenen Beitrags</b>	<b>91</b>
	<b>Erklärung über die eigenständige Abfassung der Arbeit</b>	<b>92</b>
	<b>Curriculum Vitæ</b>	<b>93</b>
	<b>Eigene Publikationen</b>	<b>94</b>
	<b>Danksagung</b>	<b>97</b>

# Abbildungsverzeichnis

1.1	Schematische Darstellung der Datenfluß-Pipeline . . . . .	3
1.2	beispielhafter DICOM-Datensatz [Nat03] . . . . .	5
1.3	texturiertes Oberflächenmodell . . . . .	5
1.4	Analyse eines Gipsabdruckes . . . . .	6
1.5	Schablone für die Kiefergelenksendoskopie . . . . .	23
2.1	Ergebnis der kephalometrischen Analyse (neben dem 3D-Oberflächenscan werden konstruierte Punkte, Linien und Ebenen dargestellt)	25
2.2	Workflow zur Erzeugung von Punkten, Ebenen und Linien im 3D-Raum . . . . .	26
2.3	Computertomographie (CT) -basierte Analyse (Berechnung diverser diverser knöcherner und weichgewebiger Parameter durch Hinzunahme von Hilfsobjekten ) . . . . .	36
2.4	Workflow Landmarkenplatzierung in der 3D-Kephalometrie: grün – Benutzer setzt Markierung auf ein 3D-Objekt; rot – erzeugt Punkt / Landmarke an der vom Benutzer markierten Position und stellt es im 3D-Fenster dar . . . . .	37
2.5	verschiedene Implantate der Hersteller Stryker, Synthes, Martin und Biomet . . . . .	44
2.6	Workflow zum Registrierablauf in FAT . . . . .	45
2.7	Darstellung der Funktionsweise von „Digitizer“ an 5 exemplarischen Datensätzen . . . . .	52
2.8	Workflow zur Darstellung der Konturen . . . . .	52
2.9	Workflow zur Darstellung der Schnittpunkte . . . . .	53



2.10	PDS-Folie . . . . .	62
2.11	Workflow zum Vergleich zweier Objekte – Unterschied wird im 3D-Fenster farbkodiert angezeigt . . . . .	63
2.12	farbige Abgrenzung der Orbitawände . . . . .	67
2.13	Workflow zur Umwandlung zum PolyData-Objekt . . . . .	68
2.14	Workflow zur Konvertierung des importierten Objektes in ein PolyData-Objekt mit anschließender Glättung und Anwen- dung auf das Ursprungsobjekt (untere blauen Linien) . . . . .	68
2.15	Darstellung einer an endokriner Orbitopathie leidenden Pati- entin mit Symmetrie-Schablone in FAT . . . . .	75
2.16	Workflow der Exophthalmus-Analyse mit Ausgabe der kon- struierten Hilfsobjekte und Ergebnisse . . . . .	76
2.17	farbkodierte Weichteildicken-Messung . . . . .	83
3.1	Exemplarische OP-Simulation – Prä - Post . . . . .	85
3.2	Visuelle und metrische Darstellung der veränderten Bereiche .	86
3.3	das Osteosynthese-Implantat wird automatisch an die knöcher- ne Unterlage angepasst – die Farbwerte zeigen die Verformung metrisch an . . . . .	86

# 1. Einführung

In der computerassistierten Chirurgie sind für viele Fragestellungen der Diagnostik und Therapie eingehende metrische Analysen notwendig. Für die cranio-maxillofaziale Chirurgie (CMF) beinhaltet dies die dreidimensionale Kephalmetrie zur Beschreibung eines Ausgangszustands und führt über die Operationsplanung bis zur Validierung/Analyse eines Operationsergebnisses. Um diese Aufgaben zu erfüllen, benötigt man zwangsläufig geeignete Softwarewerkzeuge.

Bis jetzt beinhalten kommerziell angebotene Applikationen meist nur die Beurteilung von 2-Punkt-Abständen oder einfache Winkelmessungen. Durch neue 3D-Scanning Verfahren (z.B. optische Scans) bzw. hochauflösende CT- oder Cone-Beam-Aufnahmen kamen neben der einfachen Darstellung auch Applikationen zur Rekonstruktion und intraoperativen Navigation hinzu, die auch erweiterte Messoptionen wie die Berechnung von Flächen oder Volumina beinhalten. Mit den derzeit kommerziell erhältlichen Softwarelösungen (z.B. Brainlab iPlan CMF, Fa. Brainlab AG, München; VoXim, IVS Technology GmbH i. L., Chemnitz; SurgiCase, Materialise GmbH, Gilching - Materialise HQ, Leuven (BEL) ) sind derartige Fragestellungen bisher leider nur sehr eingeschränkt oder nicht zu beantworten.

Aus diesem Grund wurden speziell für diese Anforderungen eigene Softwarelösungen konzipiert, deren Aufbau und klinische Anwendungen Inhalt dieser Arbeit sind und im Folgenden dargestellt werden. Auch wenn exemplarisch immer Fragestellungen aus dem Gebiet der CMF erläutert werden, sind diese Werkzeuge auch für andere medizinische oder tiermedizinische Fragen einsetzbar.

Ein sehr hilfreiches Werkzeug für die Realisierung ist hier das Visualization Toolkit von Kitware (Kitware VTK Paraview, [www.kitware.com](http://www.kitware.com) - Kitware, New York (USA) ) zu nennen, das als „Baukastensystem“ weltweit ein grundlegender Baustein vieler medizinischer Softwarelösungen wie auch für die in dieser Arbeit vorgestellte Software ist.

## 1.1 VTK – Visualization Toolkit

Bei dem Visualization Toolkit [Kit06] handelt es sich um ein frei verfügbares objektorientiertes Open-Source-Softwaresystem für die 3D Computergrafik, Modellierung, Bildverarbeitung und wissenschaftliche Visualisierung. Zugleich unterstützt es eine Vielzahl an Visualisierungsalgorithmen und Modellierungstechniken.

VTK wurde 1993 ins Leben gerufen und nach der Gründung der Fa. Kitware Inc. im Jahr 1998 durch diese betreut und kontinuierlich erweitert. Es wird aus heutiger Sicht als das weltweit führende Visualisierungssystem angesehen. VTK besteht aus einem kompiliertem C++ -Kern, der mit zusätzlichen interpretierten Programmiersprachen, wie z.B. Java, Python und Tcl, erweitert werden kann. Durch diese Unterstützung des automatischen Wrappings lassen sich Anwendungen performant und plattformunabhängig realisieren.

Die wesentliche Struktur von VTK ist eine Datenfluss-Pipeline, deren Hauptaufgabe darin besteht, Daten zu empfangen, diese zu verarbeiten und anschließend darzustellen. Dieser Ablauf ist in Abbildung 1.1 zu sehen und lässt sich nochmal in zwei Komponenten unterteilen, der Visualization Pipeline und der Render Engine (auch Graphics Pipeline genannt).

Als Vorbereitung für die Visualisierung, werden in der Visualization Pipeline alle eingelesenen Daten verarbeitet bzw. modifiziert und im Anschluß an die Graphics Pipeline weitergeleitet. Der Mapper dient dabei als Bindeglied zwischen den beiden Sub-Pipelines und stellt das Ende der „Datenverarbeitungs“-Pipeline dar.

In der Graphics Pipeline werden alle Objekte in einer visuellen Szene („Fenster“) abgebildet. Darunter zählen Volumen gerenderte Bilder, geometrische Datenobjekte aber auch zweidimensionale Daten.

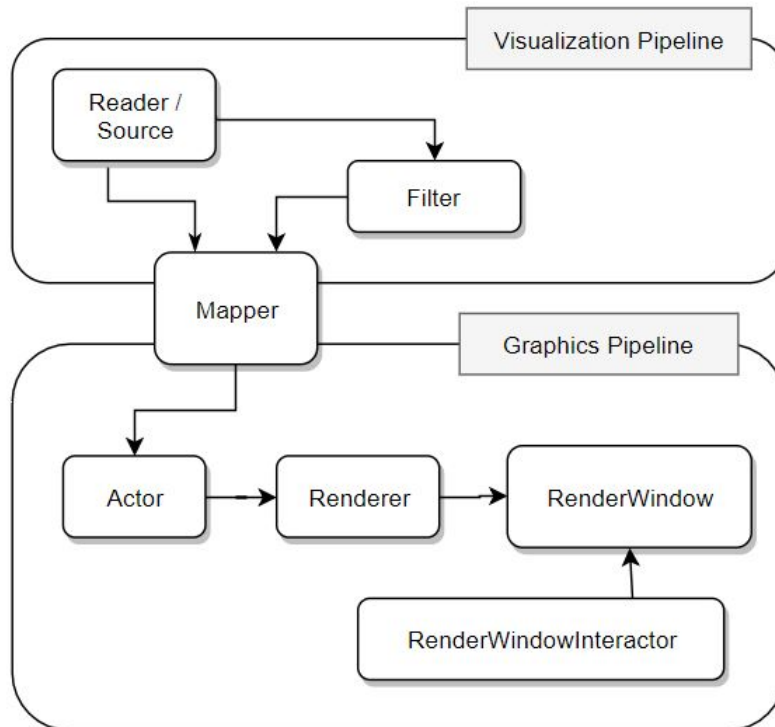


Abbildung 1.1: Schematische Darstellung der Datenfluß-Pipeline

Die Möglichkeiten von VTK und somit dessen Umfang an Funktionen reichen von diversen Visualisierungstechniken, wie z.B. Skalaren (ISO-Konturierung in 2D und 3D) und Strömungslinien, über Modellierungen von Polygonen und Meshmanipulationen bis hin zu Oberflächen- und Volumenrendering von medizinischen Bilddaten. Zudem lassen sich mittlerweile auch Entwicklungen für die Virtual-Reality umsetzen. Mit Sicherheit sind noch viele weitere Funktionen erwähnenswert, welche jedoch den Umfang dieser Arbeit überschreiten würden. Deshalb wird für weitere Informationen auf die offizielle Homepage [Kit] verwiesen.

VTK wird weltweit neben der Forschung und Entwicklung auch in unterschiedlichen Anwendungen eingesetzt. Darunter zählen beispielsweise die Visualisierungsanwendungen von ParaView oder OsiriX, aber auch die nachfolgende Anwendung FAT, welche ein Vielzahl der bisherigen Probleme lösen und fehlenden Funktionen ergänzen soll.

## 1.2 FAT – Facial Analysis Tool

Durch die eingangs erwähnte Problematik, dass keine zufriedenstellende Anwendung zur individuellen Analyse von medizinischen 3D-Daten zur Verfügung steht, wurde FAT mit Hilfe des Visualization Toolkits entwickelt.

Mit Fokus auf dreidimensionale Bilddaten und deren metrischer Analyse soll FAT ein Werkzeug für das medizinische Fachpersonal sein, um möglichst intuitiv und mit größtmöglicher Softwareunterstützung zu den gewünschten Ergebnissen zu kommen. Dabei kann FAT auf eine Vielzahl an Funktionen blicken, die aufgrund der Fülle nachfolgend nur exemplarisch und vereinfacht beschrieben werden.

### 1.2.1 Importfunktionen

Die Importfunktionen sind stets ein wichtiger Bestandteil in jeder Bearbeitungssoftware. Dabei unterscheiden wir im dreidimensionalen Raum zwischen medizinischen Volumendaten und Oberflächendaten.

Bei den Volumendaten bestehen die Daten aus einzelnen dreidimensionalen Quadern, die durch entsprechende bildgebende Verfahren, wie CT oder MRT, erzeugt wurden. Aufgrund der räumlichen Darstellung werden diese gleichmäßigen Quader auch Voxel oder Volumenpixel genannt. Der Vorteil dieser Form der Datenabspeicherung und -repräsentation ist, dass neben den Maßen auch charakteristische Eigenschaften abrufbar sind. Somit können zum Beispiel Dichtewerte (z.B. für Knochen oder Weichgewebe) durch entsprechende Algorithmen visualisiert werden (Abbildung 1.2). Anders als bei den Volumendaten, bestehen die Oberflächendaten lediglich aus einzelnen Polygonen, die zusammen ein geometrisches Objekt beschreiben. Sie stellen quasi nur die „Hülle“ dar.

Diverse Datenformate repräsentieren diese dreidimensionalen Bilddaten und finden in unterschiedlichen Branchen ihren Nutzen. Neben der Medizin nehmen auch die Automobil-, Computerspiele- und Modellbauindustrie einen sehr großen Bereich in der 3D-Verarbeitung ein. Auch FAT unterstützt eine Vielzahl dieser Formate, darunter fallen zum Beispiel STL, OBJ, 3DS, PLY, MHA, VRML sowie XYZ-Punktwolken. Etwas hervorzuheben sind hier die Formate STL und OBJ, da sie als Industriestandard einer sehr großen Beliebtheit genießen (vorrangig bei Rapid-Prototyping Herstellern). Ferner hat das Datenformat OBJ

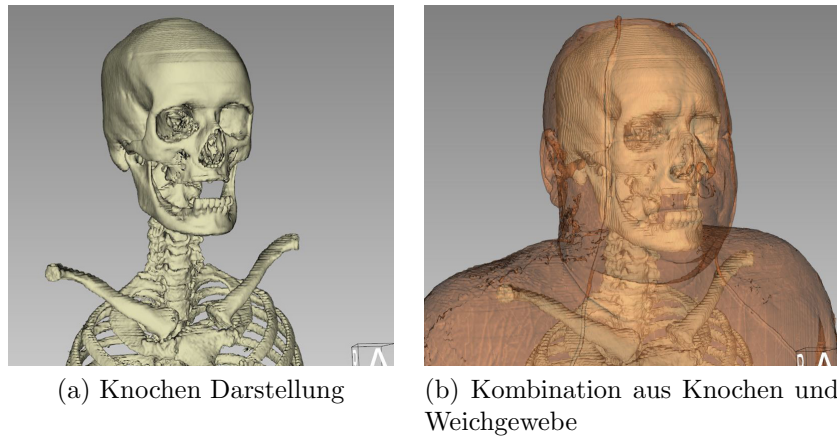


Abbildung 1.2: beispielhafter DICOM-Datensatz [Nat03]

(neben VRML) den Vorteil auch Texturen abzuspeichern. Darüber hinaus ist zu erwähnen, dass multitexturierte Oberflächendaten bisher in kaum einer bekannten medizinischen Software zur Manipulation von medizinischen Bilddaten verwendet werden konnten. Das heißt, dass vorrangig eine Textur je OBJ-Datensatz verwendet wird. Mit FAT ist es jedoch möglich auch Dateien zu öffnen, die aus mehreren Einzel-Texturen bestehen (siehe Abbildung 1.3).

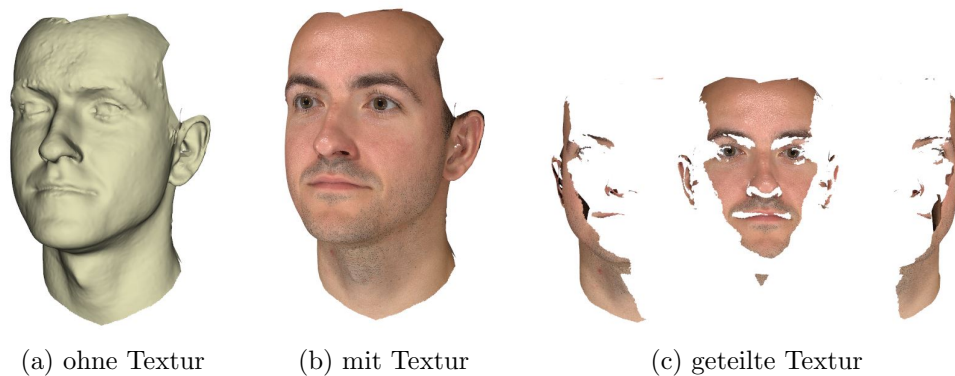


Abbildung 1.3: texturiertes Oberflächenmodell

Neben den erwähnten dreidimensionalen Daten werden auch die zweidimensionalen Bilddaten, wie zB. JPEG oder BMP, von FAT unterstützt und können beispielsweise als Röntgenbild zusätzliche Hilfestellung liefern.

### 1.2.2 Analyse-Funktion in FAT

Der Hauptbestandteil von FAT ist die 3D-kephalometrische Analyse, welche durch einen umfangreichen „Satz“ von trigonometrischen Operationen und Befehlsfolgen diverse Auswertungen zulassen. Durch abspeicherbare Makros sind vordefinierte Analysen jederzeit auf unterschiedliche Ausgangsobjekte wiederholbar.

In den digitalen Journals von „Digital Dental News“ [Hie11] und „teamwork“ [HKHH10] werden weitere Funktionen und Anwendungsbeispiele erwähnt. Ab Seite 7 lässt sich dies im Online-Beitrag von „teamwork“ nachschlagen. Im Buchbeitrag [Das09] (auf Seite 18) wird der klinische Bezug dargestellt. Hier wird ein häufiger Anwendungsfall aus der Kieferanalyse beschrieben und gezeigt wie zeitsparend die Untersuchung und Analyse eines Zahnbogens mit Hilfe der Software umgesetzt werden kann. Des Weiteren wird auf wichtige Datenformate und Exportfilter im Bezug auf chirurgische Planungen mit 3D-Bilddaten eingegangen.

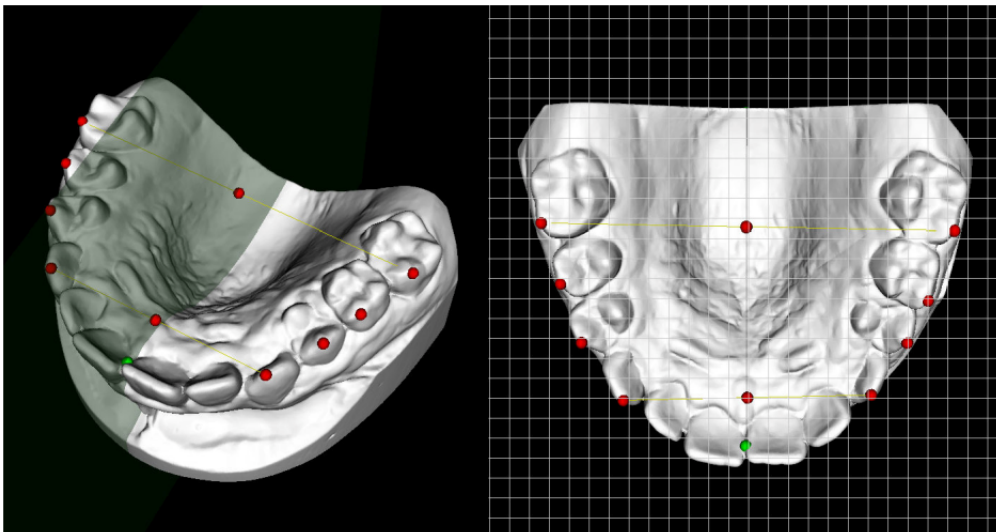


Abbildung 1.4: Analyse eines Gipsabdruckes

Eine wesentliche Grundlage für den medizinischen Einsatz ist die Validierung der Ergebnisse. In verschiedenen Studien [ [Kru], [Bri] ] erfolgte die in FAT integrierten 3D-kephalometrischen Analysesoftware.

# Chapter V

## Requirements for a Universal Image Analysis Tool in Dentistry and Oral and Maxillofacial Surgery

**Thomas Hierl**

*University of Leipzig, Germany*

**Heike Hümpfner-Hierl**

*University of Leipzig, Germany*

**Daniel Kruber**

*University of Leipzig, Germany*

**Thomas Gäbler**

*University of Leipzig, Germany*

**Alexander Hemprich**

*University of Leipzig, Germany*

**Gert Woolny**

*Universidad Polytechnica de Madrid, Spain*

### ABSTRACT

*This chapter discusses the requirements of an image analysis tool designed for dentistry and oral and maxillofacial surgery focussing on 3D-image data. As software for the analysis of all the different types of medical 3D-data is not available, a model software based on VTK (visualization toolkit) is presented. VTK is a free modular software which can be tailored to individual demands.*

*First, the most important types of image data are shown, then the operations needed to handle the data sets. Metric analysis is covered in-depth as it forms the basis of orthodontic and surgery planning. Finally typical examples of different fields of dentistry are given.*



## INTRODUCTION

Image analysis is routinely performed in all fields of dentistry, ranging from 2D X-ray analysis to the investigation of plaster model casts in orthodontics or the planning of surgical procedures based on CT data. In daily practise, different image analysis tools are used which have been designed for specialized needs, in many instances one programme for one single task. This is especially true for 3D images where landmark based analysis methods are often used. Ways to handle these data will be shown in this chapter.

## IMAGE DATA IN DENTISTRY

During the last decades, image analysis in dentistry was mostly confined to 2D bitmap images. Typical examples have been:

- Plain X-rays → cephalometric analysis in orthodontics, caries diagnostics, endodontics etc.
- Photographs → facial analysis in oral and maxillofacial surgery and orthodontics

The advent of 3D-scanning technologies has brought a wealth of new image data to dentistry. CT-scanning, magnetic resonance imaging (MRI), cone beam tomography, and optical scanning (e. g. laser scanning, fringe projection or stereophotogrammetry ) are now widely used. A short and incomplete list of reasons why such data is acquired includes:

- Optical scanning of dental crowns for prosthodontic work (CAD-CAM design and production of crowns and bridgework)
- CT and CBT for implant surgery (ranging from planning of implant position to surgical navigation during implant placement)
- CT, MRI, and optical scanning for 3D cephalometry

- Optical scanning of dental plaster casts in orthodontics
- CT, MRI, and optical scanning in epithetics (i. e. generating artificial missing facial parts after tumor surgery, accidents or due to syndromic diseases)

A key issue of most 3D scanners is the use of proprietary file formats with an inconsistent export possibility into common file formats. Most software functions of the programmes which come alongside the scanners, however, are confined to these proprietary file formats. This implies that missing import filters are limiting the use of these programmes in daily practise. Commercially used software is free of such constraints but rarely adapted to the needs of dental professionals, is rather expensive and requires profound training.

## REQUIREMENTS FOR A “UNIVERSAL” IMAGE ANALYSIS TOOL

An ideal image analysis tool should appeal to the typical software used by medical professionals (i.e. the look and feel of standard office software). Functions and drop down menus should be named in plain words, mathematical terms should be used sparsely. Regarding the data to be analysed, import filters for typical 2D and 3D format files should be available. These include:

- Bitmap formats (BMP, JPEG, ...)
- Radiologic images (DICOM standard)
- Polygon based surface data derived from optical scanners (STL, VRML, OBJ, ...)

Regarding the 3D image files export filters are required for special tasks. This includes production of rapid prototyping (RP) specimens for implant templates, epithetics or alloplastic implants (Ono et al. 2000). The most important

format is STL, which is the standard language of RP-machines. Other export formats like VRML are useful in case of surgical planning if virtual skulls or bone segments are created which will undergo surgery. For DICOM data export formats are needed if the data have to be processed as the original DICOM data should not be changed (this is a key point of this format to keep the inherent medical information).

For 2D images typical pre-analysis procedures include cropping, rotation, mirroring, colour changes and correction of contrast and brightness. Here a multitude of software solutions exists, and most tasks can be performed with any of them. In the majority, analysis of dental images is concerned with metric measurements. After calibration to the real distances landmarks are used to define distances, angulations, proportions to create new landmarks with new distances and so on. Furthermore parallel and perpendicular lines will have to be created. In the 2D world special orthodontic software exists to solve these requirements. Here a most important factor is how intuitive the analysis can be done and the time needed. Being able to perform an analysis in the shortest possible time will be a key issue in clinical practise and will define the use of any software. Also the database should allow easy access to the data for statistical analysis.

In the 3D world the situation is more complicated. As mentioned above many programmes are confined to special formats. Converting formats may lead to loss of information like an export from OBJ to STL format loses facial texture information. Programmes may read DICOM data or polygon data. The key asset of 3D data is the possibility to have a look from all sides. Thus pre-analysis features have to include:

- Moving the object (pan)
- Rotating the object
- Zoom capability

CT, MRI and CBT data may be inspected by way of image stacks, that means looking at individual slices within the scanned specimen. These planes may be parallel to the scanners gantry or perpendicular forming orthogonal  $x$ ,  $y$ ,  $z$  planes. Furthermore so-called oblique planes may be created which may lie in any direction. In case of 3D reconstruction, the image data has to be segmented (i. e. using a threshold to define which grey-scale values will be shown) to confine the displayed image to the structures to be analysed. This works easy with CT images due to the wide range of the Hounsfield scale, somewhat worse for CBT data and most complicated for MRI data. Anatomical structures may be displayed via volume or surface rendering. Regarding metric analysis, 3D images are much more difficult than 2D ones. As the object may move, the chosen landmarks have to stick. As the landmarks lie on the surface of the object, thresholding becomes a major issue analysing CT or CBT images. Changing the threshold changes the geometry und thus the landmark coordinates (that way the threshold boundaries should be stated in scientific work using segmentation procedures). A coordinate system has to be set up to attribute  $x$ ,  $y$ , and  $z$  values to calculate distances or define lines, angles and planes. More elaborate features in processing 3D-data sets include clipping, adding different aspects, loading different data-sets and manipulate them independently, or performing boolean operations (Hierl et al. 2006).

As mentioned above, image analysis can be landmark-based. In dental and medical applications, the use of landmarks is widely accepted as most areas of interest show distinct landmarks which are routinely used in clinical language to describe these specimens. As therapeutical approaches are orientated on these landmarks, too, metrical information about these landmarks is more or less self-explaining for the medical practitioner. Using 3D cephalometric measurements is the method of choice in cases of asymmetry

or severe pathology (Kragsskov et al. 1997). On the contrary, using complex ways of analysis like thin-spline-analysis (Bookstein 1996) or landmark-free methods, which describe shape changes may lead to a general understanding but can rarely be utilized for therapy. Therefore the focus of this chapter will lie on a conventional approach with stress on 3D datasets. Image analysis of time series (for example comparing pre- and posttherapeutical images) using registration procedures is an important feature, too, but is not dealt within this chapter.

## **DESIGN OF A MODEL SOFTWARE**

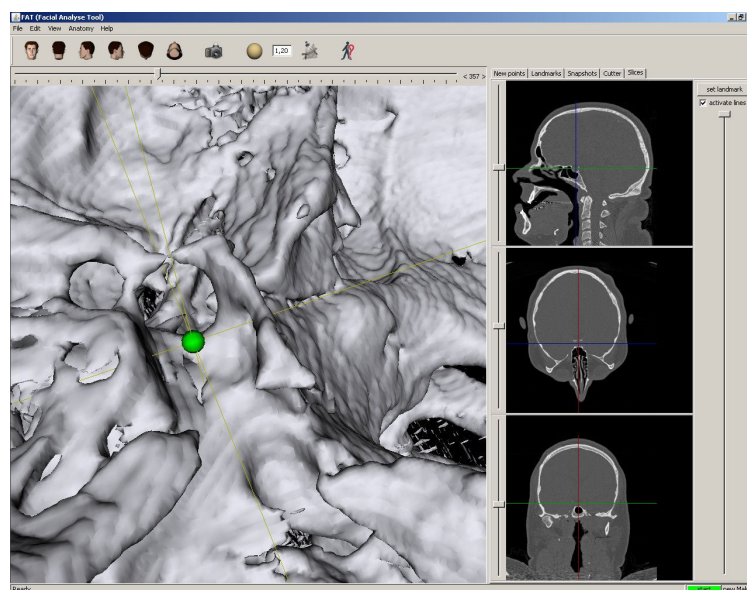
As mentioned above, an ideal, low-priced software for analysing medical 3D data is hard to find. On the other hand, open projects to furnish the background for such software have been developed. Most famous are VTK (visualization toolkit; [www.vtk.org](http://www.vtk.org), [www.paraview.org](http://www.paraview.org)

for parallel computing) and ITK (NLM insight toolkit; [www.itk.org](http://www.itk.org)) which deliver modules for data processing and visualization that are publicly available and can be combined freely. Furthermore, modules not available by now can be written by and shared with the huge VTK community. Based on VTK, a software designed for dental and medical image analysis is presented. Schroeder et al. (2006) serve for further reading on VTK. A most important feature is usability, therefore close contact between clinicians and software programmers is suggested.

First step is choosing the image formats to be read. For 2D and 3D images, the following formats were selected: 2D: BMP, JPEG, PNG, for 3D: DICOM, STL, VRML, OBJ, 3ds.

Second step is to integrate basic functions. This implies 3D rendering of DICOM images as well as functions like zooming, rotation or panning. Independent clipping planes and thresholding to segment DICOM images are needed, too. To facilitate segmentation, buttons for typical pre-set

*Figure 1. Four window display of a CT data set. The use of crosshairs allows landmark placement anywhere. The sella landmark is shown in the midst of sella turcica.*



**Requirements for a Universal Image Analysis Tool in Dentistry and Oral and Maxillofacial Surgery**

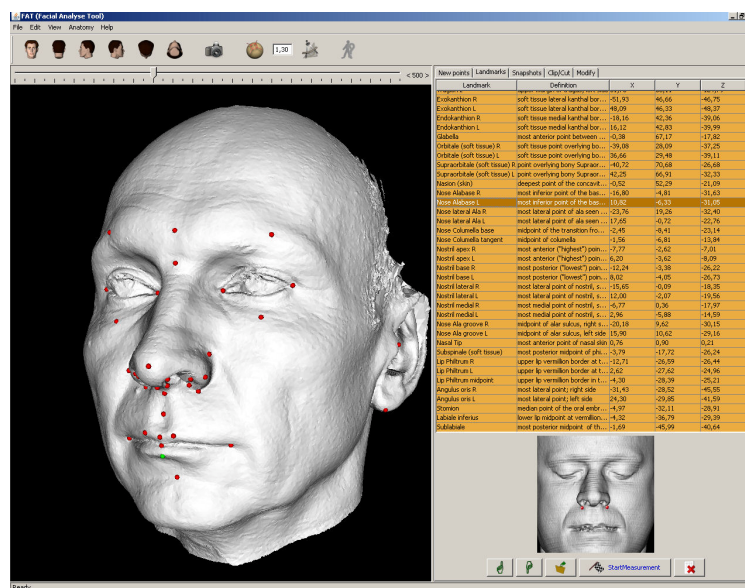
values for soft tissue surface display and bony segmentation are integrated decreasing the need for manual segmentation. In medical CT scanning an often neglected problem is the orientation of the scanner's gantry. Tilting of the gantry plane is done to avoid exposition of the lenses. During 3D reconstruction most software programmes will not correct the gantry which will lead to gross distortion of the rendered object by displacement of all axial slices in the z-plane. Automatic gantry tilt correction can be implemented in VTK and is a useful feature.

For metrical analysis, a hierarchical procedure was chosen. First step is to select the appropriate landmarks. These may be anatomical ones in case of cephalometry and orthodontics and here an open, self-defined library to choose the ones needed is helpful. Landmarks may be select by way of different means. E. g. by direct placement on the thresholded CT image, by way of using

crosshairs, or by using a maximum intensity projection to reduce a 3D image to a 2D one, in which exact landmark placement can be easier. Figure 1 shows the use of crosshairs, which is important for landmarks that do not lie on the surface of the investigated object. Furthermore the coordinates of the individual landmarks must be available for further use (Figure 2). This allows processing of the data. In case of cephalometry, Euclidian distance matrix analysis (Lele and Richtsmeier 2001) or finite element methods (Lozanoff and Diewert 1989) may be performed that way.

Having chosen the landmarks, the trigonometric operations follow. Figure 3 shows possible operations, ranging from defining distances, different ways to construct planes, proportions, angulations, to perpendicular distances, lines or planes. In addition these operations may define new points etc, which can serve as a basis for further measurements (Figure 4). So, an intricate

*Figure 2. Facial scan taken by an optical scanner. Import format is VRML. Anatomic landmarks have been placed on the surface. The individual coordinates are displayed instantly and may be used for further processing. On the far left of the table the landmark is given, then a short definition follows. Below right the location of the highlighted landmark is shown.*



**Requirements for a Universal Image Analysis Tool in Dentistry and Oral and Maxillofacial Surgery**

Figure 3. Construction table for trigonometric operations. Any operations can be performed by inserting the appropriate landmarks. Each result is shown and stored in a spreadsheet.

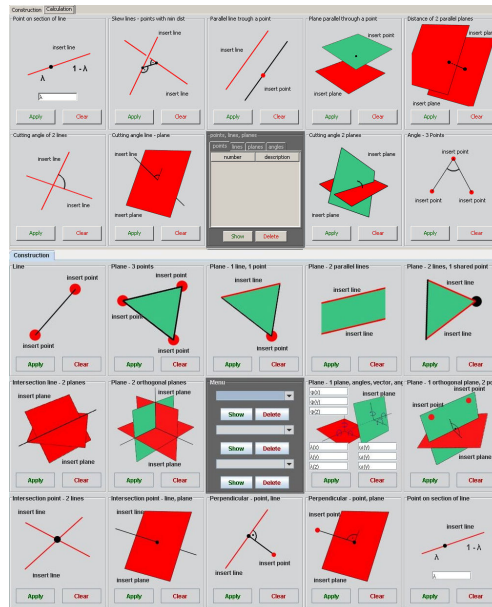
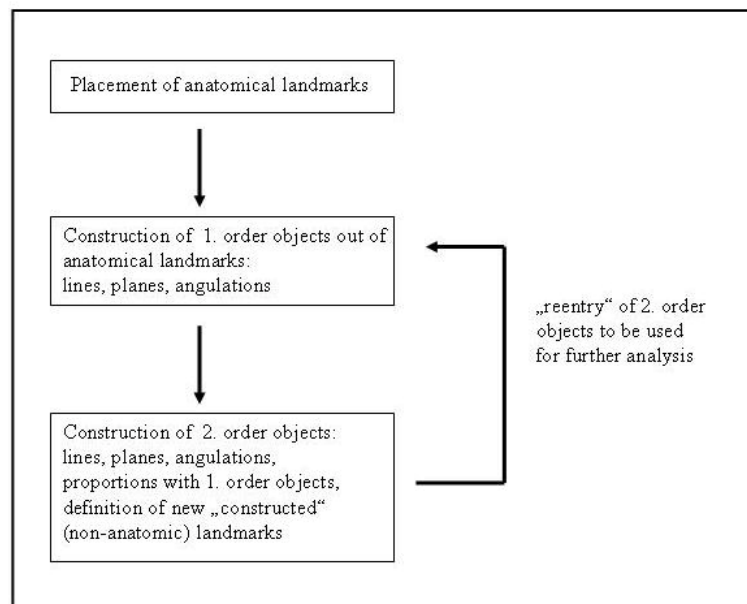


Figure 4. Pathway for a landmark based analysis. Generated objects can be used for further analysis. This way, complex metrical analysis is possible.





trigonometric analysis can be performed. In the end a spreadsheet with all the information for that individual specimen is given. The construction table has to be self-explaining. In this example a drag and drop function to allocate the landmarks and picking from a table are possible. Finally analyses are created which resemble batch programmes. In the end, an appropriate analysis is selected for the data, the landmarks are loaded automatically and the only work is to place the landmarks in the correct order. After the last landmark has been placed, the result of the full analysis is given in a spreadsheet ready for export to a statistical software programme. In addition, the landmark coordinate data can be saved, too. Thus the correct position of the landmarks may be re-evaluated or more landmarks may be added for a new analysis.

By way of segmentation, objects can be created. Adding multiple objects to a scene and handling them independently allows planning operations like surgery, orthodontic therapy or prosthodontics (Figure 5).

Boolean operations with objects will be necessary to construct CAD-CAM facial implants (Figure 6), epithetic prostheses, or in prosthodontics .

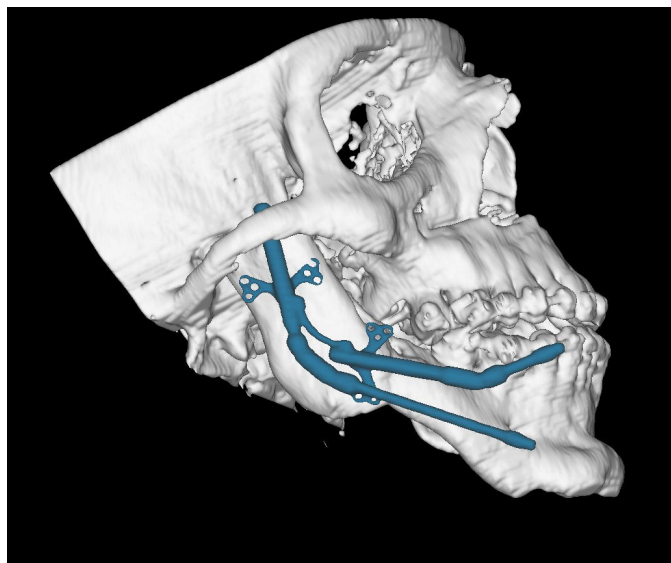
Being able to inspect intersections of multiple datasets will also allow the investigation of occlusion using virtual model casts.

Export filters are necessary to allow further work with the generated data. For practical reasons VRML and STL seem reasonable. This way objects can be created by way of rapid prototyping or used for further work (Figure 7). If finite element methods need to be applied, segmentation and export functions are needed for preprocessing of the data, too (Remmler et al. 1998).

#### SOFTWARE VALIDATION

Any kind of software used for medical inves-

*Figure 5. Virtual try-on of an internal mandibular distraction device on a patient's skull. Virtual operations help in shortening operation room times and can improve surgical outcome.*



**Requirements for a Universal Image Analysis Tool in Dentistry and Oral and Maxillofacial Surgery**

*Figure 6. Planning of a CAD-CAM generated alloplastic implant by fusion of two objects. Pink: patient's situation with traumatic nasoethmoidal and frontal deficiency; deep yellow: skull segment taken from a skull library. Both objects are superpositioned and fused. Afterwards the patients' object will be subtracted and the implant object will remain. Only minor work to correct the transition to the patient skull will be necessary. Segmented VRML data is used for these operations.*

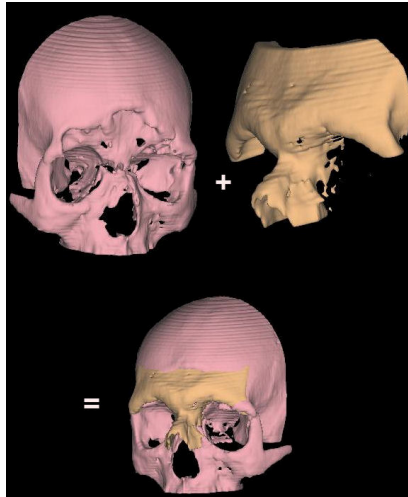


*Figure 7. Surgical template for implant placement generated via rapid prototyping. Here the STL export filter has been used to create a FDM specimen.*

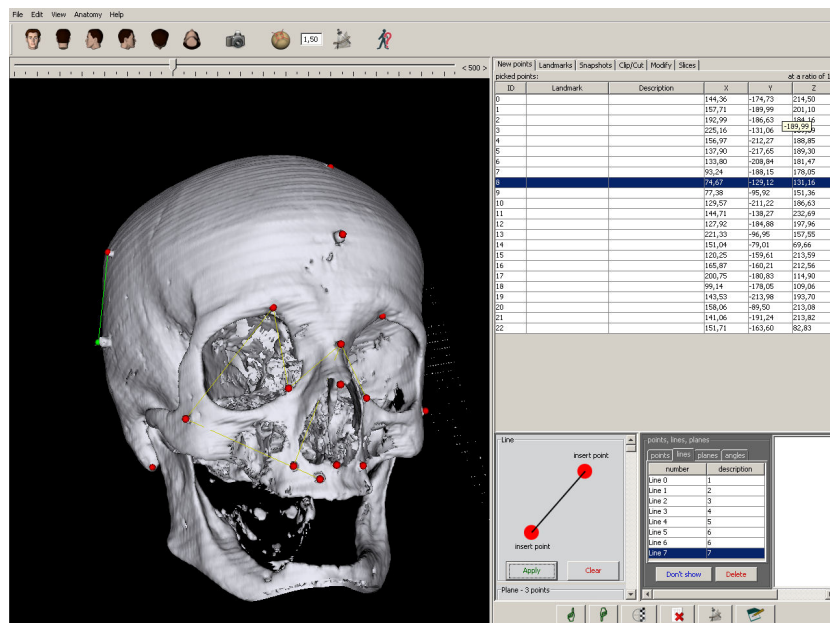


tigations needs validation. Different ways have been suggested. Human skulls have been used in many instances as they resemble best the intricate anatomy and the data set may show problems with import functions, 3D-reconstruction, segmentation, and trigonometric measurements. A common way is measuring distances on the real skull and compare the results with measurements on the virtual object (Hildeboldt and Vannier 1988). Distances on the real skull can be taken with a 3D-digitizer or with precision callipers. In our validation study, a precision calliper was used. To minimize errors due to landmark identification, titanium micro-screws were inserted on 22 landmarks before CT-scanning of the skull. Statistical analysis of 48 measurements showed not significant difference (CT parameters: 1 mm slicing, contiguous slices, Ø deviation real skull – vs. virtual skull 1 % of the measurements which equalled 0.24 mm. Students t test,  $p < 0.01$ ) (Figure 8).

## CLINICAL APPLICATION

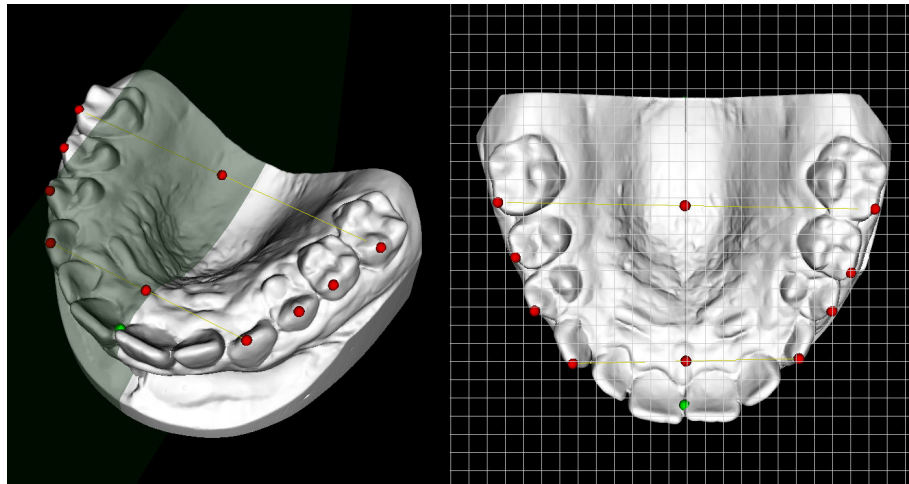
A typical application of dental image analysis is investigating a dental arch. Plaster casts are taken routinely and conventional analysis was done by placing a Perspex plate with an etched metric grid over the crowns. For precise measurements reflection microscopes or callipers were used. Now optical scanning will furnish a precise virtual model with no risk of losing information due to fractures of the brittle plaster cast. Having set up a metric analysis the file is loaded and the appropriate landmarks are placed. Then the batch programme will calculate all pre-defined measurements automatically. As the virtual model can be zoomed, moved, or rotated freely, an analysis can be performed in short time (Figure 9).

Figure 8. Software validation. Measurements between titanium micro screw markers (red dots) are performed on the real and virtual skull. Using micro screws diminishes landmark location errors.





*Figure 9. 3D-analysis of a dental plaster cast. Import format is STL. Note the high quality of the laser-scanning process. On the left landmarks, a midsagittal symmetry plane, and distances from cuspids to the reference plane are shown. Right a grid has been placed for quick visual reference.*



## **ADDITIONAL FEATURES**

Of course the above mentioned features cover only parts of dental image analysis. Measuring areas and volumes is important and will have to be included. That way manual segmentation of regions with little contrast difference is possible, too. Registration procedures are also integrated but will not be discussed within this chapter.

## **CONCLUSION**

With the increase in image data in dentistry and medicine analysis tools become more and more important. Especially the possibility to scan objects three-dimensionally increases the need for powerful instruments. As commercially available software by now lacks special features or has drawbacks in workflow, a solution to overcome these problems is using free software. VTK is presented as a possible solution. It offers a wealth of modules which can be used for almost all tasks in dental image analysis. Thus close cooperation

between informatics and medical departments is an ideal way to generate software up to the clinicians need. As these features will be communicated freely, it sounds reasonable to expect that commercial software will be developed, which will incorporate these features.

## **REFERENCES**

- Bankman, I. A. (2000). *Handbook of medical imaging*, London: Academic press.
- Bookstein, F. L. (1996). Biometrics, biomathematics and the morphometric synthesis. *Bull Math Biol*, 58, 313-65.
- Hammond, P. (2008). The use of 3D face shape modelling in dysmorphology. *Arch Dis Child*, 92, 1120-1126.
- Hierl, Th., Wollny, G., Schulze, F. P., Scholz, E., Schmidt, J. G., Berti, G., Hendricks, J., & Hemprich, A. (2006). CAD-CAM implants in esthetic and reconstructive craniofacial surgery.

*J Comp Information Tech*, 14, 65-70.

Hildebolt, C. F., & Vannier, M. W. (1988). Three-dimensional measurement accuracy of skull surface landmarks. *Am J Phys Anthropol*, 76, 497-503.

Lele, S., & Richtsmeier, J. T. (2001). *An invariant approach to statistical analysis of shapes*. London: Chapman and Hall-CRC press.

Kragoskov, J., Bosch, C., Gyldensted, C., & Sindet-Pedersen, S. (1997). Comparison of the reliability of craniofacial anatomic landmarks based on cephalometric radiographs and three-dimensional CT scans. *Cleft Palate Craniofac J*, 34, 111-116.

Lozanoff, S., & Diewert, V. (1989). A computer graphics program for measuring two- and three-dimensional form changes in developing craniofacial cartilages using finite element methods. *Comp Biomed Res*, 22, 63-82.

Ono, I., Abe, K., Shiotani, S., & Hirayama, Y. (2000). Producing a full-scale model from computed tomographic data with the rapid prototyping technique using the binder jet method: a comparison with the laser lithography method using a dry skull. *J Craniofac Surg*, 11, 527-537.

Remmler, D., Olson, L., Duke, D., Ekstrom, R., Matthews, D., & Ullrich, C. G. (1989). Presurgical finite element analysis from routine computed tomography studies for craniofacial distraction: II. An engineering prediction model for gradual correction of asymmetric skull deformities. *Plast Reconstr Surg*, 102, 1395-1404.

Schroeder, W., Martin, K., & Lorensen, B. (2006). *The visualization toolkit. An object-oriented approach to 3D graphics*. Clifton Park: Kitware

Swennen, G. R., Schutyser, F., Barth, E. L., De Groeve, P., & De Mey, A. (2006). A new method of 3-D cephalometry Part I: the anatomic Cartesian 3-D reference system. *J Craniofac Surg*, 17, 314-325.

Yu, I. H., & Wong, Y. K. (2008). Evaluation of mandibular anatomy related to sagittal split ramus osteotomy using 3-dimensional computed tomography scan images. *Int J Oral Maxillofac Surg*, 37, 521-528.

## KEY TERMS & DEFINITIONS

**CAD-CAM:** Computer-aided design and computer-aided manufacturing. Describes the use of software tools for design activities. Afterwards computer systems are used to control the tools during product manufacturing.

**CBT:** Cone-beam tomography. Radiologic method to acquire 3D data sets.

**Cephalometry:** The measurement of the human head. Standard procedure in orthodontics, anthropology, forensic medicine and maxillofacial surgery.

**DICOM:** Digital imaging and communications in medicine. Standard for the management of medical imaging.

**FDM:** Fused deposition modelling. A rapid prototyping procedure.

**OBJ:** An open geometry definition file format

**RP:** Rapid Prototyping. Automatic construction of physical objects using solid freeform fabrication.

**STL:** Standard triangulation language or surface tessellation language. Standard language for rapid prototyping and CAD.

**VRML:** Virtual reality modeling language. A common language to describe 3D objects, widely used in the internet.

# Die dreidimensionale Bildgebung

Analyse und Manipulation von Bilddaten

Der Förderpreis „Digitale Zahnmedizin“ wurde 2009 von der teamwork media GmbH und dem Deutschen Ärzteverlag ins Leben gerufen. Dieser Fachbeitrag gehört zu den erstplatzierten der zahlreichen Einsendungen.

In der Human- sowie Zahnmedizin spielt die dreidimensionale Datenerfassung eine immer größere Rolle, stetig werden neue Softwareprodukte vorgestellt. Leider handelt es sich dabei oft um proprietäre Formate, welchen keinen Export in übliche 3D-Formate – beziehungsweise dies nur durch teure Zusatzprodukte – ermöglichen. Außerdem erfordern die Softwarelösungen häufig eine umfangreiche Einarbeitung und erlauben neben der Visualisierung nur rudimentäre metrische Analysen. Die nachfolgend beschriebene Software soll die genannten Probleme verhindern und den klinisch tätigen Anwender hinsichtlich Aufwand und Zeit entlasten.

Indizes: 3D-Kephalometrie, Bilddatenanalyse, STL-Format, Rapid Prototyping

Ein Beitrag von Priv.-Doz. Dr. Dr. Thomas Hierl, Dipl.-Inf. Daniel Kruber und Dr. Dr. Heike Hümpfner-Hierl, alle Leipzig

## Aufbau von FAT

Die hier vorgestellte Software (FAT) ermöglicht die Analyse und die Manipulation von in der Zahnmedizin gebräuchlichen dreidimensionalen Bilddaten. Aufbauend auf dem Visualization Toolkit (VTK) erlaubt die Software den Import der meisten Datenformate, deren Bearbeitung und den Export in die für Rapid Prototyping gebräuchliche Formate. Außerdem ist eine dreidimensionale Bildanalyse (zum Beispiel 3D-Kephalometrie, Modellanalyse) möglich. Hierbei lassen sich umfangreiche Messungen strukturiert vornehmen und anschließend in beliebige Anwendungen exportieren. Die Möglichkeiten der Software werden an einem klinischen Beispiel demonstriert. Bei einem jungen Patienten mit Kiefergelenkankylose wird der Gesichtsschädel dreidimensional analysiert, der Ober- und Unterkiefer vermessen und abschließend Teile des Datensatzes für das Rapid Prototyping exportiert. Die Daten dienen als Grundlage für die Erstellung knöchern verankerter Kieferdistraktoren.

Die Software basiert auf dem Visualization Toolkit ([www.vtk.org](http://www.vtk.org)) und der Softwareplattform Java. Somit kann sie plattformunabhängig gestaltet werden (Windows, Linux, et cetera) und ist durch kontinuierlich entwickelte Module erweiterbar.

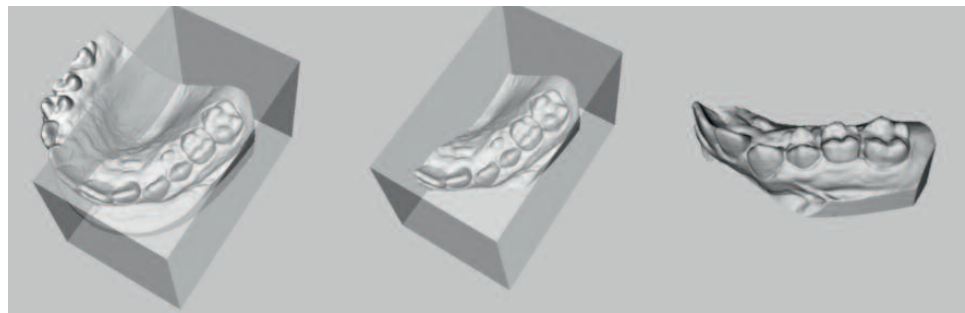
## Im- und Exportformate

Um ein breites Einsatzspektrum zu gewährleisten, sind verschiedene Importformate vorgesehen. Es können CT-, MRT- oder DVT-Datensätze in den Formaten DICOM, Nifti und Raw (Roh) Format eingelesen werden. Weiterhin stehen für dreidimensionale Daten die Importformate STL, OBJ, VRML, 3ds Max und vtk zur Verfügung. Zweidimensionale Bilddaten können in BMP, JPEG und PNG-Formaten eingelesen werden. Somit ist die Analyse verschiedener Bilddatenquellen möglich – dies reicht von Röntgengeräten über optische Scanner (Modelle beziehungsweise Gesichtsscans) und Fotografien bis hin zu Konstruktionsdaten aus CAD-Programmen. Der Export der Daten ermög-

Abb. 1  
Darstellung typischer  
Dateiobjekte.  
Von links oben begin-  
nend: CT, CT mit zusätz-  
licher Oberflächendar-  
stellung, MIP (virtuelles  
Röntgen), MRT-Angio-  
gramm, Zahnmodell,  
optischer Oberflächens-  
can, Volumen-Raycast-  
darstellung, CAD-Datei  
eines Kieferwinkel-  
implantates



Abb. 2  
Beschneiden eines  
Datensatzes mit  
einem Würfel  
(Größe und alle Flächen  
des Würfels können  
verändert werden)



licht die Weitergabe von CT-Daten an das Rapid Prototyping im STL-Format beziehungsweise die Nutzung für CAD-Aufgaben. Neben dem Hauptobjekt können Nebenobjekte geladen werden, zum Beispiel Implantate, Konstruktionselemente oder Osteosynthesematerialien.

### Visualisierung

Zur Visualisierung stehen die üblichen Werkzeuge zur Verfügung. Daten von Röntgenscannern werden im 1-Fenster (dreidimensionales Modell) oder im 4-Fenster-Modus (dreidimensionales Modell und drei orthogonale Schnittbilder) dargestellt. Über einen Schieberegler kann die Datei nach *Hounsfield*-Einheiten segmentiert werden. Das ermöglicht eine Darstellung entsprechend des Grauwerts der einzelnen Voxel. Somit werden sowohl der Knochen wie auch die Hautoberfläche sichtbar. Darüber hinaus können Daten als Maximum-Intensity-Projection (MIP=virtuelles zweidimensionales Röntgenbild) visualisiert werden. In der Zahnheilkunde dient das dazu, um aus einer CT-Aufnahme ein Fernröntgenseitbild zu generie-

ren. Weiterhin ist in der Software ein Volumenrendering implementiert, was mit einer Oberflächendarstellung kombiniert werden kann. Dies ermöglicht komplexe anatomische Strukturen zu diagnostizieren (Abb. 1). Außerdem können Transparenz, Farbe, Licht, Zoom, Rotation, Verschiebung und Hintergrund individuell eingestellt werden. Die eingelesenen Bilddaten werden über Ebenen, Volumenkörper oder einer Kombination aus beiden beschnitten (Abb.2).

### 3D-Analyse

Ein wichtiger Bestandteil der Software ist die Möglichkeit, an allen Bilddatensätzen komplexe dreidimensionale metrische Analysen vorzunehmen. Diese beruht auf Landmarken, welche auf dem Datensatz mittels Cursor oder Fadenkreuz platziert werden. Damit können Geraden, Strecken, Ebenen, Winkel und Abstände von Punkt zu Punkt definiert werden. Die dabei entstandenen Daten können rekursiv verwendet werden. So ist es realisierbar, weitere Ebenen oder Winkel zu berechnen. Insgesamt stehen 40 Möglichkeiten zur Verfügung.







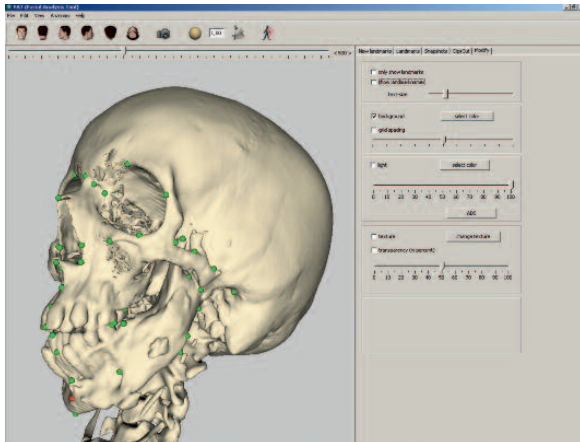


Abb. 9 Darstellung des CT-Datensatzes mit anatomischen Landmarken

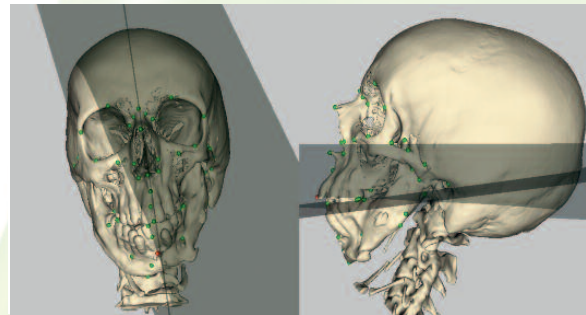


Abb. 10 Darstellung verschiedener Ebenen

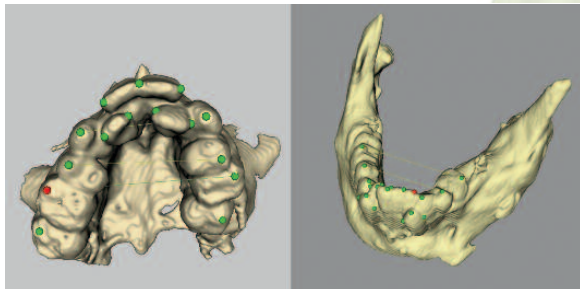


Abb. 11 Modellanalyse an Ober- und Unterkieferzahnbögen (Die Symmetrieebenen wurden aus Gründen der Übersichtlichkeit ausgeblendet)



Abb. 12 Oberkiefermodell mit individuellem knochenverankertem Distraktor zur Kieferdehnung

Vermessung des Schädels vorgenommen (3D-Kephalometrie) (Abb. 9). Neben der kephalometrischen Analyse (Abb. 10) werden Ober- und Unterkiefer isoliert und ebenfalls im Sinn einer Modellanalyse vermessen (Abb. 11). Da durch der Ankylose keine ausreichende Kieferöffnung möglich ist, können keine Modelle über Abformungen gewonnen werden. Deshalb werden der Ober- und Unterkiefer im STL-Format exportiert und über Rapid Prototyping Modelle erstellt. Auf diesen werden individuelle, knochenverankerte Distraktoren zur chirurgisch unterstützten Ober- und Unterkieferdehnung angefertigt (Abb. 12).

### Diskussion

Bei der Analyse dreidimensionaler Bilddatensätze können mithilfe der Software FAT verschiedene Fragen beantwortet werden. Neben der Visualisierung, die auch mit vielen anderen Produkten möglich ist, erlaubt FAT eine komplexe dreidimensionale metrische Vermessung. Ein weiterer Schwerpunkt in der Entwicklung der Software wurde auf eine Nutzerfreundlichkeit hinsichtlich Zeitaufwand

und Bedienbarkeit gelegt. Hierzu liegen für die verschiedenen Softwarelösungen in der Zahnheilkunde kaum Studien vor – die eigene Erfahrung der Entwicklergruppe kann jedoch große Unterschiede konstatieren. □

Literatur beim Verfasser oder im Internet unter [www.teamwork-media.de](http://www.teamwork-media.de) in der linken Navigationsleiste unter „Journale Online“.



### Korrespondenzadresse

Priv.-Doz. DDr. Thomas Hierl  
Dipl.-Inf. Daniel Kunber  
DDr. Heike Hümpfner-Hierl  
Universitätsklinikum Leipzig  
Klinik und Poliklinik für MKG-Chirurgie  
Nürnbergerstr. 57  
04103 Leipzig



### 1.2.3 Konstruktionselemente in FAT

Eine wesentliche Ergänzung der Analysewerkzeuge stellen die Konstruktionswerkzeuge dar, mit deren Hilfe unter anderem Boolesche Operationen, Deformationen oder Beschneidungen möglich sind. Ein Beispiel hierfür ist die Erstellung einer Pilotschablone.

Im Zuge einer Kiefergelenks-OP-Planung konnte mit Hilfe von FAT eine digital erstellte Pilotschablone für die minimalinvasive Chirurgie des Kiefergelenkes erstellt werden (Abbildung 1.5). Hierfür waren entsprechend den Hinweisen von [Bla92] und [HBKZ95] Markierungen zu setzen, die für den weiteren Verlauf entscheidende Positionen für die geführte Endoskopie darstellten. Der arthroskopische Zugang zum Kiefergelenk ließ sich durch Überlagerung der dreidimensionalen texturierten Oberfläche und des Volumen-Datensatzes des Patienten gut realisieren. Die zuvor festgelegten Positionen dienten der Orientierung der Führungshülsen, welche anschließend in die patientenspezifische Schablone eingebaut wurden.

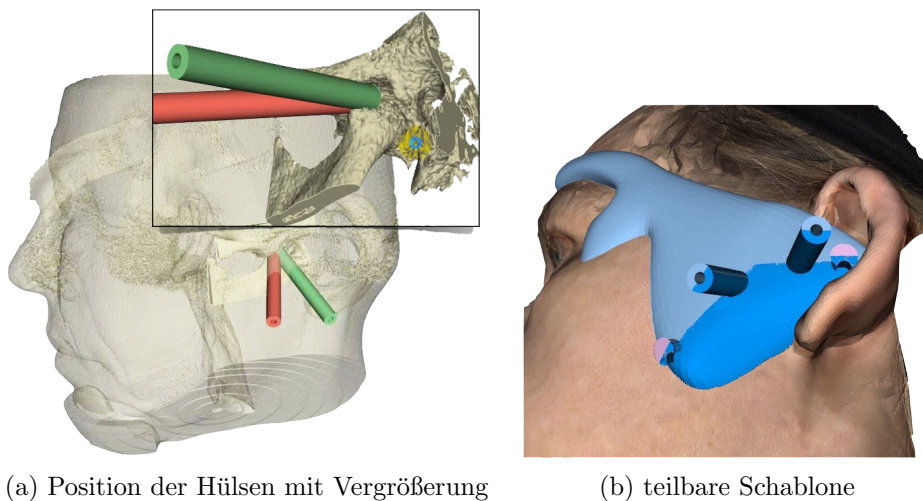


Abbildung 1.5: Schablone für die Kiefergelenksendoskopie

In den nachfolgenden Kapiteln wird gezeigt, welche weiteren medizinischen Fragestellungen mit FAT gelöst werden konnten.



## **2. FAT-Anwendungen**

### **Vergleich und Analyse komplexer Flächen**

Verschiedene Veröffentlichungen, die sich mit der Bemaßung und Analyse von Geometrien anhand von CT- oder 3D-Scan gewonnenen Daten und typischen Fragestellungen auseinandersetzen, werden nachfolgend kurz erklärt und anschließend durch die dazugehörige Publikation ergänzt.

#### **2.1 CAD-CAM–Assisted Esthetic Facial Surgery**

Zum Zeitpunkt der Veröffentlichung dieser Studie wurden bisherige Arbeitsabläufe durch diverse Rekonstruktionsvorlagen beschrieben. Eine vollständig computergestützte ästhetische Gesichtschirurgieplanung und -beratung wurde bis dato nicht vorgestellt.

Erstmalig konnte nun ein vollständig digitaler Arbeitsablauf gezeigt und analysiert werden. Dafür wurde das Kephalometrie-Modul von FAT verwendet um die OP-Planung zu unterstützen und mittels kephalometrischer Auswertung (Abbildung 2.1) der patientenspezifischen Ergebnisse einen Behandlungsplan zu präsentieren. Darauf aufbauend konnte ein geeignetes Implantat ausgewählt und eine entsprechende Schablone entworfen werden, die wiederum als intraoperative Hilfe zum Einsatz kam.

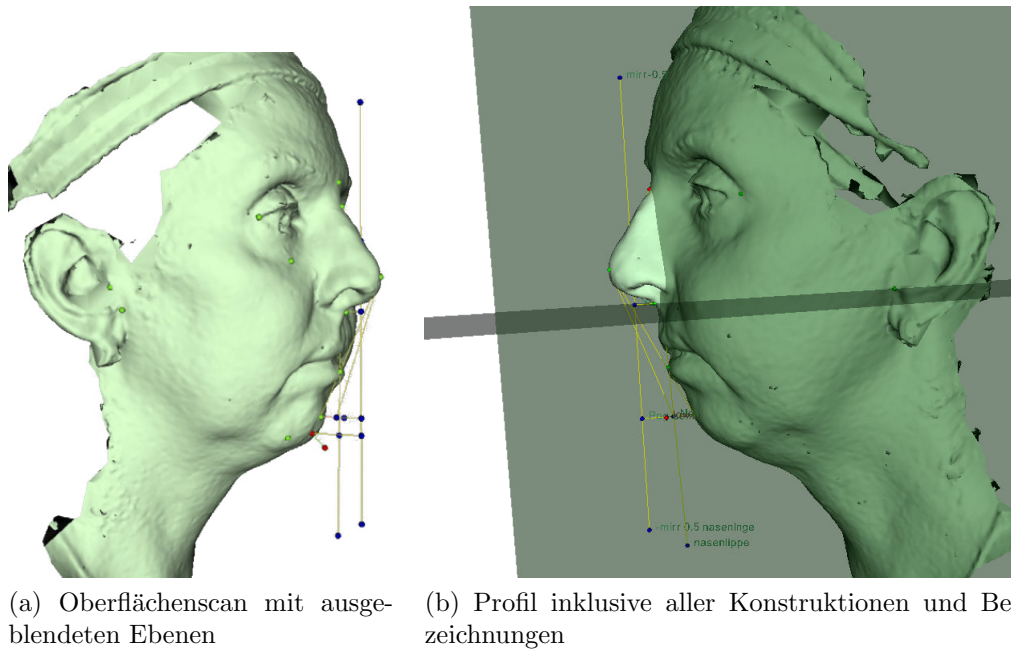


Abbildung 2.1: Ergebnis der kephalometrischen Analyse (neben dem 3D-Oberflächenscan werden konstruierte Punkte, Linien und Ebenen dargestellt)

Aufgrund der Verwendungsvielfalt des Analyse-Bereichs von FAT wird lediglich die Darstellung der VTK-Werkzeuge für die allgemeine Erzeugung von Konstruktionselementen in der Abbildung 2.2 skizziert. Aus den gesetzten Landmarken werden diverse Kombinationen von unterschiedlichen primitiven Elementen erstellt und entsprechende Ergebnisse im 3D-Raum sowie als Zahlenwert präsentiert.

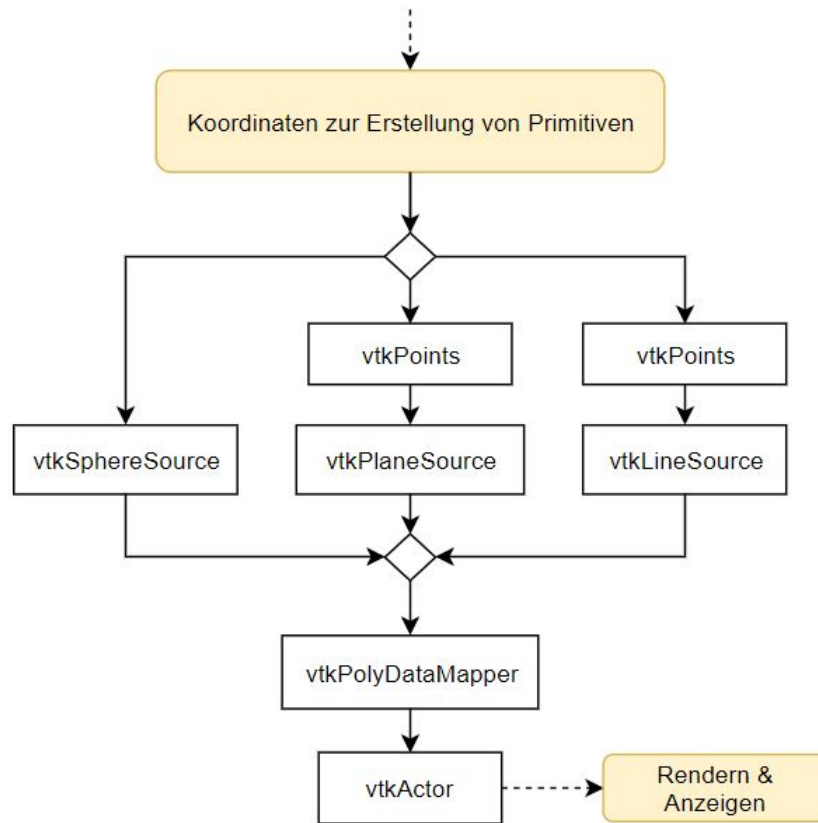


Abbildung 2.2: Workflow zur Erzeugung von Punkten, Ebenen und Linien im 3D-Raum

# CAD-CAM–Assisted Esthetic Facial Surgery

Thomas Hierl, PhD, MD, DDS,\* Steffen Arnold, Dipl-Ing,†  
Daniel Kruber, Dipl-Inf,‡ Fritz-Peter Schulze, PhD,§ and  
Heike Hümpfner-Hierl, MD, DDS||

**Purpose:** This report describes a fully digital workflow for computer-assisted esthetic facial surgery planning and guidance.

**Material and Methods:** Using optical scans, virtual surgery is performed according to the 3-dimensional cephalometric results. Next, surgical templates are generated using rapid prototyping. These templates act as a guide during surgery.

**Results:** The workflow has been tested successfully in 4 esthetic facial surgical procedures (rhinoplasty and genioplasty). In addition to surgical assistance, the advantages of the workflow include the possibility of discussing the treatment plan interactively with the patient and comparing and measuring simulation surgery with the actual outcome. As an additional benefit, the appropriate size of the alloplastic implants can be determined preoperatively.

**Conclusions:** Templates could improve special procedures in esthetic facial surgery.

© 2013 American Association of Oral and Maxillofacial Surgeons

*J Oral Maxillofac Surg* 71:e15-e23, 2013

Computer-assisted procedures are gaining more and more importance in all fields of head and neck surgery. Combined with 3-dimensional (3D) data (eg, computed tomography, cone-beam computed tomography, optical surface scanning), these methods have been used mainly for osseous surgery assistance. Applications range from surgical planning,<sup>1-3</sup> computer-assisted design (CAD), computer-assisted manufacturing (CAM) implants,<sup>4,5</sup> and surgical templates for

bone resection or bone transplant modeling,<sup>6-8</sup> to assisting in craniostylosis surgery,<sup>9</sup> osseous genioplasty,<sup>10,11</sup> or dental splints in orthognathic surgery.<sup>12</sup> Regarding facial soft tissue, full workflows from taking digital impressions to the generation of facial prostheses (eg, missing ears or noses) or orthoses have been published.<sup>13-18</sup> Thus, the last missing field within the head and neck region is integrating these methods into esthetic and reconstructive facial surgery. The first steps have been undertaken by defining average facial 3D morphology or trying to generate “universal” esthetic facial templates.<sup>19,20</sup> With regard to nasal reconstruction after ablative tumor surgery, reconstruction templates using impression taking, wax modeling, and model generation by way of rapid prototyping have been described.<sup>21,22</sup> In the present report, a novel workflow for facial surgical planning (eg, rhinoplasty, genioplasty) and intraoperative assistance fully based on digital data are introduced and the first applications shown.

## Materials and Methods

To achieve a digital workflow, 4 steps are required (Fig 1). The first step is digital impression taking using optical scanning. Optical procedures allow fast, radiation free, and precise acquisition of the facial surface. Scanning can be repeated at any time and delivers a detailed 3D surface mesh that can be used for all subsequent stages. The next step is a concise esthetic evaluation. In our workflow, a facial analysis tool,<sup>23,24</sup> a software program developed by us and based on the VTK open source libraries (available from [\\*Senior Consultant, Department of Oral and Maxillofacial Plastic Surgery, Leipzig University, Leipzig, Germany.](http://</a></p></div><div data-bbox=)

†Engineer, Department of Construction and Engineering, Rapid Prototyping, University of Applied Sciences (HTWK) Leipzig, Leipzig, Germany.

‡Computer Scientist, Department of Oral and Maxillofacial Plastic Surgery, Leipzig University, Leipzig, Germany.

§Head, Department of Construction and Engineering, Rapid Prototyping, University of Applied Sciences (HTWK) Leipzig, Leipzig, Germany.

||Consultant, Department of Oral and Maxillofacial Plastic Surgery, Leipzig University, Leipzig, Germany.

The development of the 3D cephalometric software (facial analysis tool) was partially funded by the German Federal Ministry of Economics and Technology (grant ZIM KF2036708SS0).

Address correspondence and reprint requests to Dr Hierl: Department of Oral and Maxillofacial Plastic Surgery, Leipzig University, Nuemberger Street 57, Leipzig 04103 Germany; e-mail: [hiet@medizin.uni-leipzig.de](mailto:hiet@medizin.uni-leipzig.de)

© 2013 American Association of Oral and Maxillofacial Surgeons

0278-2391/13/7101-0\$36.00/0

<http://dx.doi.org/10.1016/j.joms.2012.08.020>

www.vtk.org), is used. It enables all 3D cephalometric tasks, such as measuring distances and angles, creating planes, mirroring, and so forth. After evaluating the facial scan, the surface mesh is adjusted to the desired shape ("virtual surgery"). This can be accomplished using scanner software (eg, 3D-Mirror; Canfield Imaging Systems, Fairfield, NJ) or industrial software for automotive or aerospace development (eg, Catia, Dassault Systemes, Paris, France). The next step is a comparison of virtual surgery with the preoperative data. All changes can be visualized and evaluated using a color-coded distance map between the 2 data sets. Furthermore, the shape and size of the differences can be used to select an appropriate implant (eg, in genioplasty). As soon as the results of the virtual surgery have been accepted, templates can be designed (eg, Catia or facial analysis tool software) and built using rapid prototyping. These templates act as a guide during surgery and in the postoperative evaluation. The templates should be easy to build and handle, should include all required information, should allow sterilization, and production technology should lead to reasonable pricing. To achieve this, full 3D or 2-dimensional templates could be made. Regarding 3D templates, a transparent mold of the desired outcome is necessary. Because this would require vacuum forming over a model generated with rapid prototyping if a digital workflow is desired (which would increase the production effort and cost), we chose a less expensive and simpler method. Therefore, multiple 2-dimensional templates, which can be combined to form a 3D surface (Fig 2), were generated. The template design is straightforward, because only the desired facial contour lines must be intersected with predefined rectangular planes of 2-mm thickness. The whole planning procedure from optical scan to template data requires 1.5 to 2.5 hours.

Because all steps use and deliver 3D meshes in an open interchangeable format (in our cases, Standard Triangulation Language, Object File Format, or Virtual Reality Modeling Language), the workflow can be adapted easily to include additional software tools or to production changes.

After surgery, the patient is scanned again to compare the outcome with the preoperative and virtual surgery data.

These templates are easy to construct and build using most rapid prototyping methods. In our workflow, fused deposition modeling with acrylonitrile-butadiene-styrene, a durable hard plastic that can be sterilized, is used.<sup>4</sup> The templates are sterilized and transferred to the operating room and assist during surgery. Furthermore, outcome changes can be simply checked by placing the template during patient consultations.

The Leipzig University Ethics Committee approved the present study (Az 084-12-05032012), which followed the Helsinki Declaration.

## Results

Our workflow was evaluated in 3 patients with 4 procedures (Table 1).

A typical example is a 43-year-old patient with unilateral cleft lip and palate (Fig 3). After transversal maxillary distraction osteogenesis and Le Fort I advancement, the patient sought treatment for final esthetic surgery. After optical surface scanning (Vectra 3M, Canfield Imaging Systems), the ideal chin position was defined using 3D cephalometry.

Next, the planned procedure was simulated using 3D-Mirror software according to the cephalometric evaluation (Fig 4). The result was discussed with the patient, and the template was generated (Fig 2). Surgery included minor rhinoplasty and chin augmentation with a polyethylene implant (MEDPOR, Stryker, Freiburg, Germany). By subtracting the preoperative scan from the simulation, the dimensions of the necessary MEDPOR implant can be chosen preoperatively.

One of the advantages of the digital workflow is the possibility to compare simulation and result. Figures 5 to 8 show the original situation versus the prediction and the final outcome compared with simulation us-

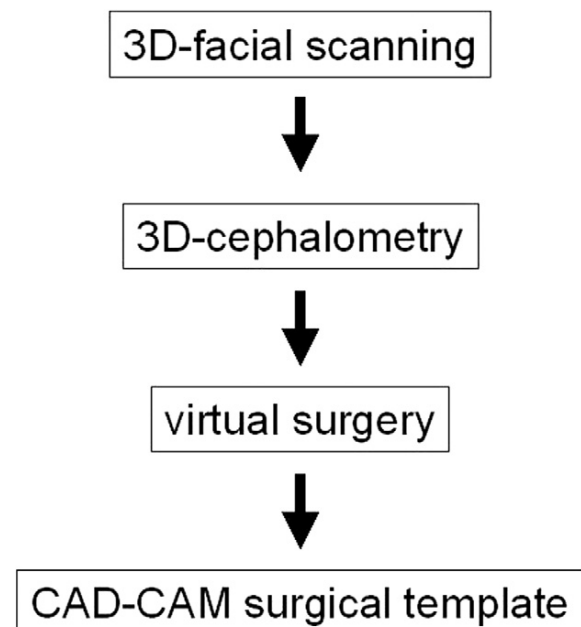


**FIGURE 1.** Workflow diagram for planning and construction of surgical templates in esthetic facial surgery.

Hierl et al. CAD-CAM-Assisted Surgery. *J Oral Maxillofac Surg* 2013.

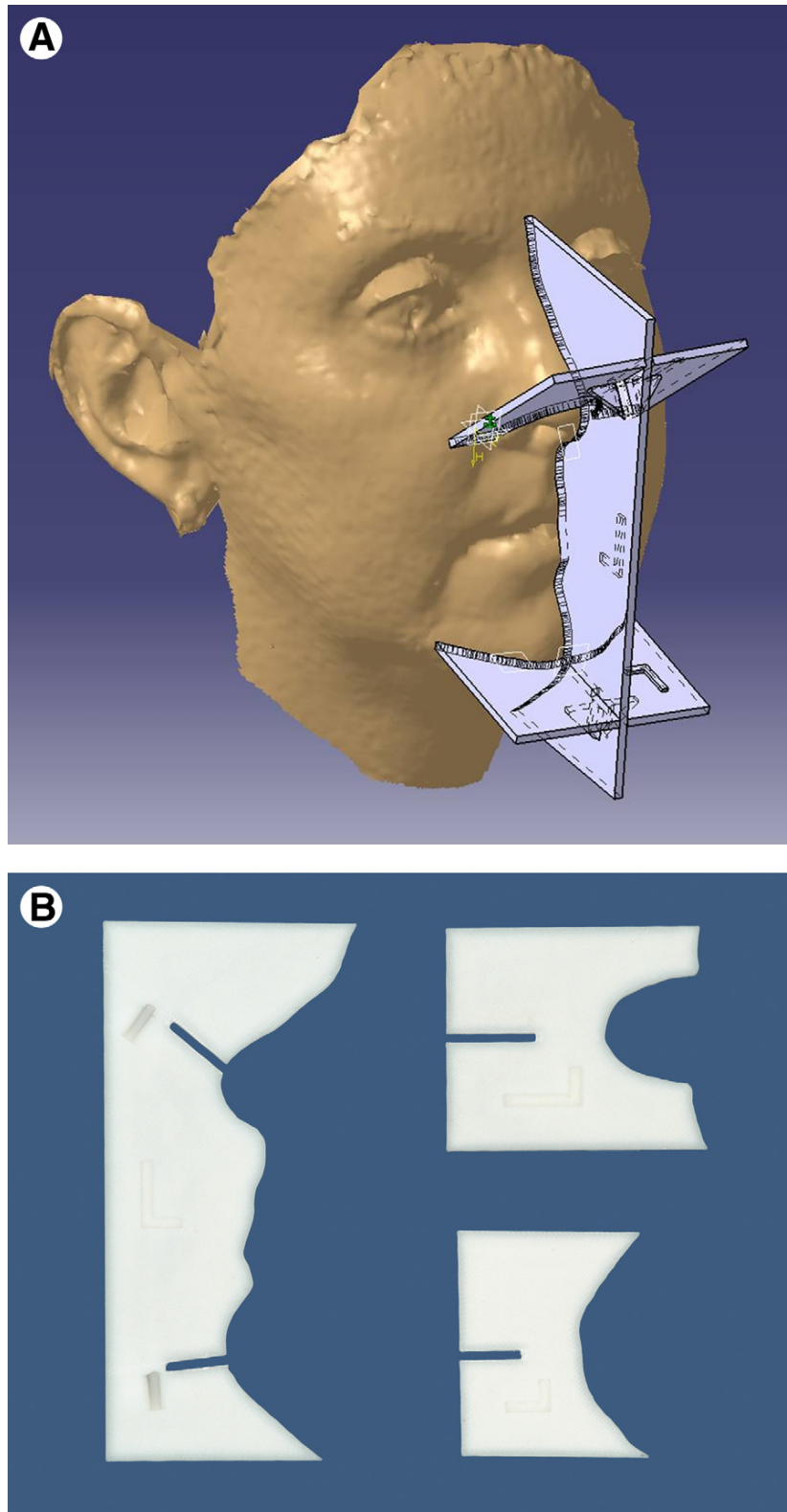


**FIGURE 2.** Surgical template consisting of 3 parts constructed with Catia. Horizontal templates can be plugged into the vertical template. Small flanges prevent unintentional mobility. Note, L imprinted on left side as a help for correct assembly.

*Hierl et al. CAD-CAM-Assisted Surgery. J Oral Maxillofac Surg 2013.*



**Table 1. PATIENT DIAGNOSES AND PROCEDURES**

Pt. No.	Diagnosis	Procedure	Template
1	Nasal deformity after complex panfacial trauma	Rhinoplasty (with costochondral graft)	3-Piece template for nose
2	Prominent chin after mandibular advancement	Setback genioplasty	1-Piece template
3	Nasal and chin dysplasia in cleft lip and palate	Rhinoplasty, chin augmentation (MEDPORE implant)	3-Piece template for nose and chin

Hierl et al. CAD-CAM-Assisted Surgery. J Oral Maxillofac Surg 2013.

ing optical scanning. Furthermore, postoperative changes can be evaluated simply by placing the template during outpatient consultations (Fig 9). To demonstrate the facial changes in conventional photographs in contrast to the facial scans, which have their own appearance and feel, the frontal face view is shown in Figure 10.

## Discussion

In the present report, a fully digital workflow for computer-assisted esthetic surgery planning and surgical assistance using CAD-CAM procedures is introduced. In contrast to earlier suggestions, which combined conventional steps such as impression taking or

real modeling of the desired outcome,<sup>21,22</sup> which must be digitized again, our method strictly uses digital data throughout the entire process. This enables easy storage and data transfer and avoids errors during the production chain. If desired, the patient can participate in the assessment of the virtual surgery, enabling a better understanding of the patients' perspectives of the present and future facial appearance. Generating 2-dimensional templates that can be combined allows reasonable pricing. From our experience, the template costs could range from 10€ to 50€ depending on the rapid prototyping procedure. Using optical scanning as the basis for the workflow permits noninvasive precise data acquisition. By subtracting the preoperative from the planned data (or vice



**FIGURE 3.** Left, lateral view of 43-year-old patient with retropositioned chin and minor nasal deformity. Right, Cephalometric analysis (face analysis tool): green, anatomic landmarks; blue, landmarks defining reference planes and lines (planes not shown for better visibility); red, preoperative and suggested chin position.

Hierl et al. CAD-CAM-Assisted Surgery. J Oral Maxillofac Surg 2013.



**FIGURE 4.** Left, Preoperative view. Right, Virtual surgery result.

*Hierl et al. CAD-CAM-Assisted Surgery. J Oral Maxillofac Surg 2013.*

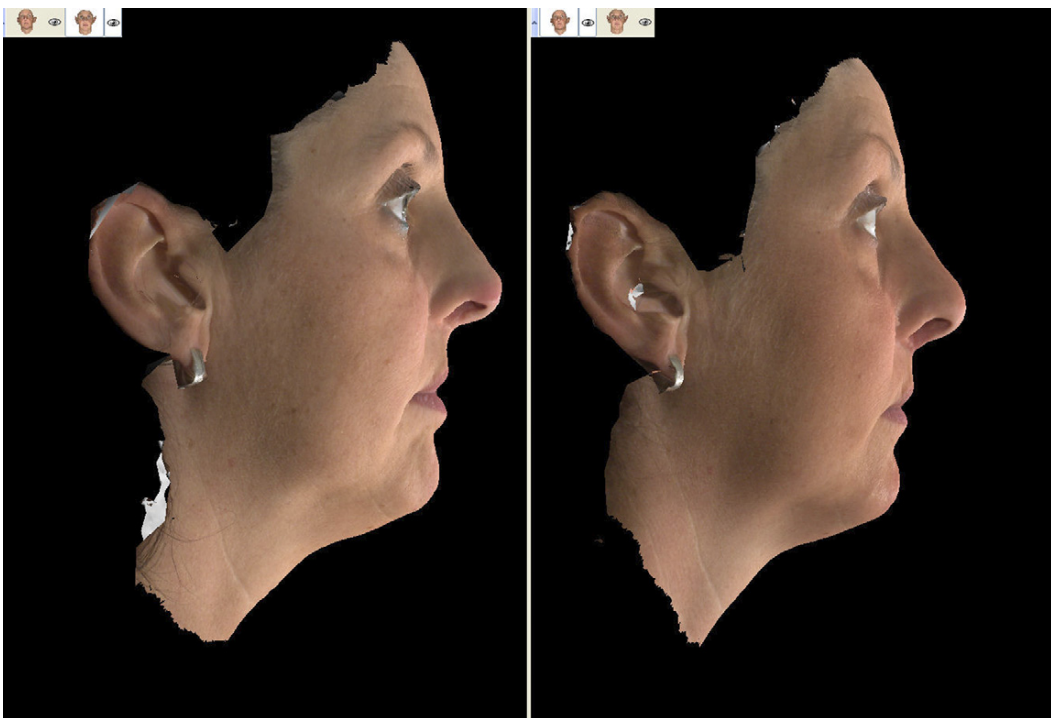


**FIGURE 5.** Left, Result of virtual surgery. Right, Actual result 3 months after surgery.

*Hierl et al. CAD-CAM-Assisted Surgery. J Oral Maxillofac Surg 2013.*



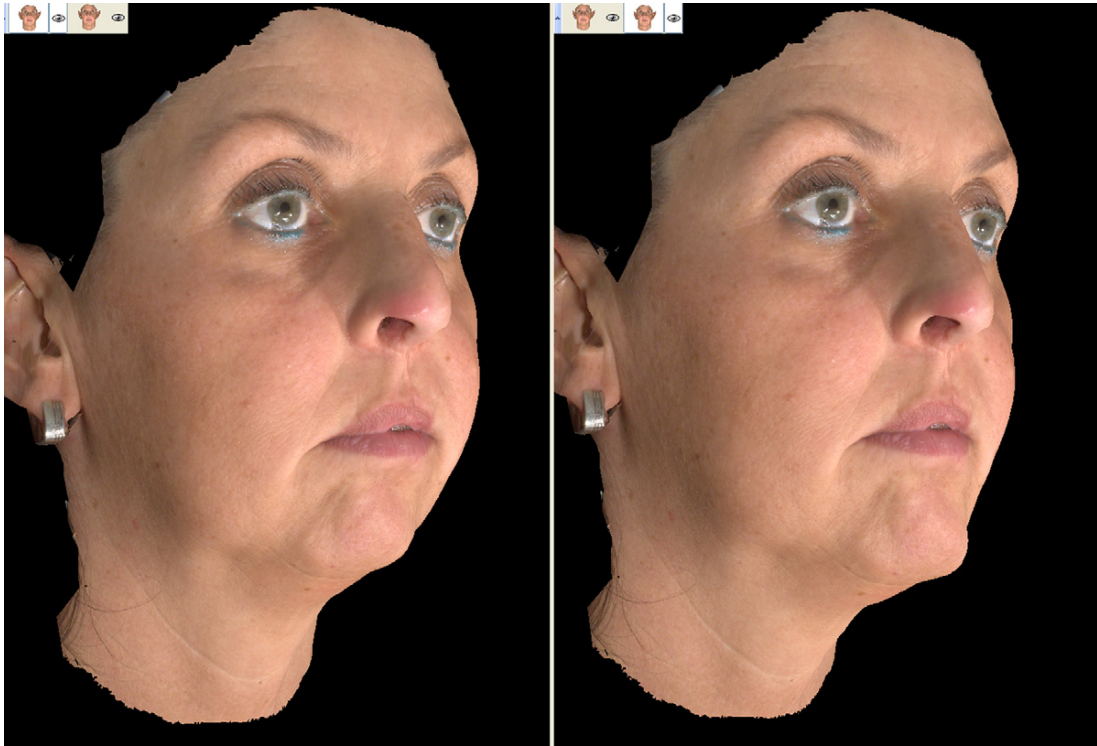


**FIGURE 6.** *Left*, Preoperative oblique scan. *Right*, Simulated effects.

*Hierl et al. CAD-CAM-Assisted Surgery. J Oral Maxillofac Surg 2013.*

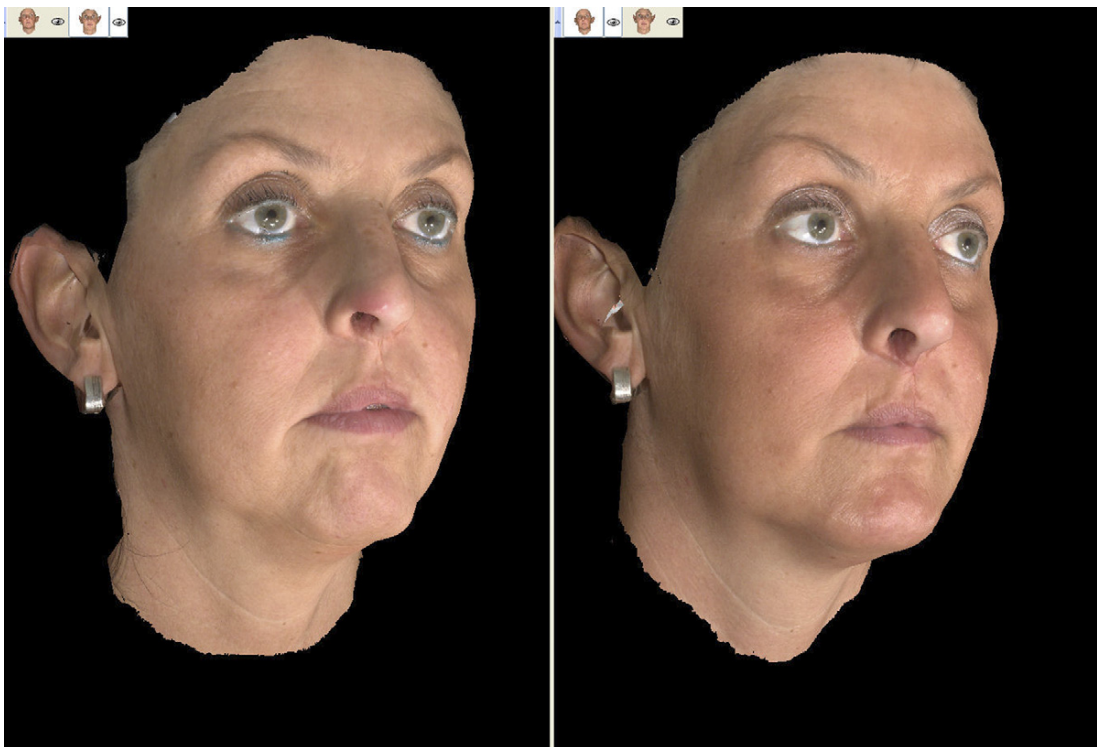


**FIGURE 7.** *Left*, Simulated surgery. *Right*, Postoperative scan.

*Hierl et al. CAD-CAM-Assisted Surgery. J Oral Maxillofac Surg 2013.*

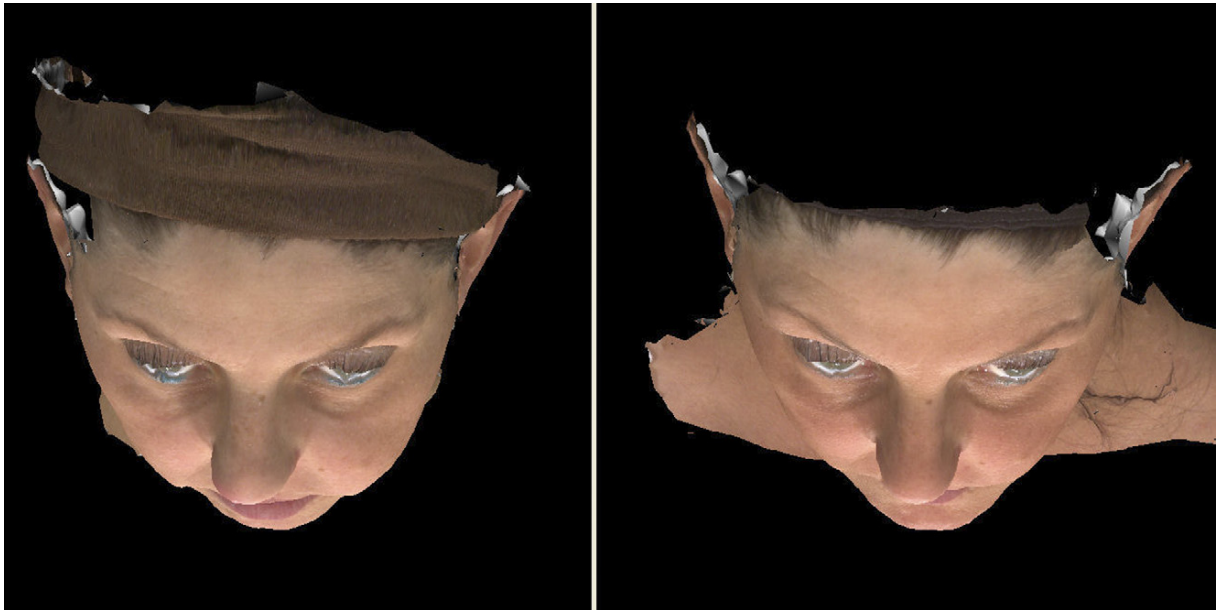


**FIGURE 8.** Pre- and postoperative comparison using facial 3D scanning. *Left*, Preoperative view. *Right*, Postoperative view. Cranial view shows changes in chin position and effects of rhinoplasty.

*Hierl et al. CAD-CAM-Assisted Surgery. J Oral Maxillofac Surg 2013.*

versa), the size of the needed implants or the amount of surgery can be assessed. Regarding rhino- or genioplasty, alloplastic sizes or individual molds can be combined with our method during surgery.<sup>25,26</sup> Furthermore, the workflow permits full review of the 3D results by comparing the final outcome with the preoperative situation and the virtual surgery, an important part of quality assessment and improvement.

Using templates for intraoperative soft tissue evaluation poses some critical aspects. First, some swelling always occurs and could hide the real amount of soft tissue change. Regarding genioplasty, a difference could exist between an osseous procedure and using alloplastic onlays. Gentle subperiosteal preparation, just enough to take the implant, will lead to less swelling and will allow a more realistic outcome evaluation than bone manipulations. During rhinoplasty, some swelling will also result; however, the nasal soft tissue envelope is comparatively thin and can be cooled with ice water during surgery. Swelling will be more prominent in the cranial parts and less in the tip area. Templates are designed to assist the surgeon during surgery, which implies they could be discarded if the result will seem esthetically unpleasant. Therefore, the surgical skills to perform such surgery using conventional outcome judgments are necessary.

An important part in any new method is to define the necessary time and costs. Because optical scanners and software have a wide price range, any such evaluation is difficult. Optical 3D scanners range from \$300 to \$30,000. The same is true for the necessary



**FIGURE 9.** Template check 3 months' postoperatively. Note, Difference in template of throat resulted from reclined head posture.

*Hierl et al. CAD-CAM-Assisted Surgery. J Oral Maxillofac Surg 2013.*





**FIGURE 10.** A, Preoperative frontal view. B, Facial changes after intervention.

Hierl et al. *CAD-CAM-Assisted Surgery. J Oral Maxillofac Surg* 2013.

software. As a rule, it can be stated that the lower price will require greater technical skills and more time spent. Depending on the available optical scanner, the needed software will vary, and the workflow described in our report is only 1 possible method.

Regarding the needed time, our setup requires 1.5 to 2.5 hours, beginning with optical scanning to the design of the template. Although this is quite long, a potential benefit of the invested time is that it forces the surgeon to analyze and plan the procedure thoroughly, which could be advantageous for lessening the operative time and improving the outcome.

The next steps are the inclusion of 3D average data and facial templates into the workflow to increase the speed and outcome of 3D cephalometry and virtual surgery, which has been suggested by Kau et al.<sup>19</sup>

## References

1. Stoker NG, Mankovich NJ, Valentino D: Stereolithographic models for surgical planning: Preliminary report. *J Oral Maxillofac Surg* 50:466, 1992
2. D'Urso PS, Barker TM, Earwaker WJ, et al: Stereolithographic biomodelling in cranio-maxillofacial surgery: A prospective trial. *J Craniomaxillofac Surg* 27:30, 1999
3. Chow LK, Cheung LK: The usefulness of stereomodels in maxillofacial surgical management. *J Oral Maxillofac Surg* 65:2260, 2007
4. Gronet PM, Waskewicz GA, Richardson C: Preformed acrylic cranial implants using fused deposition modeling: A clinical report. *J Prosthet Dent* 90:429, 2003
5. Klein M, Glatzer C: Individual CAD/CAM fabricated glass-bio-ceramic implants in reconstructive surgery of the bony orbital floor. *Plast Reconstr Surg* 117:565, 2006
6. Abou-Elfetouh A, Barakat A, Abdel-Ghany K: Computer-guided rapid-prototyped templates for segmental mandibular osteotomies: A preliminary report. *Int J Med Robotics Comp Assist Surg* 7:187, 2011
7. Hirsch DL, Garfein ES, Christensen AM, et al: Use of computer-aided design and computer-aided manufacturing to produce orthognathically ideal surgical outcomes: A paradigm shift in head and neck reconstruction. *J Oral Maxillofac Surg* 67:2115, 2009
8. Olszewski R, Reychler H: Three-dimensional surgical guide for frontal-nasal-ethmoid-vomer disjunction in Le Fort III osteotomy. *J Craniofac Surg* 22:1791, 2011
9. Burge J, Saber NR, Looi T, et al: Application of CAD/CAM prefabricated age-matched templates in cranio-orbital remodeling in craniostenosis. *J Craniofac Surg* 22:1810, 2011
10. Olszewski R, Tranduy K, Reychler H: Innovative procedure for computer-assisted genioplasty: Three-dimensional cephalometry, rapid-prototyping model and surgical splint. *Int J Oral Maxillofac Surg* 39:721, 2010
11. Xia JJ, Shevchenko L, Gateno J, et al: Outcome study of computer-aided surgical simulation in the treatment of patients

- with craniomaxillofacial deformities. *J Oral Maxillofac Surg* 69:2014, 2011
12. Yanping L, Shilei Z, Xiaojun C, et al: A novel method in the design and fabrication of dental splints based on 3D simulation and rapid prototyping technology. *Int J Adv Manuf Technol* 28:919, 2006
  13. Ciocca L, Scotti R: CAD-CAM generated ear cast by means of a laser scanner and rapid prototyping machine. *J Prosthet Dent* 92:591, 2004
  14. Reitemeier B, Notni G, Heinze M, et al: Optical modeling of extraoral defects. *J Prosthet Dent* 91:80, 2004
  15. Cheah CM, Chua CK, Tan KH, et al: Integration of laser surface digitizing with CAD/CAM techniques for developing facial prostheses. Part 1: Design and fabrication of prosthetic replicas. *Int J Prosth* 16:435, 2003
  16. Coward TJ, Watson RM, Wilkinson IC: Fabrication of a wax ear by rapid-process modelling using stereolithography. *Int J Prosth* 12:20, 1999
  17. Ciocca L, Bacci G, Mingucci R, et al: CAD-CAM construction of a provisional nasal prosthesis after ablative tumour surgery of the nose: A pilot case report. *Eur J Cancer Care* 18:97, 2009
  18. Lin JT, Nagler W: Use of surface scanning for creation of transparent facial orthoses. A report of two cases. *Burns* 29:599, 2003
  19. Kau CH, Zhurov A, Richmond S, et al: Facial templates: A new perspective in three dimensions. *Orthod Craniofac Res* 9:10, 2006
  20. Mooney LA: Cosmetic template. US Patent 4,886,076. December 12, 1989
  21. Murrell GL, Burget GC: Aesthetically precise templates for nasal reconstruction using a new material. *Plast Reconstr Surg* 112:1855, 2003
  22. Byrne PJ, Garcia JR: Autogenous nasal tip reconstruction of complex defects: A structural approach employing rapid prototyping. *Arch Facial Plast Surg* 9:358, 2007
  23. Hierl T, Wollny G, Schulze FP, et al: CAD-CAM implants in esthetic and reconstructive craniofacial surgery. *J Comp Information Tech* 16:65, 2006
  24. Hierl T, Kruber D, Borasch H, et al: Neu entwickelte 3D-Analyse software für Zahnheilkunde und MKG-Chirurgie. *Digital Dental News* 5:6, 2011
  25. McMahon D, Lin A, Reddy V, et al: Rhinoplasty sizers. *Aesthet Plast Surg* 36:72, 2012
  26. Cavusoglu T, Ayhan S, Findikcioglu K, et al: The employment of bone wax as a template in the reconstruction of nasal dorsum defects. *Aesth Plast Surg* 27:120, 2003

## 2.2 Positioning of Bone Segments During Navigated Surgery

Bei ausgeprägten Verletzungen des Gesichtsskelettes zeigen vor allem Trümmerfrakturen oder Revisionsoperationen wesentliche Probleme auf, die die Wiederherstellung der korrekten Position bzw. Passung der entsprechenden Knochensegmente beeinträchtigen können.

In der nachfolgenden Veröffentlichung wird ein innovativer Weg beschrieben, wie mittels präoperativer 3D-Planung in FAT und intraoperativer Navigation unter Zuhilfenahme eines Mini-Distraktors Knochensegmente eindeutig und sicher intraoperativ positioniert werden können.

Ähnlich wie in Kapitel 2.1 auf Seite 24, wird auch hier eine kephalometrische Auswertung mittels FAT durchgeführt.

Abbildung 2.3 zeigt eine 3D-Analyse für die Augenhöhle.

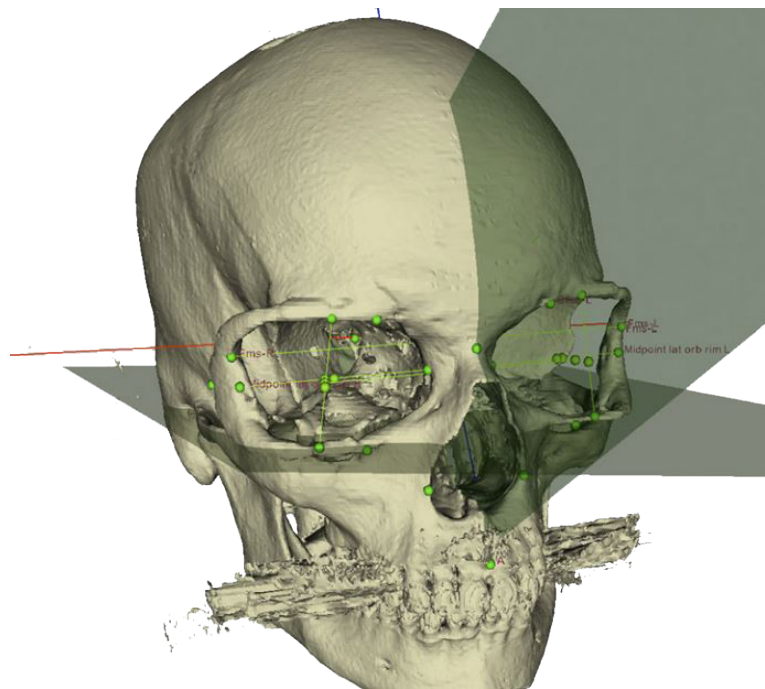


Abbildung 2.3: Computertomographie (CT) -basierte Analyse (Berechnung diverser knöcherner und weichgewebiger Parameter durch Hinzunahme von Hilfsobjekten )

## Kapitel 2. FAT-Anwendungen

### Vergleich und Analyse komplexer Flächen

---

Das Prinzip der Erzeugung von Hilfsobjekten (wie z.B. Ebenen oder Linien) wurde bereits im Diagramm des vorherigen Kapitels dargelegt. Deshalb wird stattdessen in der folgenden Abbildung 2.4 gezeigt, welche Schritte in VTK nötig sind um eine Landmarke auf ein Objekt zu positionieren. Darauf aufbauend sind dann trigonometrische Berechnungen an diesem Objekt durchführbar.

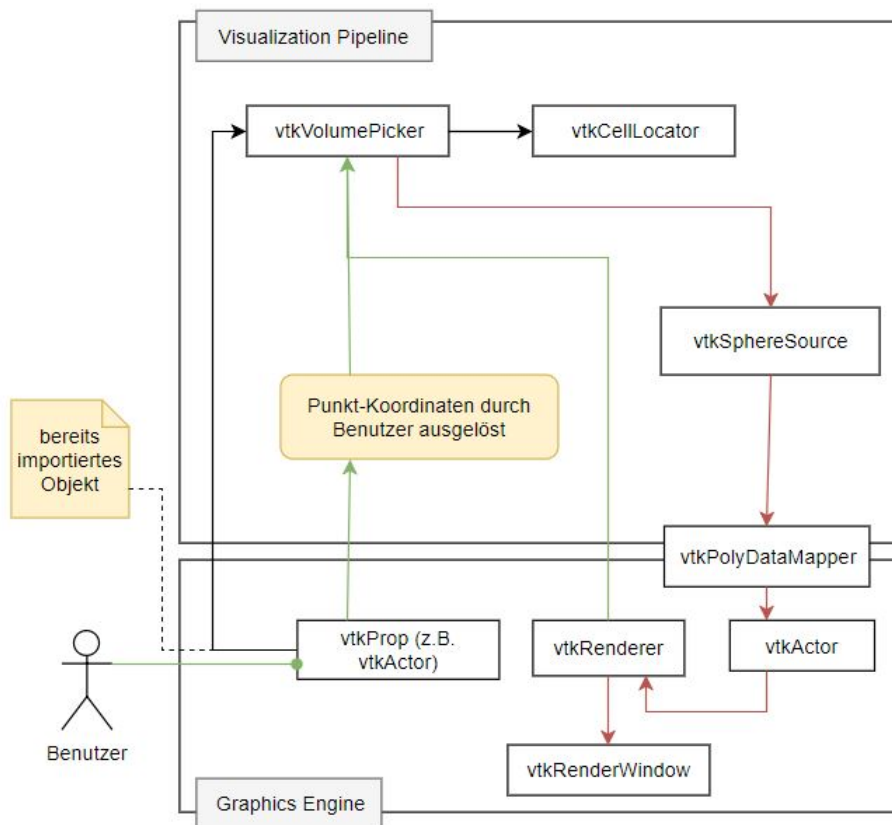


Abbildung 2.4: Workflow Landmarkenplatzierung in der 3D-Kephalometrie:  
grün – Benutzer setzt Markierung auf ein 3D-Objekt;  
rot – erzeugt Punkt / Landmarke an der vom Benutzer markierten Position  
und stellt es im 3D-Fenster dar



# Positioning of Bone Segments During Navigated Surgery

Thomas Hierl, PhD, MD, DDS,\* Matthias Krause, MD, DDS,†  
Daniel Kruber,‡ and Heike Hümpfner-Hierl, MD, DDS§

**Purpose:** In navigated craniomaxillofacial surgery, bone segments often have to be repositioned. To keep them reliably in the desired place during referencing and osteosynthesis, a miniature external distractor can be used.

**Materials and Methods:** The use of a miniature external mandibular distractor is shown in a case of bilateral lateral orbital rim advancement during endocrine orbitopathy decompression surgery.

**Results:** The advantages of using a distractor are the possibility of changing the fragment position incrementally in all directions during intraoperative control with the navigated pointer and the small size of the appliance.

**Conclusions:** Bone segments can be manipulated intraoperatively with a miniature distractor in navigated surgery.

© 2013 American Association of Oral and Maxillofacial Surgeons  
*J Oral Maxillofac Surg* 71:376-381, 2013

Three-dimensional imaging has led to great improvements in preoperative evaluation and virtual treatment planning.<sup>1</sup> Intraoperative navigation has been the next step to take the virtual planning into the operating room.<sup>2,3</sup> Because navigated oral and maxillofacial surgery is concerned with the facial skeleton in most instances, bony parts have to be repositioned, resected, or osteotomized to achieve the desired results. Concerning repositioning, this will work without major problems in straightforward situations. Problems arise when the bony parts will not fit, such as in comminuted fractures or in revision surgery when

segments have to be osteotomized and rearranged. In these cases a major problem in navigated procedures is to hold the appropriate bone segments in the correct position during referencing and osteosynthesis. Depending on the clinical situation, several possibilities are at hand. One way is to generate a 3-dimensional (3D) model through rapid prototyping, perform surgery on the model, and bend the necessary plates or meshes before surgery.<sup>4,5</sup> This works well if the possibility to generate such a model is at hand and if the bony structures allow a single well-defined way to position the hardware. In case of thin structures, a template could be generated by way of computer-aided design/computer-aided manufacturing procedures to hold the bony segment(s) during osteosynthesis.<sup>6,7</sup> Both ways will work but require some expense and time because software and rapid prototyping facilities are needed. A third way, which will be introduced in this report, is to fix the segments securely and allow incremental position changes by using a miniature external mandibular distractor. Its use is shown in a case report on endocrine orbitopathy surgery combining the technique of González-García et al<sup>8</sup> with intraoperative navigation.<sup>9,10</sup>

\*Senior Consultant, Department of Oral & Maxillofacial Plastic Surgery, Leipzig University, Leipzig, Germany.

†Consultant, Department of Oral & Maxillofacial Plastic Surgery, Leipzig University, Leipzig, Germany, and Private Practice, Berlin, Germany.

‡Computer Scientist, Department of Oral & Maxillofacial Plastic Surgery, Leipzig University, Leipzig, Germany.

§Senior Consultant, Department of Oral & Maxillofacial Plastic Surgery, Leipzig University, Leipzig, Germany.

The development of the Facial Analysis Tool (3D cephalometric software) is partially funded by the German Federal Ministry of Economics and Technology (ZIM KF2036708SS0).

Address correspondence and reprint requests to Dr Hierl: Department of Oral & Maxillofacial Plastic Surgery, Leipzig University, Nuemberger Street 57, 04103 Leipzig, Germany; e-mail: hiet@medizin.uni-leipzig.de

© 2013 American Association of Oral and Maxillofacial Surgeons

0278-2391/13/7112-0\$36.00/0

<http://dx.doi.org/10.1016/j.joms.2012.04.013>

## Materials and Methods

Our patient had had severe endocrine orbitopathy for several years. The medical history included thyroidectomy, corticoid medication, retrobulbar radiation, removal of orbital fat and parts of the lateral orbital walls, and lateralization of the orbital rims, all performed in different departments. Because there was still major exophthalmos and insufficient lid clo-

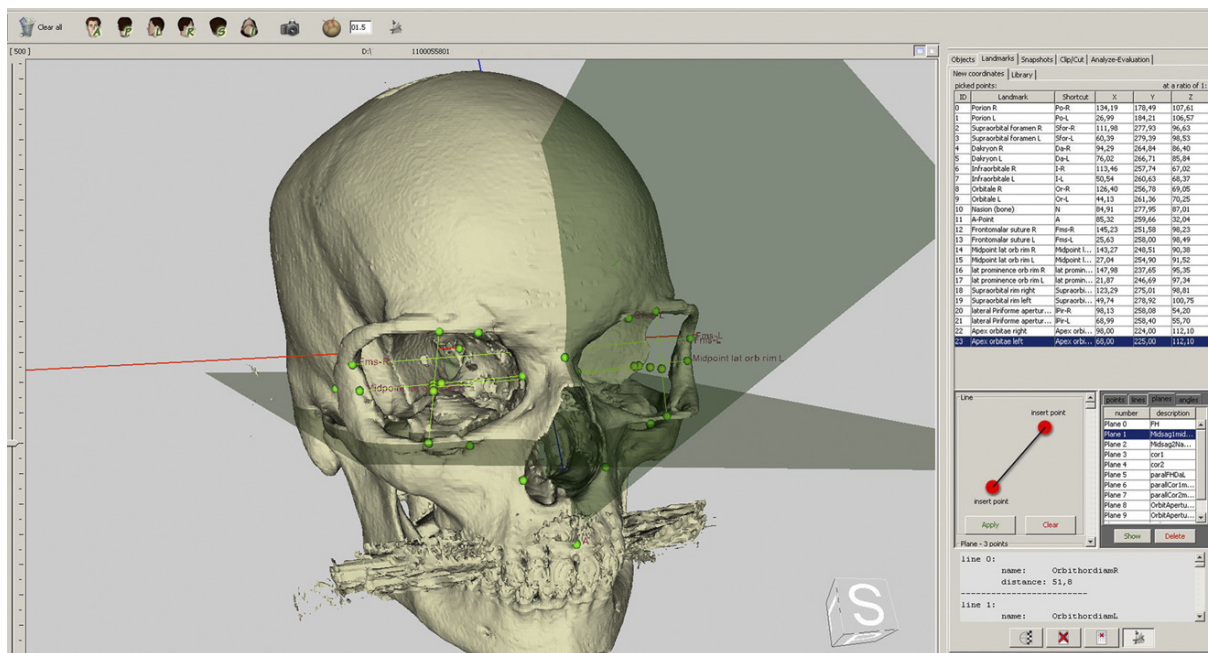


**FIGURE 1.** Preoperative 3D analysis with Facial Analysis Tool software. The landmarks and 2 planes are shown.

Hierl et al. Positioning of Bone Segments. *J Oral Maxillofac Surg* 2013.

sure, the patient was referred for further surgery. The treatment plan started with computed tomography (CT)-based analysis (Fig 1) using the Facial Analysis Tool, which is 3D cephalometric software (Facial Analysis Tool, developed at the authors' institution).<sup>11</sup>

Analysis showed a far too lateralized and repositioned lateral orbital rim leading to a shallow orbit. Comparing patient data with our orbital anatomy database delivered the information for virtual surgical planning in the Brainlab software program (Feldkirchen, Germany). As shown in Figure 2, both lateral orbital walls had to be re-osteotomized and moved forward-medially. Furthermore, remnants of the lateral orbital wall were to be removed down to the skull base.

This plan was taken into the operating room, and the orbital rims were temporarily removed through a transconjunctival and upper eyelid incision. After the remaining lateral orbital walls had been corrected according to the treatment plan, the lateral rims had to be repositioned to the desired place. In cases without any anatomic guidelines, it can be demanding to hold a bone segment in place while referencing its position with the navigation probe, to correct the position, and still not to move during osteosynthesis. In such cases, a miniature external mandibular distractor can be effectively used. In Figure 3 the Multi-Guide distractor frame (Stryker, Freiburg, Germany) was mounted on 1 pin fixed to the lateral-superior aspect of the orbital rim (first pin to be inserted) and to the free orbital rim (second pin). To ease distractor placement, the free bone part is held into

the suggested position to allow a parallel insertion of the second pin (free segment). Before the distractor is attached, it is adjusted in neutral position, allowing movements in all directions. Both fixation pins should be as parallel as possible. This will ease distractor insertion, although it is also possible when both pins are diverging. If this is the case, the first pin is inserted and the distractor attached. Then, the free segment is held in the desired position. The hole for the second pin is burred by inserting the pin in the distractor clamp, marking the point where the pin meets the bone segment, pivoting the distractor slightly around the first pin, and placing the bur hole parallel to the second pin.

The design of a multidirectional distractor allows free movement of the bone segment in all directions easily while maintaining a secure position during referencing. After the planned position had been found, the rims were fixed with 1.0-mm osteosynthesis plates to the infraorbital and supraorbital rims (Fig 4). Furthermore, small bone wedges were inserted and fixed between the rim and the frontal bone to prevent accidental postoperative rotation.

The small size of the external distractor permits easy access during osteosynthesis or further manipulation. After osteosynthesis, the segment position was referenced again. The distractor was removed and then the pins were removed, and the incisions were closed.

This report followed the Declaration of Helsinki on medical protocol and ethics. The regional ethical review board declared no need for approval.



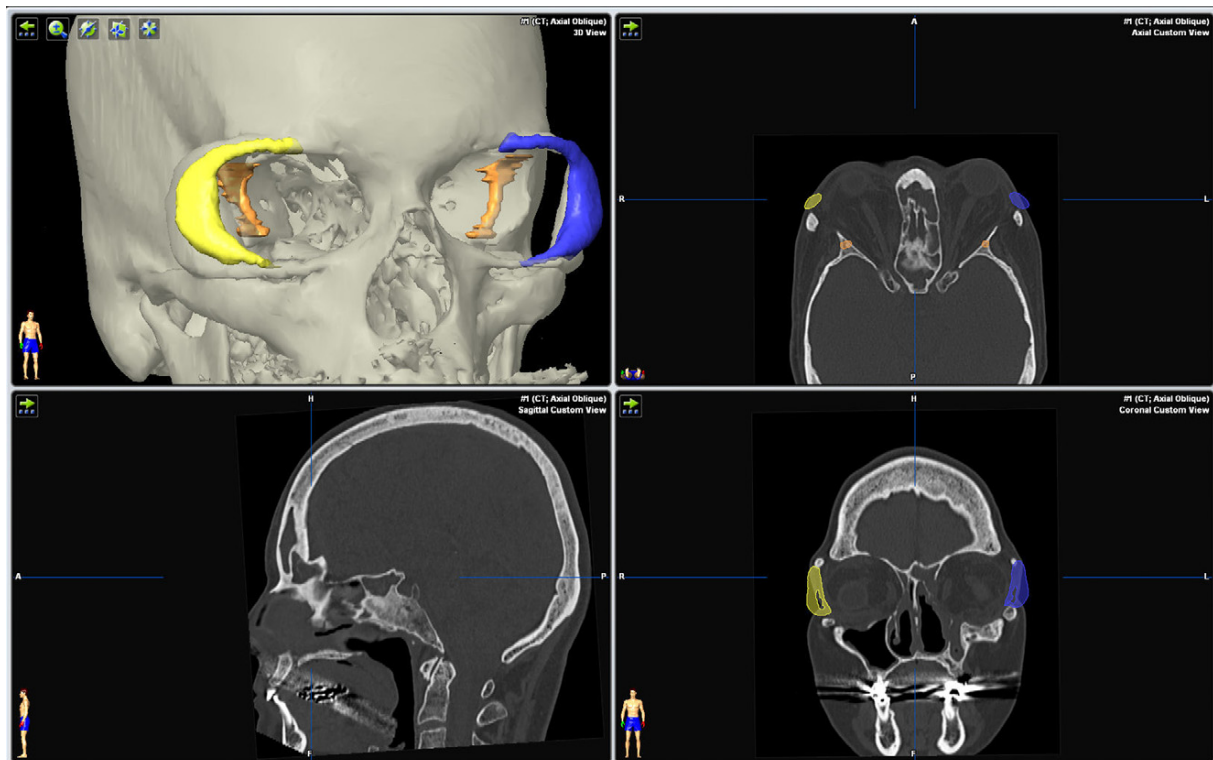


**FIGURE 2.** Preoperative planning with Brainlab software. The new position of the lateral orbital rims (*blue and yellow*) and the border of the planned lateral orbital wall resection (*orange*) are highlighted.

*Hierl et al. Positioning of Bone Segments. J Oral Maxillofac Surg 2013.*



**FIGURE 3.** *Left*, Fixation of the osteotomized lateral orbital rim with the miniature distractor before referencing. *Right*, Lateral orbital rim attached to manipulation pin. The lateral bony extension of the rim has been removed to improve the esthetic outcome.

*Hierl et al. Positioning of Bone Segments. J Oral Maxillofac Surg 2013.*

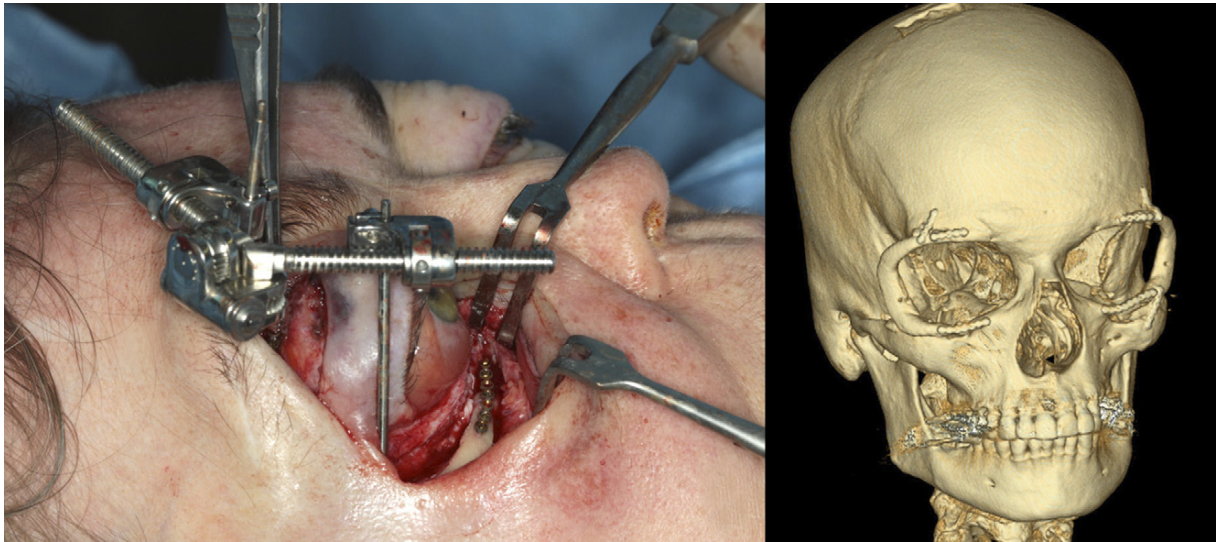


**FIGURE 4.** *Left*, Microplate osteosynthesis during fixation of the bone segments. *Right*, Postoperative CT scan showing the newly positioned lateral orbital rim and resected bone of the lateral orbital wall. (The parietal bone defect seen was created during earlier surgery for bone grafting purposes.)

Hierl et al. Positioning of Bone Segments. *J Oral Maxillofac Surg* 2013.

**Results**

Postoperative CT showed the orbital anatomy according to the virtual treatment plan (Figs 4 and 5). Figure 6 shows a comparison of the preoperative situation and the situation at 3 months after surgery.

**Discussion**

Introducing an external miniature distractor is a possible strategy to solve the problem of stable bone fragment positioning while allowing full 3D incremental movements during navigated surgery. The rigid system holds the fragments in place during osteosynthesis while permitting slight movements (eg, adaptation of fragments' ends during plate fixation).



**FIGURE 5.** Overlay of postsurgical CT scan and virtual surgery plan. Because the lateral aspects of the orbital rims have been removed, the planned and real rims have different dimensions.

Hierl et al. Positioning of Bone Segments. *J Oral Maxillofac Surg* 2013.

Distractor fixation is easily and rapidly performed by drilling 2 holes (1 for anchorage and 1 in the appropriate free segment). The only noteworthy step is to align both pins in a close-to-parallel way before distractor placement. Because small fragments are handled, large automated systems for fragment reduction seem inappropriate in the midface region.<sup>12</sup> Using the distractor as a flexible “third hand” improves intraoperative bone handling in navigated craniomaxillofacial surgery, can save operation time, and may enhance outcome quality.

The accuracy of the described method will depend on the quality of the navigation system, the slice thickness of the CT data, and the individual registration error. On average, this should lie below 2 mm and in most instances below 1.5 mm.<sup>13,14</sup> In comparison, the dimensional error of rapid prototyping models depends on the method used and, for example, is stated as 2.6% in cases of selective laser sintering.<sup>15</sup> Regarding orbital dimensions, this would imply errors at about 0.7 mm and could lead to a higher precision using surgical templates or prebent plates. Whether this theoretic difference in accuracy would be clinically noteworthy has not yet been evaluated. Comparing time, effort and costs of using rapid prototyping models, templates, or distractors is difficult because they depend on each institution’s facilities. If no rapid prototyping machine is at hand, a model of the orbits will cost, in our region, between \$200 and \$650 depending on the rapid prototyping method and the required data (ie, who will perform the segmentation and data export from DICOM [Digital Imaging and Communications in Medicine] to STL [Standard Tri-





**FIGURE 6.** Preoperative (*left*) and postoperative (*right*) optical scans to show the esthetic changes after decompression and lateral rim advancement.

*Hierl et al. Positioning of Bone Segments. J Oral Maxillofac Surg 2013.*

gulation Language] and whether the needed software exists at the institution). In this respect it is noteworthy to add that rapid prototyping models (eg, templates) that are used for “active” treatment planning and are used during surgery would fall under European Community Medical Product regulations and would need *Conformité Européenne* (CE) approval. (CE approval is a certification that must be legally affixed to products falling under the European New Approach Directives. It indicates that the product meets the legal requirements of the applicable European Union directive, in this case, the Medical Devices Directive.) Thus cheaper models from a purely industrial reverse engineering store could not officially be used in countries under European Community law. The same applies to surgical templates with costs in an identical range.

When one compares the introduced method with freehand positioning or the use of rapid prototyping auxiliary means, all methods have their pros and cons. Using templates and prebent plates will reduce operating time and may render intraoperative navigation unnecessary in some instances. On the other hand, time and effort are needed preoperatively. In this example navigated surgery would be needed even if prebent plates or templates would be at hand to define bony resection margins during orbital decompression. If, however, navigated surgery is intended and a miniature distractor is available, this could add precision in those cases where the desired postoperative segment position is difficult to estimate and handle. According to our point of view, the use of a distractor is useful if single

segments are to be repositioned, if a distractor is at hand, and if the surgeon is acquainted with its use. Furthermore, it can help in unexpected situations when holding and making incremental adjustments are difficult. In cases of multiple fragments or repositioning vectors beyond the scope of a distractor, rapid prototyping procedures would be a valuable alternative.

## References

1. Olszewski R, Tanesy O, Cosnard G, et al: Reproducibility of osseous landmarks used for computed tomography based three-dimensional cephalometric analyses. *J Craniomaxillofac Surg* 38:214, 2010
2. Schmelzeisen R, Gellrich NC, Schoen R, et al: Navigation-aided reconstruction of medial orbital wall and floor contour in cranio-maxillofacial reconstruction. *Injury* 35:955, 2004
3. Kokemueller H, Tavassol F, Ruecker M, et al: Complex midfacial reconstruction: A combined technique of computer-assisted surgery and microvascular tissue transfer. *J Oral Maxillofac Surg* 66:2398, 2008
4. Kozakiewicz M, Elgalal M, Loba P, et al: Clinical application of 3D pre-bent titanium implants for orbital floor fractures. *J Craniomaxillofac Surg* 37:229e, 2009
5. Abou-Elfetouh A, Barakat A, Abdel-Ghany K: Computer-guided rapid-prototyped templates for segmental mandibular osteotomies: A preliminary report. *Int J Med Robotics Comp Assist Surg* 7:187, 2011
6. Olszewski R, Tranduy K, Reychler H: Innovative procedure for computer-assisted genioplasty: Three-dimensional cephalometry, rapid-prototyping model and surgical splint. *Int J Oral Maxillofac Surg* 39:721, 2010
7. Xia JJ, Shevchenko L, Gateno J, et al: Outcome study of computer-aided surgical simulation in the treatment of patients with craniomaxillofacial deformities. *J Oral Maxillofac Surg* 69:2014, 2011
8. González-García R, Sastre-Pérez J, Rodríguez-Campo FJ, et al: C-modified osteotomy for bilateral advancement of the orbital

- rim in Graves orbitopathy: A technical note. *Int J Oral Maxillofac Surg* 37:853, 2008
9. Mourits MP, Bijl H, Altea MA, et al: Outcome of orbital decompression for disfiguring proptosis in patients with Graves' orbitopathy using various surgical procedures. *Br J Ophthalmol* 93:1518, 2009
  10. Millar ML, Maloof AJ: The application of stereotactic navigation surgery to orbital decompression for thyroid-associated orbitopathy. *Eye (Lond)* 23:1565, 2009
  11. Hierl T, Kruber D, Borasch H, et al: Neu entwickelte 3D-Analysesoftware fuer Zahnheilkunde und MKG-Chirurgie. *Digit Dent News* 5:6, 2011
  12. Oszwald M, Westphal R, Bredow J, et al: 3D visualized robot assisted reduction of femoral shaft fractures: Evaluation in exposed cadaveric bones. *Technol Health Care* 17:337, 2009
  13. Lübberts HT, Messmer P, Grätz KW, et al: Misjudgments at the mandibular angle: Freehand versus computer-assisted screw positioning. *J Craniofac Surg* 21:1012, 2010
  14. Chen X, Lin Y, Wang C, et al: A surgical navigation system for oral and maxillofacial surgery and its application in the treatment of old zygomatic fractures. *Int J Med Robotics Comput Assist Surg* 7:42, 2011
  15. Nascimento D, Gerhardt de Oliveira M, Meurer E, et al: Dimensional error in selective laser sintering and 3D-printing of models for craniomaxillary anatomy reconstruction. *J Craniofac Surg* 36:443e, 2008

## 2.3 Morphologic comparison of preformed orbital meshes

In der Mund-, Kiefer- und Gesichtschirurgie werden Orbitawandfrakturen oft mittels anatomisch vorgeformter Implantate [Abbildung 2.5] versorgt um die „eingebrochenen“ Stellen wieder auszugleichen.

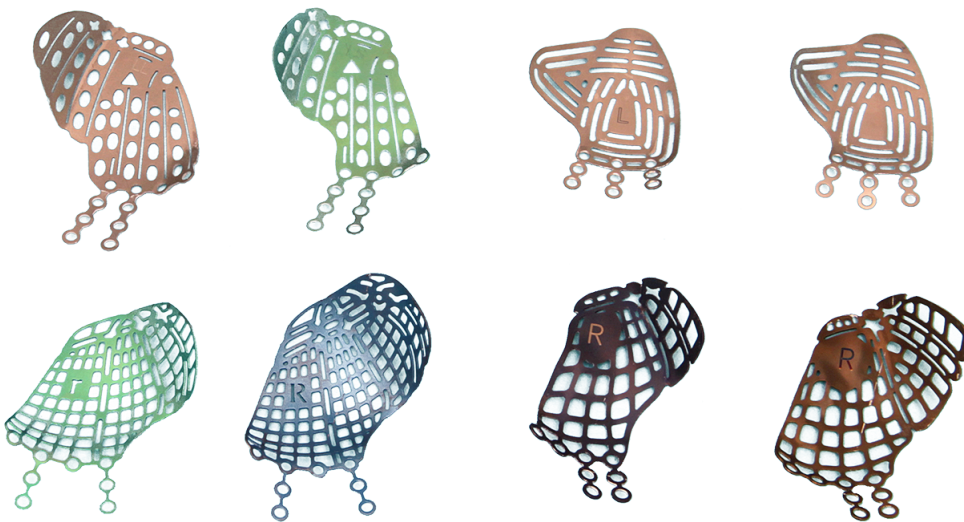


Abbildung 2.5: verschiedene Implantate der Hersteller Stryker, Synthes, Martin und Biomet

Diese anatomisch präformierten Implantate werden von verschiedenen Herstellern angeboten und als anatomisch regelrecht bezeichnet. Da sie sich jedoch schon visuell deutlich unterscheiden, wurden in dieser Studie mittels Unterstützung durch FAT ihre Geometrien sowohl untereinander wie auch mit einer eigenen statistisch-anatomischen Orbitageometrie verglichen. Diese Aussagen zur den Geometrien dieser kommerziellen Implantate und ihre Bedeutung für die chirurgische Praxis war bisher in dieser Form in einer einzigen Softwareumgebung so nicht möglich.

Die Implantate wurden in FAT per Registrieralgorithmus überlagert und anschließend deren Übereinstimmung wie in der Veröffentlichung dargestellt farbcodiert wiedergegeben. In Abbildung 2.6 wird dieser beschriebene Ablauf skizziert.

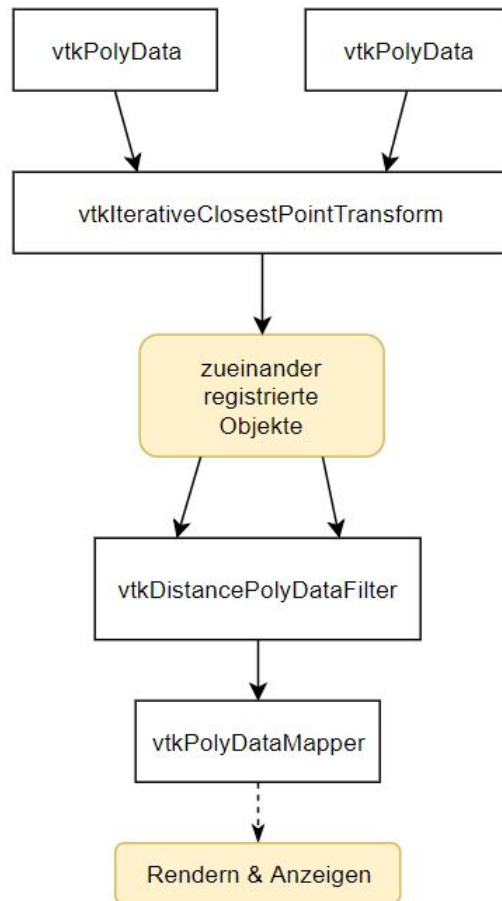


Abbildung 2.6: Workflow zum Registrierablauf in FAT

# Morphologic Comparison of Preformed Orbital Meshes

Heike Huempfer-Hierl, MD, DDS, \*Hans-Martin Doerfler, MEng, †  
Daniel Kruber, DiplIng, ‡ and Thomas Hierl, MD, DDS, PhD§

**Purpose:** Preformed orbital titanium meshes have been introduced to improve outcomes in the treatment of orbital wall fractures. This study evaluated the geometry of different commercially available orbital meshes and compared them with an average human orbit.

**Materials and Methods:** Seven commercially available preformed orbital meshes were scanned using an optical scanner. For comparison, an average orbit was generated from 113 computed tomographic scans of unaffected orbits. Meshes and the average orbit were compared by registration and the calculation of congruence.

**Results:** All meshes showed a high similarity within a  $\pm 1.5$ -mm deviation corridor. Major differences were seen in the slope between the orbital floor and the medial wall and in the upturning toward the lateral orbital rim.

**Conclusion:** Preformed orbital meshes conform highly to an average orbit, but differ in size and geometry. Using special software, the best fitting mesh could be chosen preoperatively to improve surgical outcome if its geometry were published.

© 2015 American Association of Oral and Maxillofacial Surgeons  
*J Oral Maxillofac Surg* 73:1119-1123, 2015

Fractures of the orbital walls are routinely encountered in oral and maxillofacial surgery. To reconstruct the proper geometry of the fractured walls, several methods have been introduced. Concerning titanium as a reconstruction material, plain titanium meshes,<sup>1</sup> computer-assisted designed and manufactured implants,<sup>2,3</sup> meshes adapted to rapid prototyping models,<sup>4,5</sup> and individual computer-based preformed meshes<sup>6</sup> have been used. A different approach to improve treatment is the use of anatomically preformed meshes,<sup>7,8</sup> which are currently available from major companies and should decrease bending efforts and improve fit. However, no in-depth information on how these meshes have been designed is available. Therefore, this study compared 7 preformed

orbital titanium meshes with an average orbit and investigated differences and congruency.

## Materials and Methods

Six left-sided preformed titanium meshes and 1 bending template were purchased from the manufacturers. Only the left side was chosen because the left and right sides are mirror-inverted. These consisted of a small mesh and a large mesh from DePuy Synthes (DePuy Synthes, Tuttlingen, Germany), a small mesh and a large mesh from Stryker (Stryker GmbH, Freiburg, Germany), a mesh from Biomet (large left implant; Biomet, Jacksonville, FL), and a preformed mesh from KLS Martin (KLS Martin, Tuttlingen, Germany).

\*Senior Consultant, Department of Oral and Maxillofacial Plastic Surgery, Leipzig University, Leipzig, Germany.

†Engineer, Department of Oral and Maxillofacial Plastic Surgery, Leipzig University, Leipzig; University of Applied Sciences, Leipzig, Germany.

‡Computer Scientist, Department of Oral and Maxillofacial Plastic Surgery, Leipzig University, Leipzig, Germany.

§Senior Consultant, Department of Oral and Maxillofacial Plastic Surgery, Leipzig University, Leipzig, Germany.

Development of the 3-dimensional analysis software was funded in part by the German Federal Ministry of Economics and Technology (ZIM KF 2036708SS0). Generation of the average orbit was

funded by the German Federal Ministry of Economics and Technology (ZIM KF 2036713AK2).

Address correspondence and reprint requests to Dr Huempfer-Hierl: Department of Oral and Maxillofacial Plastic Surgery, Leipzig University, Liebigstrasse 12, 04103 Leipzig, Germany; e-mail: [Heike.Huempfer-Hierl@medizin.uni-leipzig.de](mailto:Heike.Huempfer-Hierl@medizin.uni-leipzig.de)

Received September 3 2014

Accepted January 26 2015

© 2015 American Association of Oral and Maxillofacial Surgeons

0278-2391/15/00103-2

<http://dx.doi.org/10.1016/j.joms.2015.01.031>



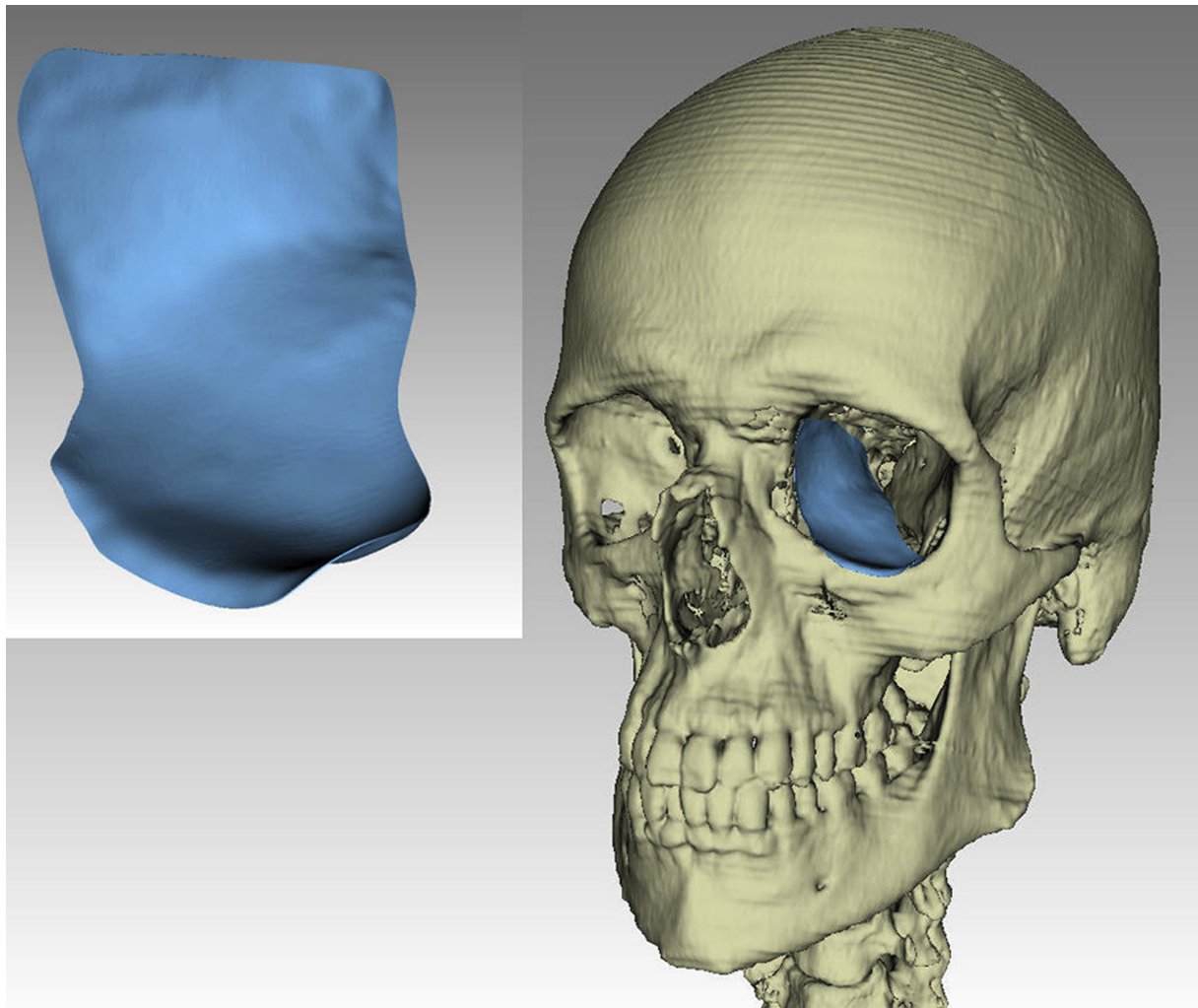


**FIGURE 1.** Average model created from 113 computed tomographic datasets consisting of the medial wall and the orbital floor. *Huempfer-Hierl et al. Morphologic Comparison of Orbital Meshes. J Oral Maxillofac Surg 2015.*

**Table 1. RESULTS OF METRIC ANALYSIS: SIZE AND CONGRUENCY REGARDING THE DISTANCE CORRIDORS OF COMMERCIAL MESHES TO THE AVERAGE MODEL**

Mesh Type	Size (cm <sup>2</sup> )	Distance Corridor of Mesh to Model			Maximum Deviation (mm)
		-0.5 to +0.5 mm (% Area)	-1 to +1 mm (% Area)	-1.5 to +1.5 mm (% Area)	
Stryker small	7.9	77.7	98.0	100	1.24
Stryker large	9.6	76.8	98.7	100	1.15
DePuy Synthes large	9.2	72.7	96.5	99.5	1.69
DePuy Synthes small	7.4	65.4	94.2	99.1	1.78
Biomet	8.7	62.1	93.7	100	1.66
KLS Martin pre-bent	5.9	67.1	95.8	100	1.32
KLS Martin template		92.6	99.0	100	1.17
KLS Martin vs KLS Martin template		65.2	91.5	100	1.45

*Huempfer-Hierl et al. Morphologic Comparison of Orbital Meshes. J Oral Maxillofac Surg 2015.*

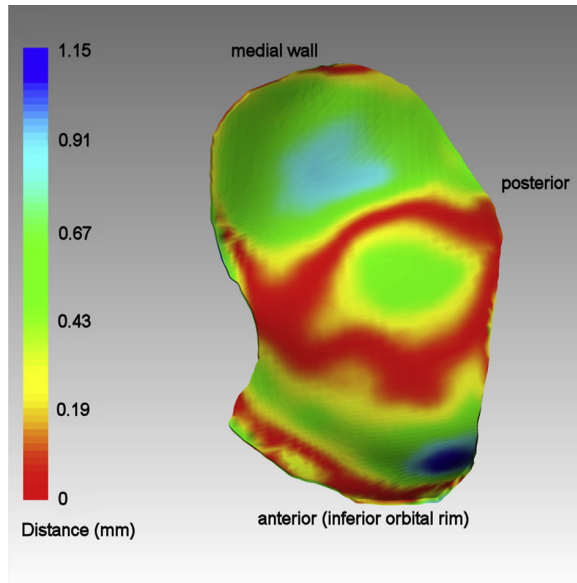


**FIGURE 2.** Three-dimensional congruency of the large Stryker mesh with the average model. The color-coded legend (*left*) indicates the deviation.

*Huempfer-Hierl et al. Morphologic Comparison of Orbital Mesbes. J Oral Maxillofac Surg 2015.*

Furthermore, an unbent KLS Martin mesh was adapted to the company’s bending template. The large and small Stryker meshes differ only in size (medial and posterior extensions), whereas the 2 DePuy Synthes meshes present different shapes. To acquire the geometry, all meshes were scanned using a high-resolution industrial

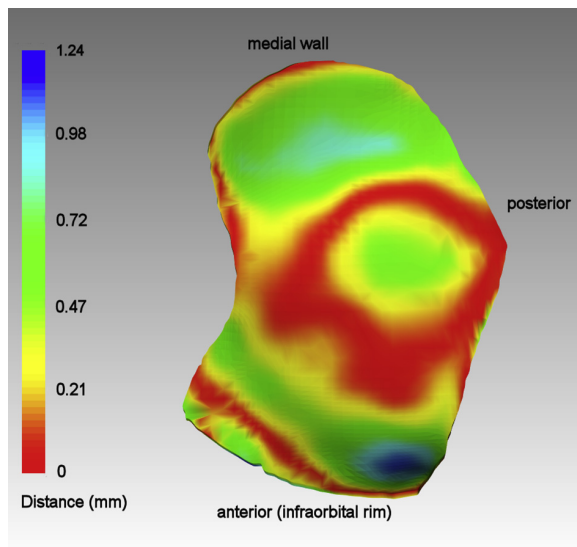


**FIGURE 3.** Three-dimensional congruency of the small Stryker mesh with the average model. Owing to the smaller size, the registration algorithm shows different results compared with the larger Stryker mesh. The color-coded legend (*left*) indicates the deviation.

*Huempfer-Hierl et al. Morphologic Comparison of Orbital Mesbes. J Oral Maxillofac Surg 2015.*

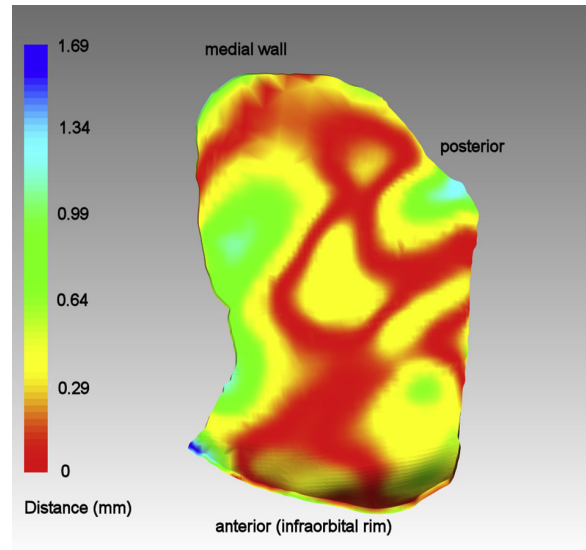


**FIGURE 4.** Shape deviation of the large DePuy Synthes mesh. The color-coded legend (*left*) indicates the deviation.

*Huempfer-Hierl et al. Morphologic Comparison of Orbital Mesbes. J Oral Maxillofac Surg 2015.*

scanner (0.015-mm resolution; ATOS IIe revised 01, GOM, Braunschweig, Germany). Because a comparison of meshes consisting of holes and struts was not suitable, all meshes were covered with ultrathin flexible tape before scanning. A high-resolution file in stereolithographic (STL) format was created for each mesh. All STL files were compared to an average left orbit model, which was created from 113 computer

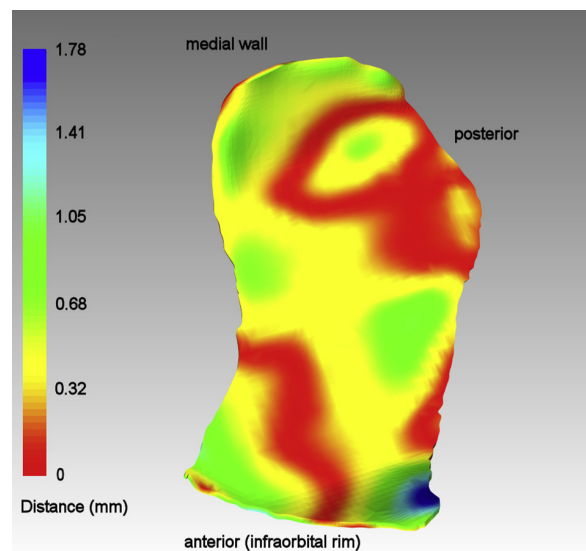


**FIGURE 5.** Comparison of the small DePuy Synthes mesh with the average model. The color-coded legend (*left*) indicates the deviation.

*Huempfer-Hierl et al. Morphologic Comparison of Orbital Mesbes. J Oral Maxillofac Surg 2015.*

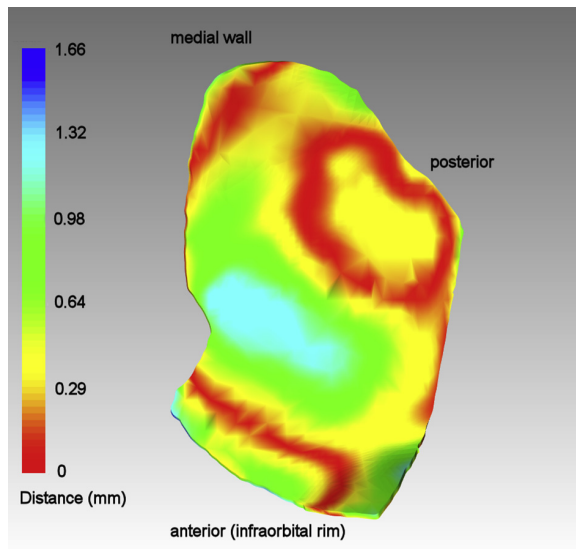


**FIGURE 6.** Biomet titanium mesh and average orbital model. The color-coded legend (*left*) indicates the deviation.

*Huempfer-Hierl et al. Morphologic Comparison of Orbital Meshes. J Oral Maxillofac Surg 2015.*

tomographic (CT) scans. Only 1 side was chosen because previous investigations have shown high congruency of the 2 sides.<sup>9</sup> The datasets derived from unaffected orbits were obtained from Caucasian adults (32% female, 68% male). CT data were segmented using the Brainlab CMF segmentation tool (Brainlab AG, Feldkirchen, Germany). For minor discrepancies be-

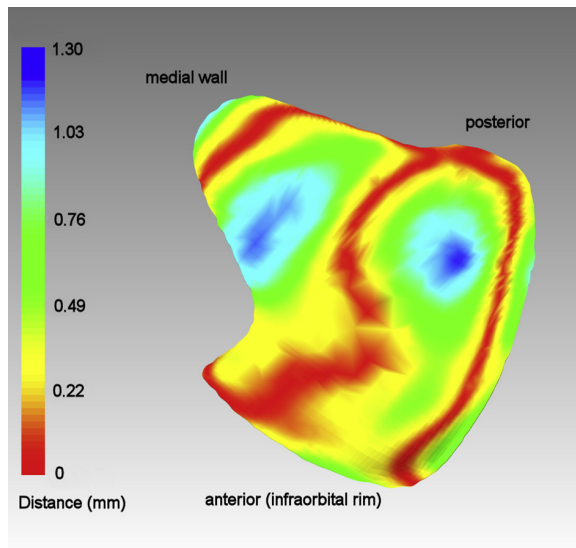


**FIGURE 7.** Preformed KLS Martin mesh registered and analyzed. The medial wing is angulated inferiorly. The most marked difference is in the central orbital floor of all compared meshes. The color-coded legend (*left*) indicates the deviation.

*Huempfer-Hierl et al. Morphologic Comparison of Orbital Meshes. J Oral Maxillofac Surg 2015.*

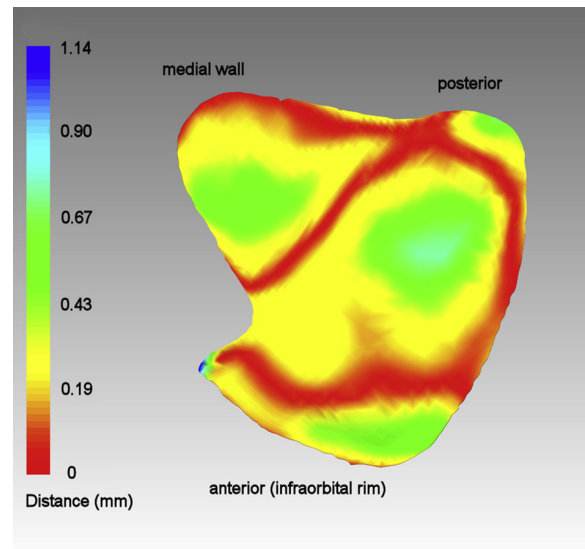


**FIGURE 8.** Result of comparison with template-based KLS Martin plate. The color-coded legend (*left*) indicates the deviation.

*Huempfer-Hierl et al. Morphologic Comparison of Orbital Meshes. J Oral Maxillofac Surg 2015.*

tween the model and the actual anatomy, the model was manually adjusted to the appropriate geometry. The orbits were exported into STL format and trimmed by removing the lateral wall and ceiling. After preregistration using anatomic landmarks, an average geometry of the orbital floor and medial wall was created with ATOS Professional 7.5 SR2 software (GOM; Fig 1). The final model extended from the optic foramen to the nasolacrimal fossa and from the superior medial wall to the inferior fissure.

To compare congruency of the meshes with the average model, they were registered using the iterative closest point algorithm. This was performed using FAT software,<sup>10</sup> which is a modular VTK-based framework. VTK is open-source software and provides a huge and powerful range of libraries for biomedical 3-dimensional display and analysis (VTK, Kitware, Clifton Park, NY). After registration, congruency was visualized by calculating the distances between the model and the mesh. For comparison, 3 corridors of congruency were assigned ( $\pm 0.5$  mm, corridor of 1 mm;  $\pm 1$  mm, corridor of 2 mm;  $\pm 1.5$  mm, corridor of 3 mm) and the percentage of the corresponding area was calculated. Besides the pre-bent and template-adjusted KLS Martin meshes, no metric comparison between the different meshes was performed because these differ greatly in size (Table 1) and do not fully overlap. Therefore, all nonoverlapping regions would have to be discarded, thus further decreasing mesh size.

This study followed the Declaration of Helsinki on medical protocol and ethics. The regional ethical review board declared no need for approval.

## Results

Table 1 presents the congruency of the different meshes with the average orbit. Figures 2 to 8 present the shape differences by a color-coded distance map.

Within the  $\pm 1.5$ -mm corridor, all plates presented almost 100% concordance with the average orbit. An interesting finding was that, in the  $\pm 0.5$ -mm range, the pre-bent KLS Martin mesh scored worse than the template-bent KLS Martin mesh, which scored best. As seen in Figures 2 to 8, major geometric discrepancies were found in the slope of the medial wall (KLS Martin and Biomet) and the upturning toward the lateral rim of the inferior border (Stryker and DePuy Synthes).

## Discussion

Although the proportion of the different types of hardware used in orbital traumatology is unknown, it can be judged that titanium meshes constitute a large part. Pre-bent meshes have been introduced to ease intraoperative adaptation and improve fit.<sup>7,8</sup> Although many major companies have introduced anatomically formed meshes, none has declared how the geometry was obtained. Stryker claims in their product flyer that their geometry is based on 300 orbital CT scans of subjects largely (92%) of European descent. Some information on how the DePuy Synthes meshes were generated has been published,<sup>9,11</sup> but no detailed information on the calculation, number, and origin of their data has been stated. Kamer et al<sup>9</sup> stated that they used 70 CT datasets within their study, but whether these results served as a basis for the DePuy Synthes mesh is unknown to the investigators. Also, no information regarding the Biomet and KLS Martin meshes with respect to the bending template could be found. Therefore, the authors were interested in whether these different meshes would be similar and whether they conformed to an average orbit. The results show that all geometries resemble the orbit more or less and none of the commercially available meshes are identical one another. Within a 3-mm corridor, they are fully congruent with the authors' model orbit. Analysis showed that 2 regions presented the largest differences: the upturning along the inferior border toward the lateral wall (Stryker and DePuy Synthes) and the angulation of the medial wall (KLS Martin and Biomet anteriorly). The maximum deviation from the authors' model ranged from 1.76 to 1.15 mm. Interestingly, the surface area differed greatly among manufacturers, the largest being almost twice as large as the smallest. From a clinical viewpoint, all meshes could be used in orbital traumatology depending on the individual defect size and location and the geometry of the individual orbit. It would be a great benefit if the

manufacturers would provide users with the STL files of their products. These could be imported into surgical planning software to decide preoperatively which would fit best and where to perform bends before first insertion. If needed, this also would be a great help during navigated surgery.<sup>12,13</sup> When comparing the slope of the medial wall, the Stryker and KLS Martin templates scored best. Perhaps the most striking finding was the difference between the pre-bent KLS Martin mesh and their bending template, which showed no congruency. In a clinical situation, the congruency of the mesh's border to the surrounding bone is crucial. Therefore, further investigations using CT datasets of trauma patients will be needed to elucidate this point.

Commercially available pre-bent orbital meshes show a high grade of congruency but differ in size, angulation of the medial wall, and curvature along the inferior orbital rim. All seem to be clinically useful. For the best results, the STL files should be made available by the manufacturers for preoperative virtual try-outs and—if applicable—*intraoperative navigation*.

## References

- Gabrielli MF, Monnazzi MS, Passeri LA, et al: Orbital wall reconstruction with titanium mesh: Retrospective study of 24 patients. *Craniomaxillofac Trauma Reconstr* 4:151, 2011
- Klein M, Glatzer C: Individual CAD/CAM fabricated glass-bioceramic implants in reconstructive surgery of the bony orbital floor. *Plast Reconstr Surg* 117:565, 2006
- Kozakiewicz M, Elgalal M, Walkowiak B, et al: Technical concept of patient-specific, ultrahigh molecular weight polyethylene orbital wall implant. *J Craniomaxillofac Surg* 41:282, 2013
- Mustafa SF, Evans PL, Bocca A, et al: Customized titanium reconstruction of post-traumatic orbital wall defects: A review of 22 cases. *Int J Oral Maxillofac Surg* 40:1357, 2011
- Kozakiewicz M, Elgalal M, Piotr L, et al: Treatment with individual orbital wall implants in humans—1 Year ophthalmologic evaluation. *J Craniomaxillofac Surg* 39:30, 2011
- Metzger MC, Schoen R, Zizelmann C, et al: Semiautomatic procedure for individual performing of titanium meshes for orbital fractures. *Plast Reconstr Surg* 119:969, 2007
- Scolozzi P, Momjian A, Heuberger J, et al: Accuracy and predictability in use of Ao three-dimensional preformed titanium mesh plates for posttraumatic orbital reconstruction: A pilot study. *J Craniofac Surg* 20:1108, 2009
- Gordon CR, Sursala SM, Yaremchuk MJ: Quantitative assessment of medial orbit fracture repair using computer-designed anatomical plates. *Plast Reconstr Surg* 130:698e, 2012
- Kamer L, Noser H, Schramm A, et al: Orbital form analysis: Problems with design and positioning of precontoured orbital implants. A serial study using post-processed clinical CT data in unaffected orbits. *Int J Oral Maxillofac Surg* 39:666, 2010
- Hierl T, Kruber D, Borasch H, et al: [A newly developed 3D-analysis software for dentistry and oral and maxillofacial surgery]. *Digit Dent News* 5, June 6, 2011 (in German)
- Kamer L, Noser H, Lamecker H, et al: Three-dimensional statistical shape analysis—A useful tool for developing a new type of orbital implant? *AO Dev News* 2:20, 2006
- Schmelzeisen R, Gellrich NC, Schoen R, et al: Navigated-aided reconstruction of medial orbital wall and floor contour in cranio-maxillofacial reconstruction. *Injury* 35:955, 2004
- Markiewicz MR, Dierks EJ, Potter BE, et al: Reliability of *intraoperative navigation* restoring normal orbital dimensions. *J Oral Maxillofac Surg* 69:2833, 2011



## 2.4 Template-Based Orbital Wall Fracture Treatment Using Statistical Shape Analysis

In der folgenden Veröffentlichung wurde die medizinische Fragestellung betrachtet, ob eine anatomisch regelrechte und dabei kostengünstige Versorgung von Orbitawandfrakturen möglich ist, ohne sich dabei auf ein bestimmtes Implantatmaterial festlegen zu müssen.

Die Lösung war die Entwicklung eines statistisch-anatomischen Modells der Orbitawände als Grundlage eines Stempels zum Verformen verschiedener planer Implantatmaterialien. Daraufhin wurde ein statistisch-anatomisches Modell der Orbitawände entwickelt, das als Grundlage eines Stempels zum Verformen verschiedener planer Implantatmaterialien dient.

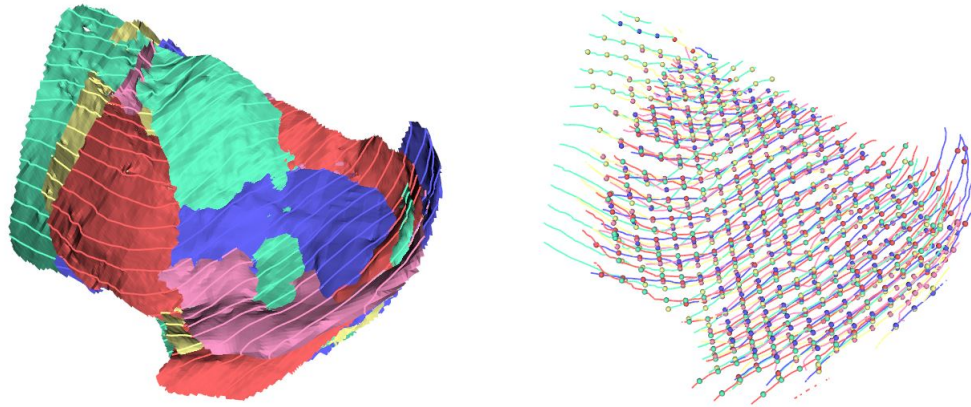
Bezüglich der Lösung bestanden verschiedene Probleme die zum Einen mit kommerziell erhältlichen Softwarepaketen nur schwer lösbar waren, zum Anderen einen mehrfachen Im- und Export in verschiedene Programme mit jeweils einem Wechsel des Datenformats und der räumlichen Koordinaten erfordert hätten.

In FAT wurden Lösungen zur Erstellung eines statistisch-anatomischen Modells basierend auf CT-Datensätzen, zur Bemaßung und zum Beschneiden komplexer anatomischer Geometrien mittels anatomischer Landmarken implementiert.

Eine der evaluierten Optionen aus der folgenden Publikation war, die Zuhilfenahme des integrierten Moduls „Digitizer“. Damit konnten aus den Konturen der jeweiligen segmentierten Dateien Punktwolken erzeugt werden, die die Erstellung eines statistisch-anatomischen Modells ermöglichten.

In Abbildung 2.7 wird dies beispielhaft an fünf unterschiedlich eingefärbten Datensätzen verdeutlicht.

Aufgrund der hohen Komplexität wurde diese Variante jedoch schlussendlich durch die Evaluierung einer weiteren Möglichkeit ersetzt.



(a) Konturen mit einem definierten Abstand auf den 5 farbigen Objekten (b) farblich differenzierte Punktwolken je Datensatz auf zuvor erzeugten Konturen

Abbildung 2.7: Darstellung der Funktionsweise von „Digitizer“ an 5 exemplarischen Datensätzen

Der grobe Ablauf zur Konturerstellung mittels Digitizer wird als Diagramm in Abbildung 2.8 angezeigt.

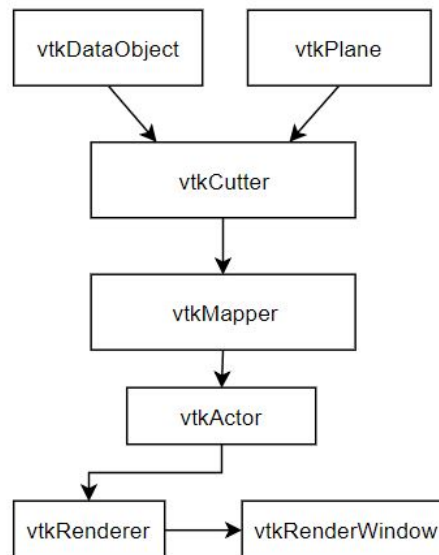


Abbildung 2.8: Workflow zur Darstellung der Konturen

Für die Erzeugung der Schnittpunkte aus Abbildung 2.8 werden die zuvor gewonnenen Konturen zu Grunde gelegt und das Ablaufdiagramm etwas modifiziert (Abbildung 2.9). Hier werden nun die `vtkPolyData`-Informationen von `vtkCutter` verwendet um die Schnittpunktkoordinaten zu schaffen, die anschließend per `vtkSphereSource` als ein entsprechendes Kugelobjekt an den `vtkMapper` übergeben und dann im `RenderWindow` angezeigt werden. Aus der Vielzahl an Koordinatendaten kann so die Grundlage für die statistische Analyse zur Bestimmung der durchschnittlichen Form gewonnen werden. In der nachfolgenden Veröffentlichung wurde diese Herangehensweise allerdings nicht für das Endergebnis verwendet.

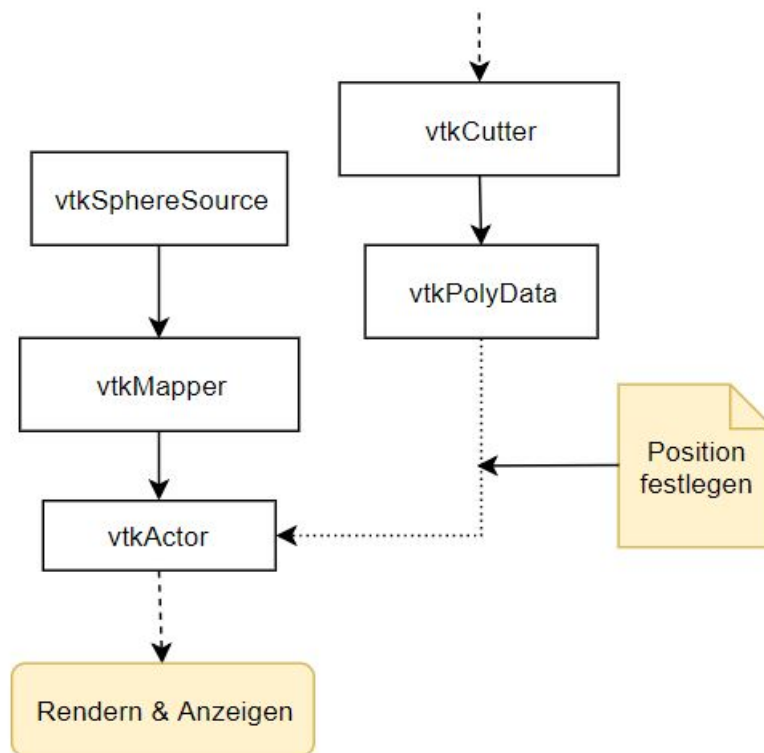


Abbildung 2.9: Workflow zur Darstellung der Schnittpunkte



# Template-Based Orbital Wall Fracture Treatment Using Statistical Shape Analysis



Hans-Martin Doerfler, MEng, \*Heike Huempfer-Hierl, MD, DDS, PhD, †  
Daniel Kruber, Dipl-Inf, ‡Peter Schulze, PhD-Eng, § and Thomas Hierl, MD, DDS, PhD||

**Purpose:** Aim of this study was to investigate whether a mold generated from a statistical shape model of the orbit could be generated to provide a cost-efficient means for the treatment of orbital fractures.

**Materials and Methods:** A statistical shape model was created from 131 computed tomographic (CT) scans of unaffected adult middle European human orbits. To generate the model, CT scans were segmented in Brainlab software, preregistered using anatomic landmarks, trimmed to an identical size, and definitely registered. Then, the model was created using the global master algorithm. Based on this model, a mold consisting of a male part and a female part was constructed and printed using a rapid prototyping technique.

**Results:** A statistical shape model of the human orbit was generated from 125 CT scans. Six scans (4.5%) presented major anatomic deviations and were discarded. A solid mold based on this model was printed. Using this mold, flat titanium mesh could be successfully deformed to serve as an orbital implant.

**Conclusion:** A mold based on the statistical orbital shape could serve as a cost-effective means for the treatment of orbital fractures. It allows the anatomic preformation of titanium or resorbable implant material for orbital reconstruction. Because these materials could be cut from larger sheets, the use of a mold would be a cost-effective treatment alternative.

© 2017 American Association of Oral and Maxillofacial Surgeons  
*J Oral Maxillofac Surg* 75:1475.e1-1475.e8, 2017

The human orbit is anatomically complex and demands precise reconstruction of fractures to preserve esthetics and function. In recent decades, a multitude of materials and procedures has been suggested.<sup>1,2</sup> Concomitant with the technical progress in image acquisition and implant manufacturing has been a trend toward the optimal fit of orbital implants.

Materials used range from autologous bone grafts,<sup>3</sup> intraoperatively bent titanium meshes,<sup>4</sup> preformed titanium meshes,<sup>5,6</sup> to patient-specific implants (PSIs) generated from bioceramics, polyethylene, or titanium.<sup>7-10</sup> As an alternative to PSIs, alloplastic materials have been preoperatively modified using patient models created by rapid prototyping.<sup>11,12</sup>

\*Engineer, Department of Oral and Maxillofacial Plastic Surgery, Leipzig University and University of Applied Sciences (HTWK), Leipzig, Germany.

†Senior Consultant, Department of Oral and Maxillofacial Plastic Surgery, Leipzig University, Leipzig, Germany.

‡Computer Scientist, Department of Oral and Maxillofacial Plastic Surgery, Leipzig University, Leipzig, Germany.

§Professor, Faculty of Mechanical and Energy Engineering, University of Applied Sciences (HTWK), Leipzig, Germany.

||Senior Consultant, Department of Oral and Maxillofacial Plastic Surgery, Leipzig University, Leipzig, Germany.

This investigation was funded by the German Federal Ministry of Economics and Technology (ZIM KF 2036713AK2). The development of the 3-dimensional analysis software was funded I part by

the German Federal Ministry of Economics and Technology (ZIM KF2036708SS0).

Conflict of Interest Disclosures: None of the authors have a relevant financial relationship(s) with a commercial interest.

Address correspondence and reprint requests to Dr Hierl: Department of Oral and Maxillofacial Plastic Surgery, Leipzig University, Liebigstrasse 12, Leipzig 04103, Germany; e-mail: [Thomas.Hierl@medizin.uni-leipzig.de](mailto:Thomas.Hierl@medizin.uni-leipzig.de)

Received January 27 2017

Accepted March 27 2017

© 2017 American Association of Oral and Maxillofacial Surgeons

0278-2391/17/30366-X

<http://dx.doi.org/10.1016/j.joms.2017.03.048>

Furthermore, intraoperative navigation has been used to increase surgical precision irrespective of the chosen implant material.<sup>13,14</sup> The technical progress from flat and individually contoured titanium meshes to solid and intraoperatively barely adjustable PSIs also has caused a massive increase in costs for orbital implants. Pre-contoured titanium meshes are an intermediate state between flat sheet meshes and PSIs. In a previous study, the authors investigated the different shapes of commercially available pre-bent titanium meshes<sup>15</sup> and noticed major differences in their shape and conformance with a self-created statistical orbital model. Therefore, this study investigated whether a cost-saving but nevertheless anatomically correct method in the treatment of orbital floor fractures could be established. Such a method should be superior to conventional sheet titanium meshes and more flexible than existing pre-contoured meshes. In this study, a mold and plunger based on a model generated by statistical shape analysis was judged preferable. Thus, flexibility of the used material and the needed implant size would be combined with the closest anatomic fit compared with the gold standard of PSIs.

## Materials and Methods

Two steps were needed to create the mold and plunger: 1) the generation of a model based on statistical shape analysis and 2) the construction and fabrication of the device.

### CREATING A STATISTICAL SHAPE MODEL

A model of the full orbit with plunger-type male and female molds was impractical because it would have shown undercuts. Therefore, a model of the typical fracture sites, namely the inferior and medial walls, was chosen. The generation consisted of the following steps:

- Segmentation of bony orbits
- Removing surplus areas and placing anatomic landmarks for preregistration
- Preregistration using landmarks and definite registration of surfaces
- Generation of the statistical shape model
- Clinical analysis and final modification if necessary

One hundred forty computed tomographic (CT) scans of adult patients of local origin (ie, middle European ethnicity) with unaffected orbits were chosen for the model. All were segmented using the atlas-based automatic segmentation algorithm of iPlan software (Brainlab, Munich, Germany). Because previous studies have shown that the left and right sides do not show statistically relevant differences,<sup>16,17</sup> only 1 side was selected. If necessary, the generated files

were manually modified to the anatomically correct shape within Brainlab software. Manual correction included using the “paint” and “erase” tools for cleanup and the “wand tool” for major deviations. Next, all orbits were exported in stereolithographic (STL) file format. Nine scans were omitted because of quality problems in the exported STL file; thus, 131 orbits remained. These had been obtained from 38 women and 93 men 18 to 68 years old. Three anatomic landmarks were set to serve for the preregistration (anterior inferior orbital fissure, inferior optic foramen, and inferior lacrimal groove) and the orbits were coarsely trimmed as presented in Figure 1.

The resulting orbital shapes were preregistered in 3matic software (Materialise, Gilching, Germany). The next step was a fine trimming using 3matic software to create an almost identical size of all 131 orbital areas. Then, all orbits were registered in 3matic using N-points registration and global registration. Then, the statistical model was created. Three ways to do so were evaluated. The first way was Procrustes registration, the generation of semi-landmarks, decrease of semi-landmark energy by sliding movements, computation of new landmarks by principal component analysis, and creating the final model.<sup>18,19</sup> This would have necessitated the use of several software packages and different operating system platforms; thus, the entire algorithm was programmed using VTK (Visualization Toolkit, Kitware, Clifton Park, NY), which served as the second software strategy. The third way was using the best-fit and global master algorithms implemented in GOM Inspect 8 (Atos Professional 7.5SR2, GOM, Braunschweig, Germany).<sup>20,21</sup> Because the third method turned out to be the fastest and easiest, it was chosen.

### GENERATION OF THE PLUNGER AND EVALUATION OF THE RESULTING SHAPE

After the statistical shape model was generated, a male mold and a female mold had to be constructed using Catia 5 R2012 SP4 (Catia 5, Dassault Systèmes, Paris, France). To test the effectiveness of the mold, 2 flat titanium meshes were chosen randomly and deformed and the resulting shape was compared with the statistical shape model. The authors used the same approach as in their previous comparison of the statistical shape model with commercially available pre-bent meshes.<sup>15</sup> The meshes (Stryker, Freiburg, Germany; and DePuy Synthes, Zuchwil, Switzerland) were cut to the size of the template and deformed. Then, the meshes were coated with ultra-thin flexible tape, sprayed with matt white paint, and digitized using a high-resolution industrial scanner (0.015-mm resolution; ATOS IIe revised 01, GOM). The digitized meshes were compared with the

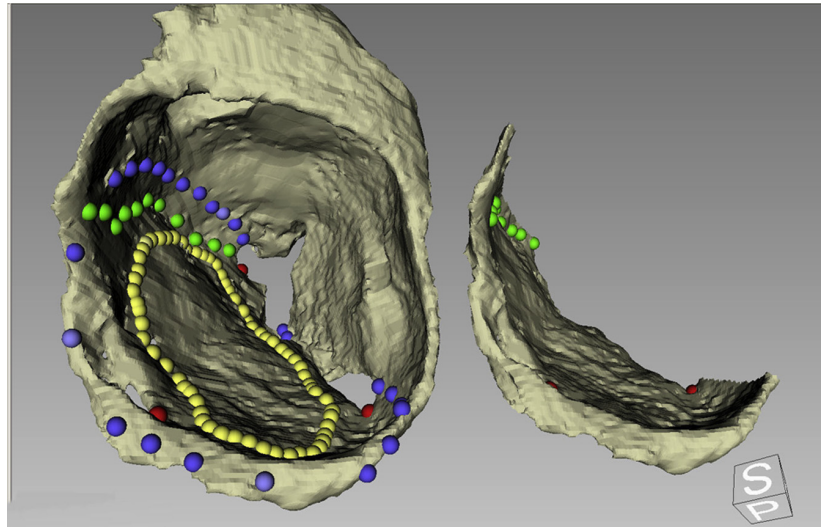


**FIGURE 1.** Process used to generate orbital areas for the statistical model. *Left*, The stereolithographic file of the orbit exported from Brainlab iPlan software. *Blue* areas delineate removed areas (outside removed). *Yellow* areas depict typical areas of orbital wall fractures. *Green* areas denote the transition from the medial wall to the roof. *Red* areas denote points used for preregistration. *Right*, Trimmed surface.

*Doerfler et al. Template for Orbital Wall Fracture Treatment. J Oral Maxillofac Surg 2017.*

statistical shape model after registration using the iterative closest-point algorithm and differences were displayed in a color-coded distance map.

This study was approved by the local ethics committee (Medical Faculty, Leipzig University, Leipzig, Germany). According to the ethics committee decision, no consent for participation was needed. This study was performed according to the Declaration of Helsinki.

## Results

Using the best-fit and global master algorithms, a statistical shape model of the medial and inferior orbital

walls was generated. Comparison of all 131 orbits with the resulting model for tolerance and deviation showed that 6 orbits (4.5%) were outliers in exhibiting major differences. [Figure 2](#) shows a case of typical outlier geometry, and [Figure 3](#) presents a good anatomic fit.

When the outliers were analyzed, no correlation with age, gender, or specific anatomic regions could be found. Therefore, a new model without these outliers was generated, consisting of 125 CT scans. [Figure 4](#) displays the final statistical shape model.

Analysis of the final model showed that the greatest variation in the test population existed in the periphery of the model. Thus, the transition from the medial

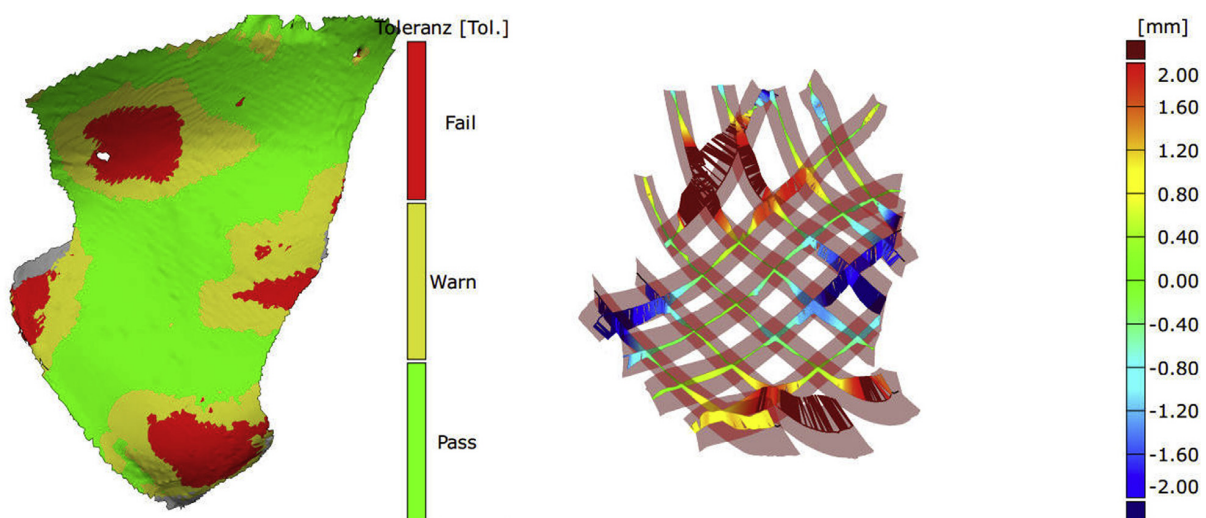


**FIGURE 2.** One example of the 6 outliers. Distinct shape differences in the lateral and posterior medial orbital floor and medial wall are visible.

*Doerfler et al. Template for Orbital Wall Fracture Treatment. J Oral Maxillofac Surg 2017.*

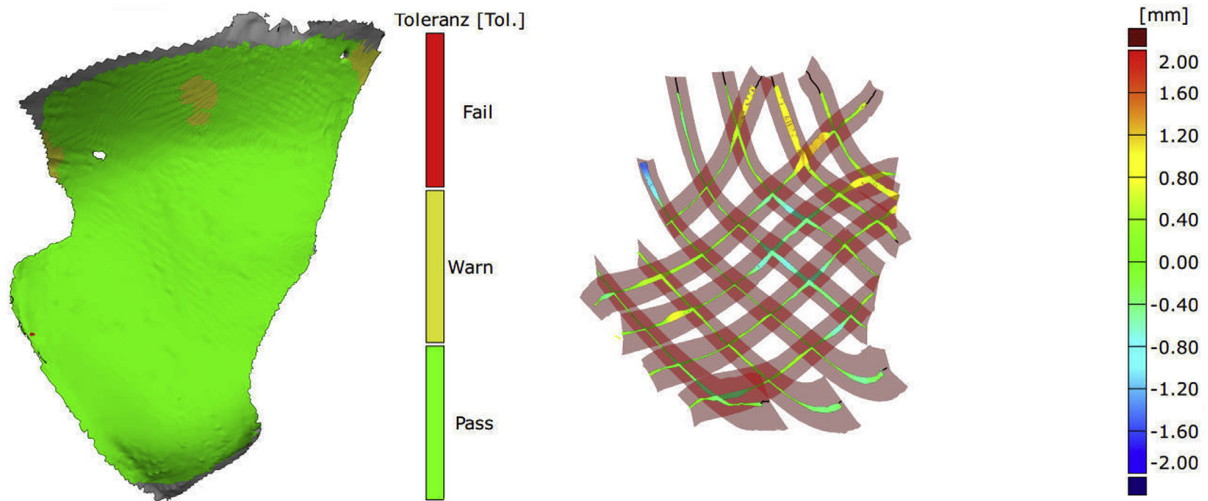


**FIGURE 3.** Example of a good fit, with anatomy consistent with the statistical shape model.

Doerfler et al. *Template for Orbital Wall Fracture Treatment. J Oral Maxillofac Surg* 2017.

to the superior wall (especially near the optic foramen), the transition from the inferior to the lateral wall, and the inferior orbital rim showed the greatest variation (Fig 5). However, the typical fracture sites presented good interpatient conformity.

After the statistical shape model was generated, a male mold and a female mold were constructed in Catia 5. The surface was arranged to prohibit undercuts, and guide bars were created on the left and right sides to guarantee a straight downward movement of

the plunger. Right and left molds were generated in solid ABS plastic with a rapid prototyping technique (FDM Titan, Stratasys Co, Rheinmünster, Germany) using a 0.2-mm nozzle for fine printing (Figs 6, 7).

As an alternative to the flat titanium meshes, resorbable or polyethylene-coated meshes could be inserted. Furthermore, orbital size meshes could be cut from larger rectangular mesh sheets, which are available in various strengths and mesh geometries from several companies. In the mold references could be integrated to help cut the desired size of the implant. The mold could be sterilized and thus the device could be used intraoperatively. Because it would have been impossible to evaluate all possible materials and sizes for conformity of the resulting shape with the mold, 2 meshes were chosen randomly for evaluation. The evaluation was performed by choosing conformity corridors, that is, stating the percentage of the area within a given deviation. In the corridor of  $\pm 0.2$ -mm deviation for the statistical shape model, 81% of the Stryker mesh was within these boundaries. Maximum deviation was 0.34 mm in the lateral anterior border (Fig 8). For the Synthes mesh, 71% of its area was within the  $\pm 0.2$ -mm deviation corridor. The maximum discrepancy was found in the anterior lateral region (0.6 mm).

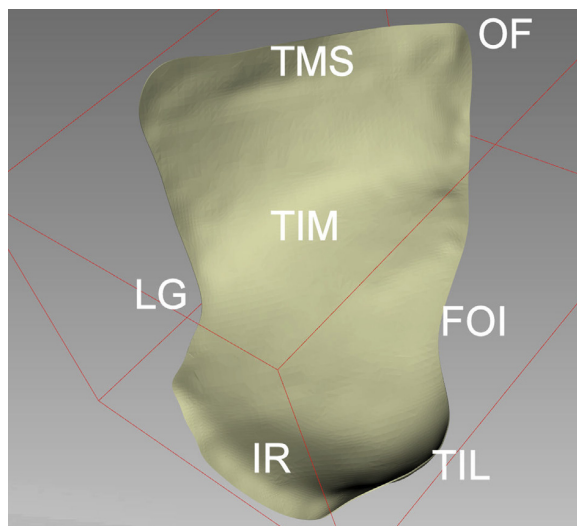


**FIGURE 4.** The final statistical shape model generated from 125 left orbital computed tomographic scans. FOI, fissura orbitalis inferior; IR, infraorbital rim; OF, optical foramen; TIL, transition from inferior to lateral wall; TIM, transition from inferior to medial wall; TMS, transition from medial to superior wall.

Doerfler et al. *Template for Orbital Wall Fracture Treatment. J Oral Maxillofac Surg* 2017.

## Discussion

For the creation of the statistical shape model, the specimen was compared with pre-existing models. To the authors' knowledge,<sup>15</sup> 3 companies offer 7 preformed orbital titanium meshes. Two companies offer large and small meshes that differ only in size and not in shape, whereas 1 company offers large and small implants with different shapes. For size of the patient group and the procedures chosen by



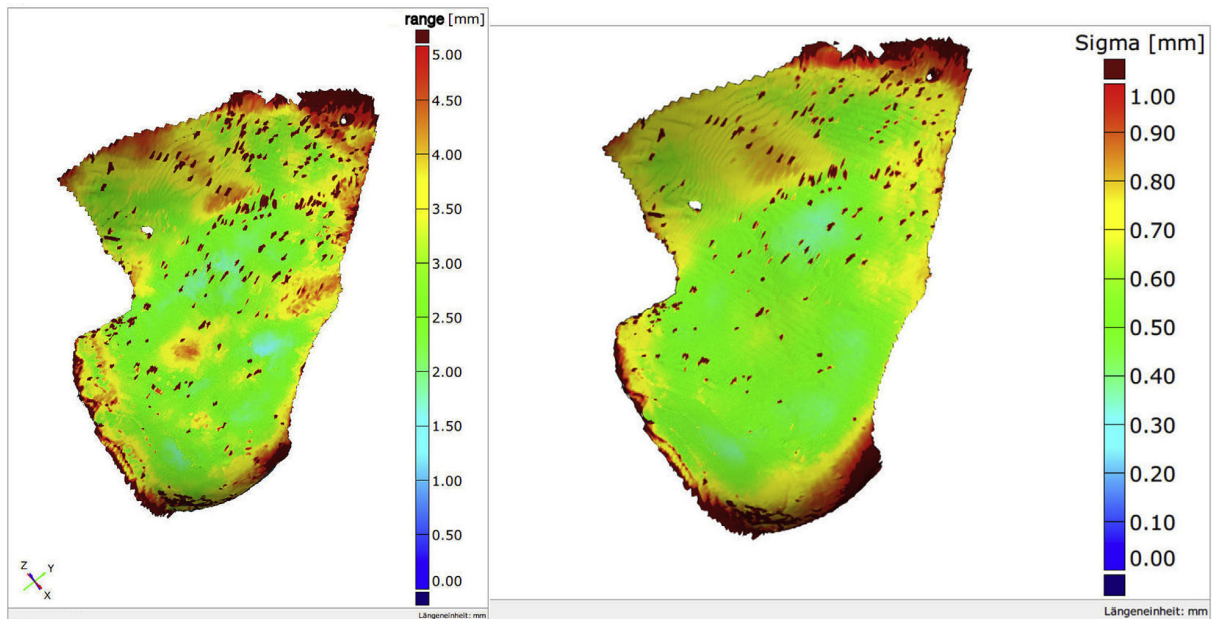


**FIGURE 5.** Display of range and standard deviation of the statistical shape orbital wall model. The greatest deviations occurred in the transition from the medial to the superior wall, especially near the optic foramen. The second zone is the upturning of the caudal wall toward the lateral wall. The infraorbital rim geometry is the third area with the greatest shape differences.

*Doerfler et al. Template for Orbital Wall Fracture Treatment. J Oral Maxillofac Surg 2017.*

these companies, KLS Martin (Tuttlingen, Germany) and Zimmer-Biomet (Freiburg, Germany) have provided no information. Stryker stated that their model is based on 300 CT scans but provided no information on the patient group or on the way the model was generated. Only DePuy Synthes has provided more substantial information on their meshes.<sup>16,17</sup> Sixty-eight of 70 CT sets were included. Thus, 125 of 131 CTs of patients for the present final model seem acceptable for a given ethnicity. Because of anatomic

differences between Europeans and non-Europeans,<sup>22,23</sup> further studies would be necessary if a similar approach were to be used in a non-European environment. For methods to generate a statistical shape model, the most widely used procedure would be the first one discussed in the Materials and Methods. Digitizing a given specimen using semi-landmarks has been used in numerous investigations.<sup>18,19</sup> To the authors' knowledge, no studies have

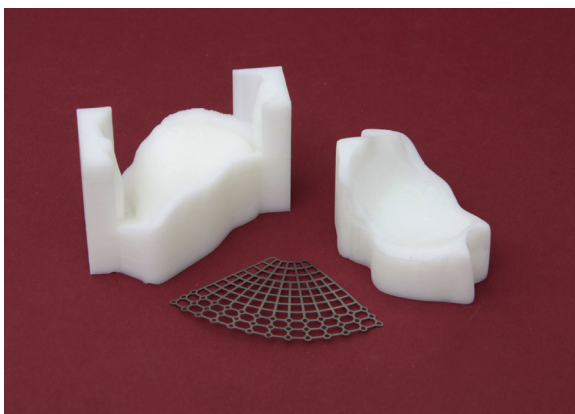


**FIGURE 6.** The resulting parts of the mold (left) with the lateral guiding wings for exact downward movement.

*Doerfler et al. Template for Orbital Wall Fracture Treatment. J Oral Maxillofac Surg 2017.*

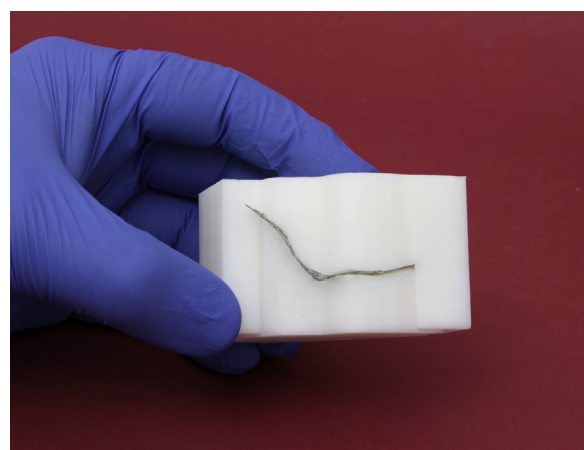


**FIGURE 7.** The plunger is inserted and the desired mesh is held between the 2 parts. The mesh is deformed by manual downward pressure.

*Doerfler et al. Template for Orbital Wall Fracture Treatment. J Oral Maxillofac Surg 2017.*

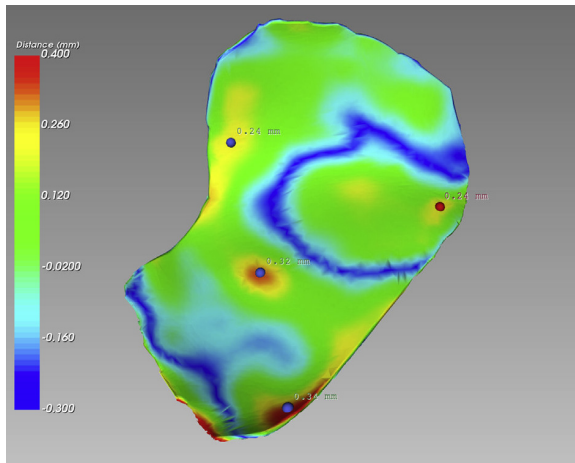


**FIGURE 8.** Shape evaluation of a deformed flat titanium sheet (Stryker). Eighty-one percent of the area is within a  $\pm 0.2$ -mm deviation corridor. Regions of maximum deviation are stated, reaching 0.34 mm in the anterior lateral area.

Doerfler et al. *Template for Orbital Wall Fracture Treatment. J Oral Maxillofac Surg* 2017.

reported potential differences among methods to create statistical shape models, but because the global master algorithm has been used successfully in previous medical studies,<sup>20,21</sup> the present approach seems acceptable. Concerning the variation within the statistical shape model, the present findings are similar to those of Kamer et al<sup>16</sup> and Noser et al.<sup>17</sup> They reported on identical regions of greater variation, namely the transition from the medial to the cranial wall, the transition from the inferior to the lateral wall, and the region of the optic foramen as major deviation regions and the infraorbital rim and posterior floor as minor deviation areas. Nevertheless, the authors' model shows differences as they previously reported in detail.<sup>15</sup> Different from Kamer et al<sup>16</sup> and Noser et al,<sup>17</sup> the authors modified their initial model by removing distinct outliers. Almost 5% of the present patients exhibited scattered major differences in clinically critical orbital regions. Thus, the authors created a model from all 131 patients rather than eliminate a small group of nonuniform outliers to obtain an even better fit in the vast majority. The authors believe that anatomically preformed implants will never cover all possible variations but are a rational means for most patients. Thus, they abandoned the 6 outliers. They could not determine any pre-existing trauma or other causes, but unnoticed trauma or inflammation cannot be ruled out.

The idea to create a mold to deform orbital implants has been applied to PSIs in some cases.<sup>24-26</sup> In those cases, a mold was generated to deform a resorbable or titanium mesh by an individually generated rapid

prototyping mold. The present approach differs because a generic mold was created that could serve most patients presenting with inferior and medial orbital wall fractures. The main advantage of a male mold and a female mold (piston and plunger in the present template) is to create a maximum adaption of a given material to the needed specific shape. In contrast to a mold, an anatomic statistical shape model of the full orbit would cover all walls, but the exact control of fit and manual adaptation would be more difficult. This applies to the commercially available orbital models, which are provided by KLS Martin and Medartis AG (Basel, Switzerland). In these models adaptation will work by manual pressure or using blunt rounded instruments or pliers. In addition to the piston-and-plunger mechanism of the present template, manual adaptation of implant materials in the present template is facilitated because a male mold and a female mold are provided. The only known approach for a template of the inferior and medial walls serving all shape variations has been the robotic press suggested by Metzger et al,<sup>27</sup> which has not been introduced into clinical practice. Concerning possible implant materials, only spring hard meshes or materials with increased thickness would be difficult to deform. Although most companies do not state the rigidity of their meshes (tension free to spring hard), spring hardness is the least likely to be encountered. Because the present prototype mold is designed to work as a hand-operated device, titanium meshes thicker than 0.4 to 0.6 mm would be difficult to deform. The 2 implant materials tested showed that the resulting meshes were within clinically acceptable differences for the mold.

Because a small percentage of patients will present a major anatomic deviation, a preoperative virtual try-in seems reasonable. The STL file of the present statistical orbital wall model might be used in surgical software such the Brainlab iPlan to examine the fit of the template. A typical example is shown in Figure 9.

Thus, implant alternatives for major shape differences could be considered.

This investigation showed that a statistical anatomic model of the orbit is feasible because human orbits present a distinct conformity. A generic mold to adapt different materials could be a cost-saving approach for most patients with orbital fracture compared with preformed implants or PSIs. The present virtual model and the generated implant material can be used in combination with navigation systems to show their concordance with the specific patient situation and to display possible modifications. Because the local ethics committee consented only to the generation of the mold prototype but explicitly not to its clinical use, the authors have performed only virtual try-ins in patients. However, these



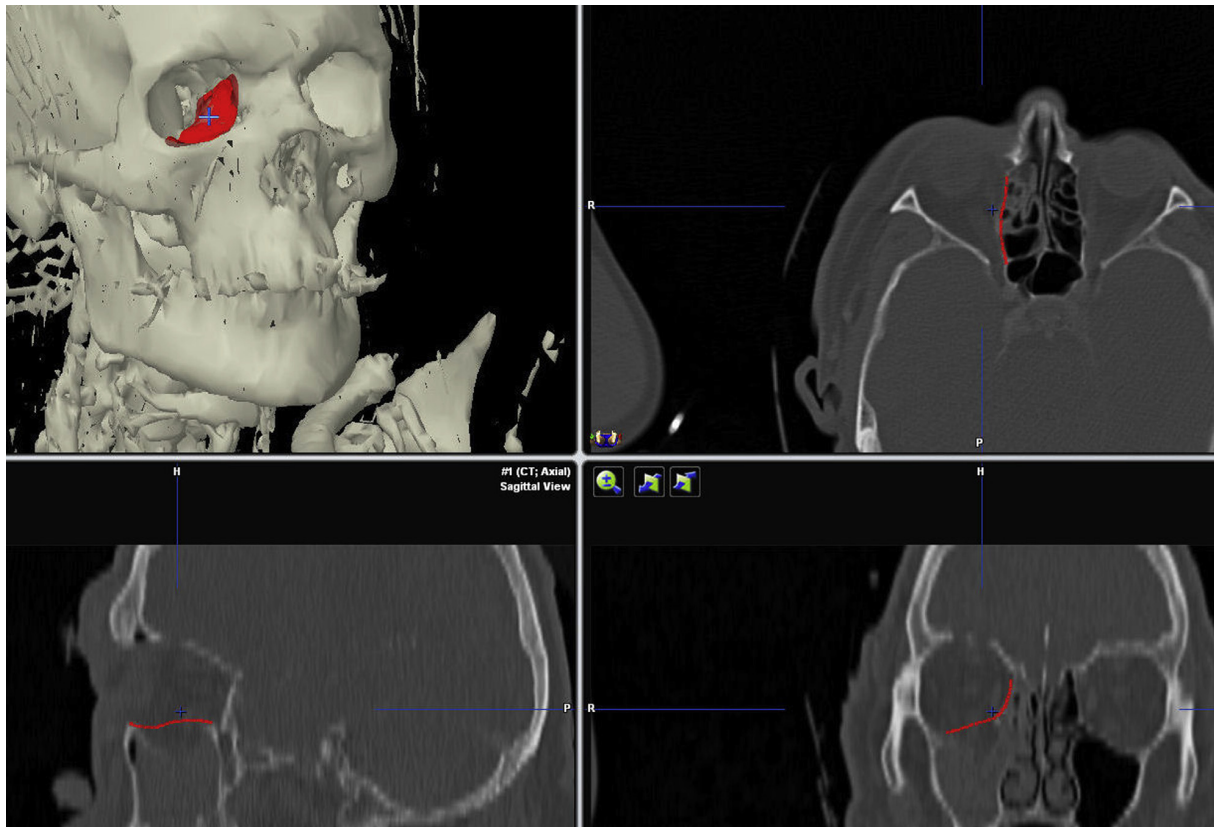


**FIGURE 9.** Presurgical virtual try-in of the template created in Brainlab iPlan software (2-wall fracture case). This patient was not included in the scans used for the model. The template shows an exact anatomic fit.

Doerfler et al. *Template for Orbital Wall Fracture Treatment. J Oral Maxillofac Surg* 2017.

suggest that the present approach would be effective in clinical practice.

## References

- Baino F: Biomaterials and implants for orbital floor repair. *Acta Biomater* 9:3248, 2011
- Dubois L, Steenen SA, Gooris PJJ, et al: Controversies in orbital reconstruction—I. Defect-driven orbital reconstruction: A systematic review. *Int J Oral Maxillofac Surg* 44:308, 2015
- Kronig SAJ, van der Mooren RJG, Strabbing EM, et al: Pure orbital blowout fractures reconstructed with autogenous bone grafts: Functional and aesthetic outcomes. *Int J Oral Maxillofac Surg* 45:507, 2016
- Gabrielli MF, Monnazzi MS, Passeri LA, et al: Orbital wall reconstruction with titanium mesh: Retrospective study of 24 patients. *Craniomaxillofac Trauma Reconstr* 4:151, 2011
- Gordon CR, Susarla SM, Yaremchuk MJ: Quantitative assessment of medial orbit fracture repair using computer-designed anatomical plates. *Plast Reconstr Surg* 130:698e, 2012
- Scolozzi P, Momjian A, Heuberger J, et al: Accuracy and predictability in use of AO three-dimensionally preformed titanium mesh plates for posttraumatic orbital reconstruction: A pilot study. *J Craniofac Surg* 20:1108, 2009
- Klein M, Glatzer C: Individual CAD/CAM fabricated glass-bioceramic implants in reconstructive surgery of the bony orbital floor. *Plast Reconstr Surg* 117:565, 2006
- Kozakiewicz M, Elagal M, Walkowiak B, et al: Technical concept of patient-specific, ultrahigh molecular weight polyethylene orbital wall implant. *J Craniomaxillofac Surg* 41:282, 2013
- Stoor P, Suomalainen A, Lindqvist C, et al: Rapid prototyped patient specific implants for reconstruction of orbital wall defects. *J Craniomaxillofac Surg* 42:1644, 2014
- Gander T, Essig H, Metzler P, et al: Patient specific implants (PSI) in reconstruction of orbital floor and wall fractures. *J Craniomaxillofac Surg* 43:126, 2015
- Kozakiewicz M, Elagal M, Loba P, et al: Clinical application of 3D pre-bent titanium implants for orbital floor fractures. *J Craniomaxillofac Surg* 37:229, 2009
- Mustafa SF, Evans PL, Bocca A, et al: Customized titanium reconstruction of post-traumatic orbital wall defects: A review of 22 cases. *Int J Oral Maxillofac Surg* 40:1357, 2011
- Schmelzeisen R, Gellrich NC, Schoen R, et al: Navigation-aided reconstruction of medial orbital wall and floor contour in cranio-maxillofacial reconstruction. *Injury* 35:955, 2004
- Dubois L, Schreurs R, Jansen J, et al: Predictability in orbital reconstruction: A human cadaver study. Part II: Navigation-assisted orbital reconstruction. *J Craniomaxillofac Surg* 43:2042, 2015
- Huempfer-Hierl H, Doerfler HM, Kruber D, et al: Morphologic comparison of preformed orbital meshes. *J Oral Maxillofac Surg* 73:1119, 2015
- Kamer L, Noser H, Schramm A, et al: Orbital form analysis: Problems with design and positioning of precontoured orbital implants. A serial study using post-processed clinical CT data in unaffected orbits. *Int J Oral Maxillofac Surg* 39:666, 2010
- Noser H, Hammer B, Kamer L: A method for assessing 3D shape variation of fuzzy regions and its application on human bony orbits. *J Digit Imaging* 23:422, 2010

18. Gunz P, Mitteroecker P: Semilandmarks: A method for quantifying curves and surfaces. *Hystrix* 24:103, 2013
19. Mitteroecker P, Gunz P: Advances in geometric morphometrics. *Evol Biol* 36:235, 2009
20. Von Wilmowsky C, Bergauer B, Nkenke E, et al: A new, highly precise measurement technology for the in vitro evaluation of the accuracy of digital imaging data. *J Craniomaxillofac Surg* 43:1335, 2015
21. Szymor P, Kozakiewicz M, Olszewski R: Accuracy of open-source software segmentation and paper-based printed three-dimensional models. *J Craniomaxillofac Surg* 44:202, 2016
22. Dean D, Bookstein FL, Koneru S, et al: Average African American three-dimensional computed tomography skull images: The potential clinical importance of ethnicity and sex. *J Craniofac Surg* 9:348, 1998
23. De Silva DJ, Rose GE: Orbital blowout fractures and race. *Ophthalmology* 118:1677, 2011
24. Lim CGT, Campbell DI, Cook N, et al: A case series of rapid prototyping and intraoperative imaging in orbital reconstruction. *Craniomaxillofac Trauma Reconstruct* 8:105, 2015
25. Tabakovic SZ, Konstantinovic VS, Radosavljevic R, et al: Application of computer-aided designing and rapid prototyping technologies in reconstruction of blowout fractures of the orbital floor. *J Craniofac Surg* 26:1558, 2015
26. Podolsky DJ, Mainprize JG, Edwards GP, et al: Patient-specific orbital implants: Development and implementation of technology for more accurate orbital reconstruction. *J Craniofac Surg* 27:131, 2016
27. Metzger MC, Schoen R, Zizelmann C, et al: Semiautomatic procedure for individual preforming of titanium meshes for orbital fractures. *Plast Reconstr Surg* 119:969, 2007

## 2.5 Preforming of Polydioxanone sheets for orbital wall fractures – a technical note

Das abbaubare und biokompatible Material Polydioxanon findet bei der operativen Versorgung von Orbitabodenfrakturen große Verwendung. Aufgrund seiner Eigenschaften bzw. Beschaffenheit können Folien aus diesem Material kleine Defekte bis zu  $2 \text{ cm}^2$  [ML94] im Orbitaboden gut ausgleichen. Bei größeren Defekten ist eine anatomische Anpassung bereits deutlich schwieriger, da ein Verformen lediglich durch „händisches-Drücken“ wie es im OP-Saal während des Eingriffs üblich ist, der komplexen S-förmigen Geometrie der Orbitawände nicht gerecht wird.

In der anschließenden Machbarkeitsstudie wird ein Verfahren erläutert, welches erstmalig die dreidimensionale anatomisch regelrechte Deformation von PDS-Folien mit Hilfe eines Stempels beschreibt.

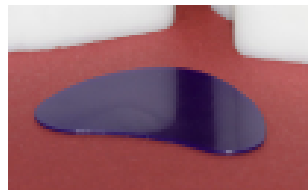


Abbildung 2.10: PDS-Folie

Von Seiten der Softwarelösung stellten sich die Probleme, die in den beiden zuvor behandelten Veröffentlichungen aufgeführt wurden. Darunter zum Einen die Generierung der Stempelform mittels statistisch-anatomischen Modell, zum Anderen der Vergleich der deformierten PDS-Folie mit der Stempelform. Mit Hilfe von FAT wurde dies in einer Softwarelösung ohne Wechsel der Anwendung bzw. Datenumwandlungen gelöst.

In Abbildung 2.11 wird der farbkodierte Distanzunterschied zwischen Folie und Stempelform mittels der VTK-Bibliothek beschrieben.

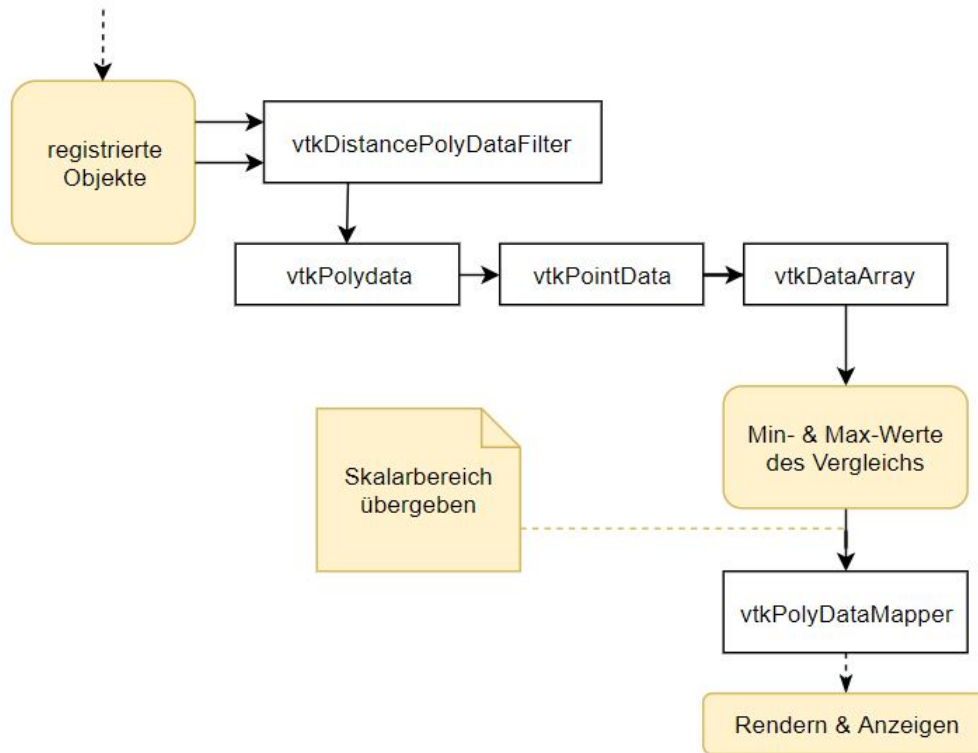


Abbildung 2.11: Workflow zum Vergleich zweier Objekte – Unterschied wird im 3D-Fenster farbkodiert angezeigt



## Preforming of polydioxanone sheets for orbital wall fractures – A technical note

Daniel Kruber <sup>a,1</sup>, Thomas Hierl <sup>c,\*</sup>, Hans-Martin Doerfler <sup>b</sup>, Heike Huempfer-Hierl <sup>a</sup>, Matthias Krause <sup>a</sup>

<sup>a</sup> Department of Oral and Maxillofacial Plastic Surgery, (Head: Prof. Dr. Dr. Alexander Hemprich), Leipzig University Hospital, Liebigstr. 10-14, 04103, Leipzig, Germany

<sup>b</sup> Faculty of Mechanical and Energy Engineering, (Head: Prof. Dr. Peter Schulze), University of Applied Sciences (HTWK) Leipzig, Karl-Liebknecht Str. 145, 04277, Leipzig, Germany

<sup>c</sup> Department of Oral and Maxillofacial Plastic Surgery, (Head: Prof. Dr. Dr. Thomas Hierl), Helios Vogtlandklinikum Plauen, Roentgenstr. 2, 08529, Plauen, Germany



### ARTICLE INFO

**Article history:**  
Paper received 22 January 2018  
Accepted 2 May 2018  
Available online 9 May 2018

**Keywords:**  
Orbital wall fracture  
PDS sheet  
Preforming  
Statistical shape model

### ABSTRACT

**Introduction:** Polydioxanone (PDS) sheets are commonly used in the treatment of orbital wall fractures. A potential drawback of PDS is that it may be difficult to adapt to the anatomy of the orbital walls. Therefore a study was conceived to test the feasibility of preforming PDS sheets.

**Material and methods:** PDS sheet material was water-heated and preformed using a template based on a statistical anatomical model. Then the deformed sheet was cooled, stored and compared to the original model to investigate post-deformation changes.

**Results:** PDS sheet material could easily be deformed using a mould. No significant post-cooling shape changes were noticed.

**Conclusions:** PDS sheet material can be preformed into complex geometric shapes. This could be a benefit in the treatment of orbital wall fractures.

© 2018 European Association for Cranio-Maxillo-Facial Surgery. Published by Elsevier Ltd. All rights reserved.

## 1. Introduction

Polydioxanone (PDS) sheets (Ethicon, Norderstedt, Germany) have been successfully used in orbital floor fracture treatment for over 27 years (Baumann et al., 2002; Beck-Broichsitter et al., 2015; Dietz et al., 2001; Iizuka et al., 1991). PDS is a resorbable biocompatible material that will be replaced by firm scar tissue or bone and will withstand the forces encountered in the orbit (Birkenfeld et al., 2013). A major drawback of PDS is that it is supplied as a flat sheet that has to be bent prior to insertion. Using the edges of instruments, these sheets may be shaped into spherical segments that may be sufficient to treat smaller orbital floor defects. As the orbital walls are not shaped like a sphere (Noser et al., 2010), larger defects of the floor might not be adequately reconstructed. The same applies to combined medial and caudal defects. To overcome

this deficiency, a new technique to preform polydioxanone sheets is presented. By preforming, the flat sheet is transformed into an implant presenting the shape of a realistic average orbit.

## 2. Materials and methods

A generic polyethylene mould generated by rapid prototyping based on statistical shape analysis of 131 central European orbits was used for this task (Doerfler et al., 2017). The mould consisted of a male and female part that slide along a defined path and that are manually closed by finger pressure. As orbital floor and medial wall fractures are the most common fracture sites; both walls were addressed in the generic mould. Sheet material (0.25 and 0.5 mm) was inserted into the mould, and the mould with the enclosed PDS material was put into a 90 °C water bath. After 30 s the mould was firmly closed and put into cold water. After cooling, the mould was opened and the geometry was checked. It should now sit passively and present the new geometry (Figs. 1 and 2). The ideal temperature was found by slowly increasing the temperature and measuring the softness of the PDS sheet material during closure of

\* Corresponding author. Fax: +49 (0)3741 493679.

E-mail address: [Thomas.Hierl@helios-gesundheit.de](mailto:Thomas.Hierl@helios-gesundheit.de) (T. Hierl).

<sup>1</sup> Daniel Kruber and Thomas Hierl contributed equally to this work.



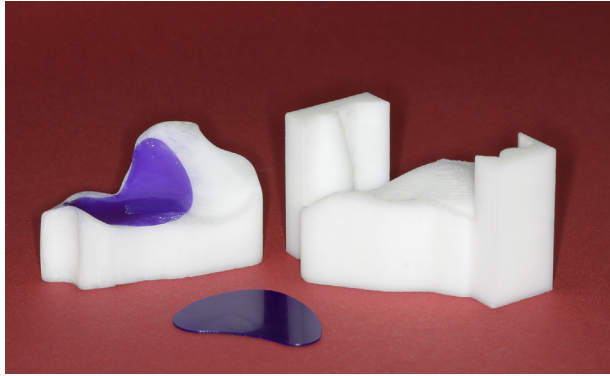


**Fig. 1.** Male and female mould parts demonstrating the PDS sheet deformation. The modified sheet adapts well to the mould. In front of the mould, a non-deformed PDS sheet can be seen.

the mould. Ten sheets were tested, and three were destroyed by overheating.

As seen in Figs. 2 and 3, the new shape has an anterior extension that rests on the infraorbital rim for proper placement. If desired, it could even be fixed with a small tack, as in pre-prosthetic membrane fixation.

The main question regarding preforming is whether the implant will retain the desired shape. To test this, the following procedure was chosen: the preformed implant was coated with matte white scanning spray to prevent reflections. Then it was scanned using a high-resolution industrial scanner (0.015-mm resolution; GOM ATOS IIe Rev. 01, Braunschweig, Germany). The resulting STL file was compared to the original data of the mould with FAT software, which is based on the VTK framework (VTK Org., Kitware, Clifton Park, NJ, USA). Both were first rigidly registered using the iterative closest point algorithm. Then congruency was visualized by calculating the distance of the sheet and mould and showing the result in a color-coded display (Fig. 3). Next, the percentage of the area within the distance corridors between the sheet and mould

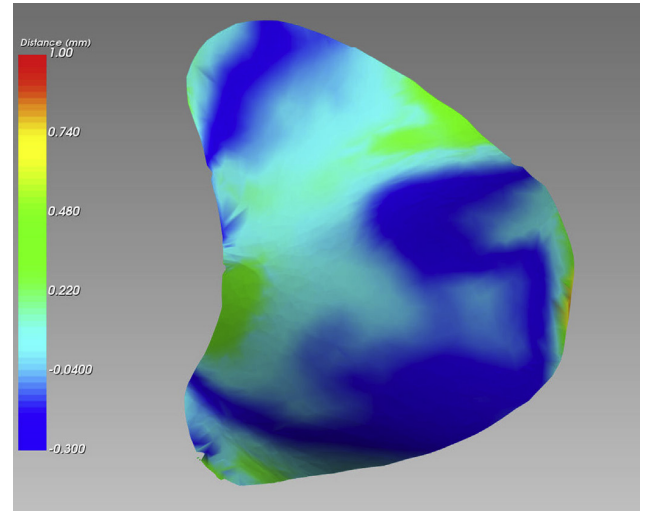


**Fig. 3.** Comparison of the preformed sheet with the original geometry of the mould by way of a color-coded distance map. Of the sheet area, 98.5% lies within a  $\pm 0.4$ -mm corridor compared to the original mould geometry.

was calculated (Huempfer-Hierl et al., 2015). Three corridors were chosen: 0 to  $\pm 0.3$  mm,  $\pm 0.3$ – $0.4$  mm; and  $0.4$ – $1$  mm. Scanning was performed 4 days after preforming and outside storage of the mould at room temperature to reveal potential post-deformation changes.

### 3. Results

Preforming was easily achieved using the described method. However, 0.25 mm of material was easier to deform, and required shorter immersion time and less force in the mould. Using boiling water led to a distortion of the sheet, whereas colder water did not allow shape changes. Comparing the preformed sheet geometry to

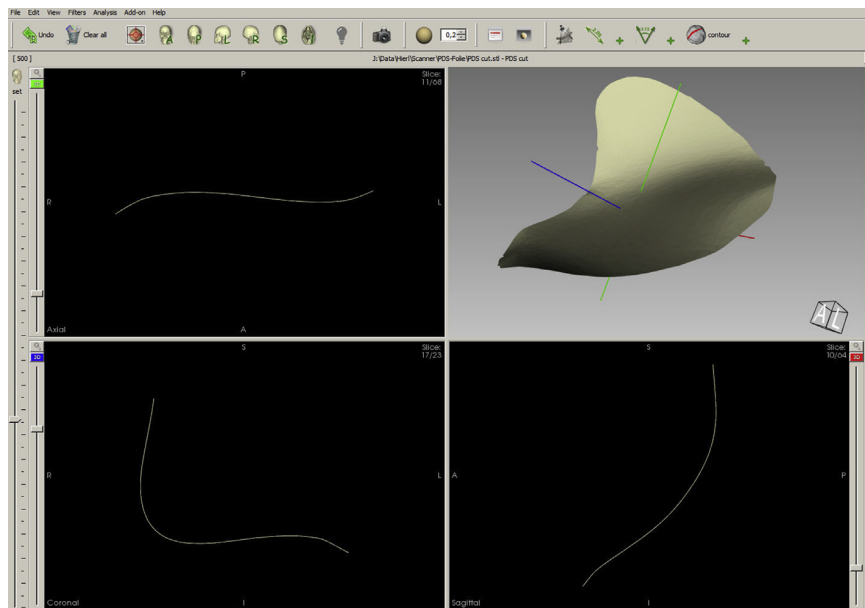


**Fig. 2.** STL file of the scanned preformed PDS sheet. FAT software shows the three-dimensional aspect and three cuts along the main axes. The geometric changes of the initial flat sheet are evident.

the original mould shape showed that 93.4% of the preformed sheet area lay within a deviation of  $\pm 0.3$  mm to the original mould. Of the sheet area, 5% had a distance to the mould ranging between 0.3 and 0.4 mm; 1.5% of the area ranged at a distance between 0.4 and 0.8 mm in the most posterior orbital floor region (Fig. 3). Measuring the sheet thickness after preforming with a precision caliper revealed only minimal changes. The comparatively low temperature and the low force created by digital compression did not create a roll-out deformation (i.e., increasing the area by diminishing the thickness). Using our software tools to compare the geometry of the mould and sheet permitted us to compare the percentage of the distance corridors between the sheet and mould. To our understanding, this is clinically relevant information. However, it is not possible to define the location of potential differences other than by visual inspection. As the corridors were almost identical with regard to the number of tests, no further diagrams are presented.

#### 4. Discussion

Our results show that PDS sheet material can be preformed according to the orbital geometry. After deformation, the sheet material showed no clinically relevant deformation or distortion. Sheet deformation depends on variable temperature, immersion time, pressure of the mould closure and temperature conductivity of the mould. Therefore a temperature diagram is not provided, as this would be valid only if the other factors did not change.

Using this novel method, PDS material could be used for more complex defects than small orbital floor fractures.

It may be argued that PDS might not be stable enough to maintain the complex geometry during and after resorption. This can be seen as a general problem of resorbable materials in orbital reconstruction irrespective of the fracture location. As PDS sheets have been in use for over 27 years, and according to the biomechanical testing of PDS (Birkenfeld et al., 2013), it seems that this is of minor concern. A potential benefit of preformation could be a better fit on the remaining bony orbital structures. In the authors' experience, cold bending of PDS material has a tendency to create an offset between the remnant bone and the sheet. This dead space is then filled by hematoma. Whether this is clinically relevant is unclear, but a better fit without dead space using a preformed sheet might be an advantage. By moulding the sheet over the infraorbital rim it can be firmly fixed in the desired position (e.g., using a tack), which is not possible in the conventional use whereby a hematoma might lift the sheet into the orbit or cause a dislocation. This might ensure that the sheet will rest on firm bone along all fracture borders, as lack of support could result in a tilting of the sheet.

#### 5. Conclusion

Our technical report shows that preformation of PDS sheet material is possible. If doing so, a generic mould based on a statistical shape model seems appropriate. At present, neither the generic mould nor the heating deformation is certified as a medical product or a medically acceptable procedure. Our technical report, however, might serve as an incentive to medical companies to take our findings into consideration.

#### Ethics statement

No patient data were used, and no patient permission was needed.

#### Conflicts of interest

The authors declare that they have no conflicts of interest.

#### Acknowledgements

This investigation was funded by the German Federal Ministry of Economics and Technology ZIM KF 2036713AK2. The development of the 3D analysis software was partially funded by German Federal Ministry of Economics and Technology ZIM KF2036708SS0.

#### References

- Baumann A, Burggasser G, Gauss N, Ewers R: Orbital floor reconstruction with an alloplastic resorbable polydioxanone sheet. *Int J Oral Maxillofac Surg* 31: 367–373, 2002
- Beck-Broichsitter BE, Acar C, Kandzia C, Jochens A, Wiltfang J, Becker ST: Reconstruction of the orbital floor with polydioxanone: a long-term clinical survey of up to 12 years. *Br J Oral Maxillofac Surg* 53: 736–740, 2015
- Birkenfeld F, Steiner M, Kern M, Wiltfang J, Moeller B, Lucius R, Becker ST: Forces affecting orbital floor reconstruction materials—a cadaver study. *J Craniomaxillofac Surg* 41: e24–e28, 2013
- Dietz A, Ziegler CM, Dacho A, Althof F, Conrad C, Kolling G, von Boehmer H, Steffen H: Effectiveness of a new perforated 0.15 mm poly-p-dioxanone-foil versus titanium-dynamic mesh in reconstruction of the orbital floor. *J Craniomaxillofac Surg* 29: 82–88, 2001
- Doerfler HM, Huempfer-Hierl H, Kruber D, Schulze P, Hierl T: Template-based orbital wall fracture treatment using statistical shape analysis. *J Oral Maxillofac Surg* 75: 1475.e1–1475.e8, 2017
- Huempfer-Hierl H, Doerfler HM, Kruber D, Hierl T: Morphologic comparison of preformed orbital meshes. *J Oral Maxillofac Surg* 73: 1119–1123, 2015
- Iizuka T, Mikkonen P, Paukku P, Lindquist C: Reconstruction of orbital floor with polydioxanone plate. *Int J Oral Maxillofac Surg* 20: 83–87, 1991
- Noser H, Hammer B, Kamer L: A method for assessing 3D shape variations of fuzzy regions and its application on human bony orbits. *J Digit Imaging* 23: 422–429, 2010

## 2.6 Calculation of resected orbital wall areas in the treatment of endocrine orbitopathy

Patienten mit endokriner Orbitopathie (EO), welche eine autoimmunologisch bedingte Zunahme des Orbitainhalts darstellt, leiden an verschiedenen Problemen. Das vordergründigste Stigma ist der mitunter sehr ausgeprägte Exophthalmus.

An erster Stelle der chirurgischen Verfahren steht bei ausgeprägten Schweregraden die Entfernung knöcherner Wände der Augenhöhle, um so Platz für die vermehrten Weichgewebe zu schaffen (Dekompression). Da das Ziel der Behandlung eine patientenspezifische Korrektur ist, liegt es nahe, als Grundlage einer statistischen Analyse die chirurgischen Einflussgrößen zu quantifizieren. Obwohl die knöcherne Dekompression seit vielen Jahren [NAF32], [SEW36] ausgeübt wird, war dies bisher auf Grund der hohen messtechnischen Schwierigkeiten nicht erfolgt. Mittels FAT wurde im nachfolgenden Artikel erstmalig die Flächen der intraoperativ resizierten Knochenwände (lateral, medial, kaudal) bestimmt (Abbildung 2.12).

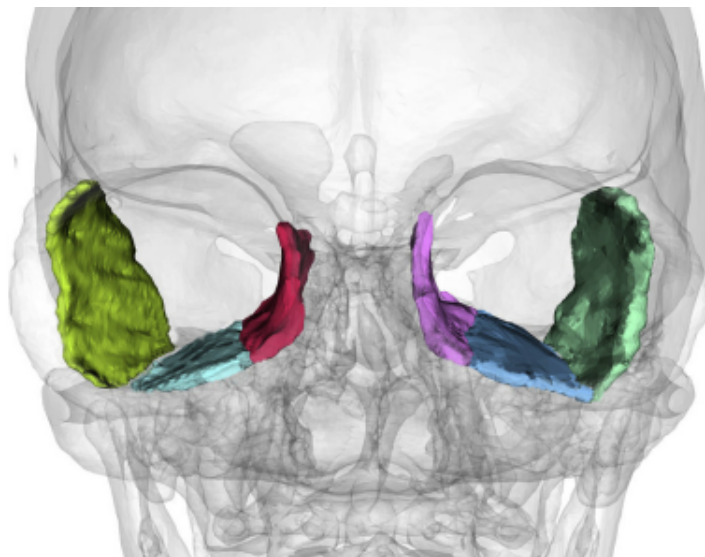


Abbildung 2.12: farbige Abgrenzung der Orbitawände

Zur Realisierung in FAT wurden zunächst die chirurgische Planung und

## Kapitel 2. FAT-Anwendungen

### Vergleich und Analyse komplexer Flächen

---

der postoperative Datensatz aus der Brainlab Planungssoftware (Brainlab iPlan CMF, Fa. Brainlab AG, München) importiert. Anschließend erfolgte die Übernahme der Differenzstrukturen im Bereich der Orbitawände (= die resizierten Knochenabschnitte) für jede Wand getrennt. Zuletzt mussten entsprechende Anpassungen (wie z.B. Glättung und Fehlstellen) in FAT vorgenommen werden, um die abschließende Bemaßung durchzuführen.

Jeder segmentierte Bereich der Orbitawände, welche als `vtkActor`'s in der „Render Engine“ dargestellt wurden, durchlief eine Konvertierung zum `vtkPolyData`-Objekt. Erst dadurch war eine Flächenberechnung möglich. Dies wird in Abbildung 2.13 veranschaulicht.

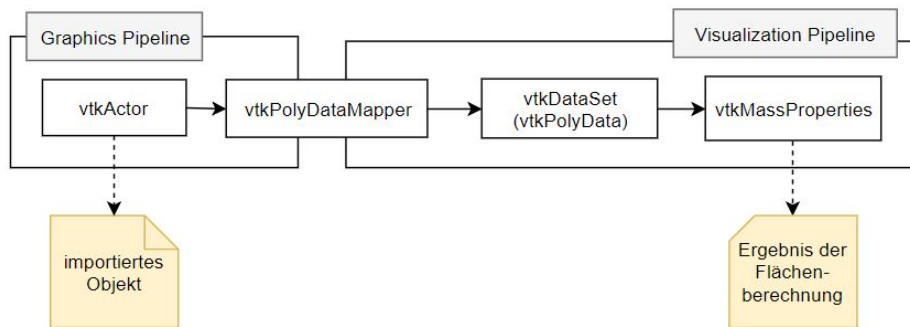


Abbildung 2.13: Workflow zur Umwandlung zum PolyData-Objekt

Durch die automatische und teilweise händische Segmentierung (im Programm Brainlab) entstanden raue Oberflächen, welche zusätzlich für die weitere Bearbeitung geglättet werden mussten (Abbildung 2.14).

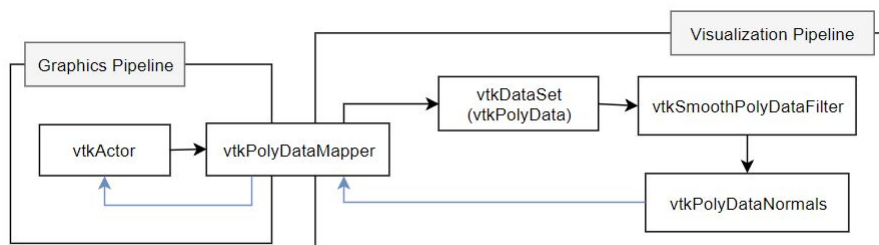
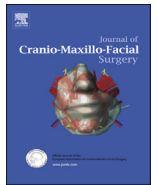


Abbildung 2.14: Workflow zur Konvertierung des importierten Objektes in ein PolyData-Objekt mit anschließender Glättung und Anwendung auf das Ursprungsobjekt (untere blauen Linien)



Contents lists available at ScienceDirect

## Journal of Cranio-Maxillo-Facial Surgery

journal homepage: [www.jcmfs.com](http://www.jcmfs.com)

# Calculation of resected orbital wall areas in the treatment of endocrine orbitopathy



Matthias Krause<sup>a</sup>, Heike Hümpfner-Hierl<sup>a</sup>, Daniel Kruber<sup>a</sup>, Ina Sterker<sup>b</sup>,  
Thomas Hierl<sup>a,\*</sup>

<sup>a</sup> Department of Oral & Maxillofacial Plastic Surgery (Head: Alexander Hemprich MD DDS PhD), Leipzig University, Liebigstr. 12, 04103 Leipzig, Germany

<sup>b</sup> Department of Ophthalmology, Leipzig University, Liebigstr. 12, 04103 Leipzig Germany

## ARTICLE INFO

### Article history:

Paper received 23 September 2016

Accepted 11 January 2017

Available online 25 January 2017

### Keywords:

Endocrine orbitopathy

Decompression

Navigated surgery

## ABSTRACT

**Purpose:** Orbital wall decompression is routinely used to treat proptosis in endocrine orbitopathy. Until now, however, there has been no investigation to measure the area/extent of the removed walls.

**Materials and methods:** The inner areas of 154 orbital walls (lateral, inferior, medial) which had been resected in 38 patients were measured using pre- and postsurgical computed tomographic data in Brainlab iPlan software. Furthermore the effect of concomitant centrolateral orbital rim advancement was calculated in 48 cases. Surgery was performed after preoperative planning using intraoperative navigation.

**Results:** The mean area of resected inferior and medial orbital walls lay at 6.7 cm<sup>2</sup> and 6.2 cm<sup>2</sup>, while the area of the lateral orbital wall was 6.9 cm<sup>2</sup>. Rotation-advancement of the lateral rim added an area of 1.8 cm<sup>2</sup> (~25% of the lateral orbital wall). Comparison of the pre- and postsurgical computed tomographic data showed excellent conformity of the presurgical planning and postsurgical results.

**Conclusions:** This investigation is a first step in analyzing the potential surgical effect of bony decompression surgery by stating the metric amount of orbital wall removal. Using these data, further studies will be performed in the future.

© 2017 European Association for Cranio-Maxillo-Facial Surgery. Published by Elsevier Ltd. All rights reserved.

## 1. Introduction

Endocrine orbitopathy (EO) is the most frequent and important extrathyroidal sign of Graves' disease (Bartalena et al., 2008a, 2008b). Early restoration and maintenance of euthyroidism and immunosuppressive treatment is the first-line therapy during the active phase of disease, whereas rehabilitative surgery (orbital decompression by enlargement of the bony orbit and/or orbital fat resection, squint surgery, eyelid surgery) is postponed until a stable euthyroid and inactive stage of at least 6 months is reached (Bartalena et al., 2008a, 2008b, 2000; Bonara et al., 2008; Graham and Carter, 1999; Kamber et al., 2009; Mourits et al., 1990; Schaefer et al., 2003; Wulc et al., 1990; Kirsch et al., 2009; Zielinski et al., 1989).

Since 1911, when Dollinger first described surgical orbital decompression (Dollinger, 1911), many different techniques and approaches have been endorsed, including one-, two-, three-, and four-wall decompressions with or without orbital fat removal (Leong and White, 2010). Further surgical techniques include the advancement or lateral expansion of the laterocentral orbital frame (González-García et al., 2008; Tavassol et al., 2012; Tessier, 1969; Wolfe, 1979).

The primary goal of orbital decompression surgery is the reduction of proptosis. This is supposed to depend on the number of the removed orbital walls, the extent of their removal, and the anatomy of the bony orbit and periorbital spaces (Lee et al., 2003).

There are a few references that suggest that the reduction of proptosis is related proportionally to the number of removed walls, with about 2–3 mm per wall (Lee et al., 2003; Mourits et al., 2009). The anatomy of the orbital walls are well described (Holck and Ng, 2005), but until now there has been no investigation on the real metric extent of orbital wall decompression. The reasons for this are presumably the difficulties encountered in the measuring.

\* Corresponding author.

E-mail addresses: [KrauseMa@medizin.uni-leipzig.de](mailto:KrauseMa@medizin.uni-leipzig.de) (M. Krause), [Heike.Huepfner-Hierl@medizin.uni-leipzig.de](mailto:Heike.Huepfner-Hierl@medizin.uni-leipzig.de) (H. Hümpfner-Hierl), [danielkruber@gmx.de](mailto:danielkruber@gmx.de) (D. Kruber), [Ina.Sterker@medizin.uni-leipzig.de](mailto:Ina.Sterker@medizin.uni-leipzig.de) (I. Sterker), [hiet@medizin.uni-leipzig.de](mailto:hiet@medizin.uni-leipzig.de) (T. Hierl).



Therefore the purpose of this study was to define the areas of the removed walls in orbital decompression for the first time. This seems to be a necessary prerequisite to improving the understanding of decompression surgery, to permit comparison between future investigations, and eventually to allow patient-specific surgical simulation. Furthermore, real measurements should be performed, as purely anatomical measurements of the orbital wall area in unaffected orbits will include regions not accessed during decompression surgery.

## 2. Material and methods

From 2010 to 2015, a total of 38 patients with endocrine orbitopathy were treated by bony decompression surgery and were retrospectively evaluated. Of the patients, 34 underwent operation bilaterally and four patients unilaterally, resulting in 72 operated orbits (150 orbital walls). The mean age was  $51.6 \pm 9.3$  years (range 31–76 years), and the group consisted of 25 women and 13 men. Ten patients (26.3%) had dysthyroid optic neuropathy. Surgical procedures included uni- or bilateral one-, two-, and three-wall decompression with or without advancement of the laterocentral orbital rim (lateral rim advancement [LARA]) according to Gonzales-Garcia et al. (González-García et al., 2008). LARA was performed as the standard procedure in 25 cases. It increases the depth of the orbit in the lateral aspect and moves the lateral canthal ligament anteriorly. This leads to an instant esthetic improvement of proptosis (it changes Hertel values even without globe movements) and diminishes lateral skin retraction caused by lateral canthal tension. LARA leaves the orbital rim as a circular structure intact and prevents lateral skin retractions that might result in cases in which the lateral orbital rim is removed. During decompression surgery, the temporary removal of the lateroorbital rim eases the access to the lateral and inferior orbital walls and prevents excessive retraction and pressure on the orbital contents.

In 13 patients, the lateral orbital rim was not changed due to the following reasons: unilateral decompression ( $n = 4$ ); isolated massive enlargement of the rectus medialis muscles ( $n = 1$ ); mild proptosis with only bilateral lateral wall decompression ( $n = 1$ ); and endocrine orbitopathy without major exophthalmus but ophthalmologic symptoms ( $n = 7$ ).

Table 1 shows the relevant patient data. In the first three cases, surgery was performed via bicoronal open access, and in all subsequent cases a transconjunctival incision with lateral canthotomy was performed. In cases of LARA, a small secondary upper eyelid crease incision was added to permit the osteotomy of the superior-medial orbital rim lateral to the supraorbital foramen. In LARA, the upper and lower osteotomy cuts on the orbital rim served as a hinge to rotate the lateral aspect anteriorly using two microplates. After defining the desired advancement, a third microplate was inserted at the lateral aspect of the orbital rim to the zygomatic bone to prevent backward rotation. Furthermore, milled bone chips gathered during decompression were inserted in the superior and inferior gaps to stabilize the advancement/rotation. No lateral

expansion of the orbital frame was performed with LARA. Orbital wall removal was performed using piezosurgical instruments, rongeurs, or forceps (Hierl et al., 2016). All patients underwent planning preoperatively in iPlan Brainlab software (Brainlab, Feldkirchen, Germany), and the Brainlab navigation system was used intraoperatively to control the amount of decompression and rim advancement. Preoperatively, the resection borders were planned as described below.

### 2.1. Lateral orbital wall

For cranial and posterior borders, the skull base contour was interpolated into orbit with removal of sharp cortical edges. The anterior border was drawn 4–5 mm posterior and parallel to the anterior border of the lateral orbital rim; and the inferior border was defined as follows: anteriorly the turning point between lateral and inferior wall, in the posterior region the inferior orbital fissure.

### 2.2. Inferior orbital wall

Anterior border: 3–4 mm posterior and parallel to the anterior border of the infraorbital rim; Posterior border: turning point between inferior wall and pterygopalatine fossa; medial border: upturning between inferior and medial wall (inferomedial strut); lateral border: anteriorly the turning point between lateral and inferior wall, in the posterior region the inferior orbital fissure.

The area of the inferior orbital fissure was not included in area calculation.

### 2.3. Medial wall

Anterior border: 3–4 mm posterior to the lacrimal fossa parallel to the medial orbital rim; posterior border: vertical line 4–5 mm anterior to the optic canal; inferior border: turning point to inferior wall (inferomedial strut); superior border: line parallel to skull base (2–3 mm caudal of skull base).

### 2.4. LARA

Superior extension: midorbital plane lateral to supraorbital foramen; inferior extension: midorbital plane (cranial-lateral to infraorbital foramen).

Fig. 1 shows a typical preoperative planning situation with display of resection borders, LARA osteotomy and LARA advancement (light blue and yellow, respectively). The optic and infraorbital nerves are colored red. All other markings resemble the planned resection borders.

All patients underwent pre- and postsurgical computed tomography (CT) scans, the findings from which were used for this analysis (0.4–1 mm contiguous slicing, bone windowing).

When measuring the area of the removed walls, several problems were encountered. Simply measuring the area of the orbital walls would have been possible, but this would be an anatomic

**Table 1**  
Distribution of examined orbital walls.

	Unilateral			Bilateral without LARA			Bilateral with LARA		
	Patients	Orbits	Walls	Patients	Orbits	Walls	Patients	Orbits	Walls
1 wall (lateral)				1	2	2	3	6	6
2 walls (inferior + lateral)	2	2	4	3	6	12	20	40	80
2 walls (inferior + medial)				1	2	4			
3 walls (lateral + inferior + medial)	2	2	6	4	8	24	2	4	12
Orbital walls: 150		Lateral = 70	Inferior = 64		Medial = 16				

LARA, lateral rim advancement.

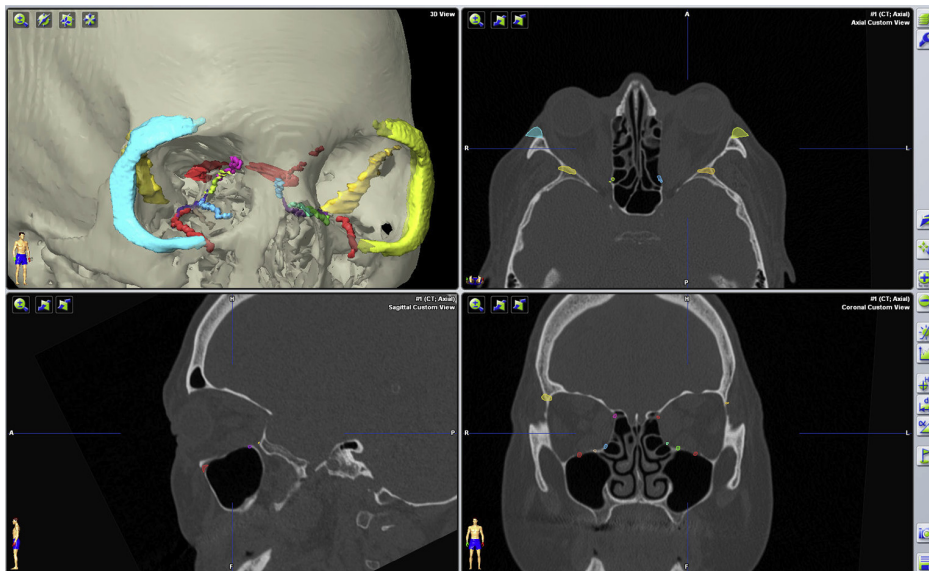


**Fig. 1.** A typical preoperative planning situation with display of resection borders, lateral rim advancement (LARA) osteotomy and LARA advancement (light blue and yellow, respectively). The optic and infraorbital nerves are colored red. All other markings resemble the planned resection borders.

study and would include regions not resected during surgery. If the measurements were performed according to the preoperative plan, this would suppose that each resection would follow exactly the above-mentioned anatomic structures. Many publications show isolated axial CT slices as examples, and when comparing these, some discrepancies can be found even if they are classified identically. Therefore the measurement of the real extent of wall removal was judged to be necessary. It was considered that the postoperative scans would represent the resection borders correctly but would lead to straight areas instead of the curved surface of the orbital walls. Thus pre- and postoperative CT scans were necessary to display the resected area.

In the first step, the resected walls were generated as isolated files. The following workflow was used: pre- and postsurgical CT data were imported into iPlan Brainlab software and registered. Next the removed orbital walls were manually segmented with the brush tool on the presurgical data. Toggling between pre- and postsurgical CTs allowed us to define the exact resection borders. In cases of LARA, the space between the inner posterior border of the pre- and postsurgical position of the lateral orbital rim was measured. After adjusting the resection borders in the axial, coronal, and sagittal planes, the segmented walls were exported in STL file format.

Thus the exact anatomical configuration and size of the resected orbital walls was generated.

In the second step, the area was measured. As this is not possible in iPlan software, the following procedure was chosen. The STL files were imported into Facial Analysis Tool (FAT) software (Hierl et al., 2009) and the surface and borders of the segmented walls were slightly smoothed to counter the effect of manual segmentation (Figs. 2–4). Finally, the inner orbital areas of the removed walls were measured in FAT (all walls have an inner and outer surface). All measurements were made by one investigator. To check accuracy, 10 walls were calculated by a second investigator and compared. As this showed only minor differences of 0.1–0.2 cm<sup>2</sup> per wall, the accuracy was seen as clinically acceptable.

In addition to the above-mentioned measurements, the conformity of the preoperative resection plan and the result was checked by overlaying the resection borders on the postsurgical CT scan in iPlan software (Fig. 5).

Statistical analysis was performed with SPSS 14.0 (SPSS Inc., Chicago, IL, USA).

This retrospective study was approved by the Local Ethic Committee. This report followed the Declaration of Helsinki on medical protocol and ethics.

### 3. Results

The areas of 150 removed orbital walls were segmented and analyzed according to our workflow. There were 70 lateral orbital wall areas (35 right, 35 left), 64 orbital floor areas (32 right, 32 left), and 16 medial orbital wall areas (8 on both sites). Furthermore the additional effect of LARA was measured in 50 lateral walls (Table 2).

All wall areas showed a wide size range, depending on the individual anatomy (Table 2). The mean removed orbital wall area ranged between 6.2 cm<sup>2</sup> (medial), 6.7 cm<sup>2</sup> (inferior), and 6.9 cm<sup>2</sup> (lateral wall). Performing an additional lateral rim advancement (LARA) added 1.8 cm<sup>2</sup> in area increase. For the lateral orbital wall, this equaled 25% of the average lateral wall. Regarding the average area values, no statistically significant difference among the three orbital wall areas could be found.

After registration of the pre- and postsurgical CT data in iPlan software, the potential deviation between plan and result was analyzed. Here no major partial aberrations exceeding 1.5–2 mm in each direction could be found.

### 4. Discussion

Since the advent of orbital decompression surgery, a major goal has been to correlate surgery and its effects on proptosis reduction. Until now, this has focused on the statement of the number of removed walls. However, this statement does not give any information on the extent of removal of the appropriate wall and the real area of the resulting orbital expansion. Therefore this study was launched to define metrically the effects of decompression surgery. In addition, the resection borders were clearly defined. Thus our investigation allows, for the first time, the statement of the resected areas according to the defined resection borders. It seems probable that the size of the resected orbital wall area plays

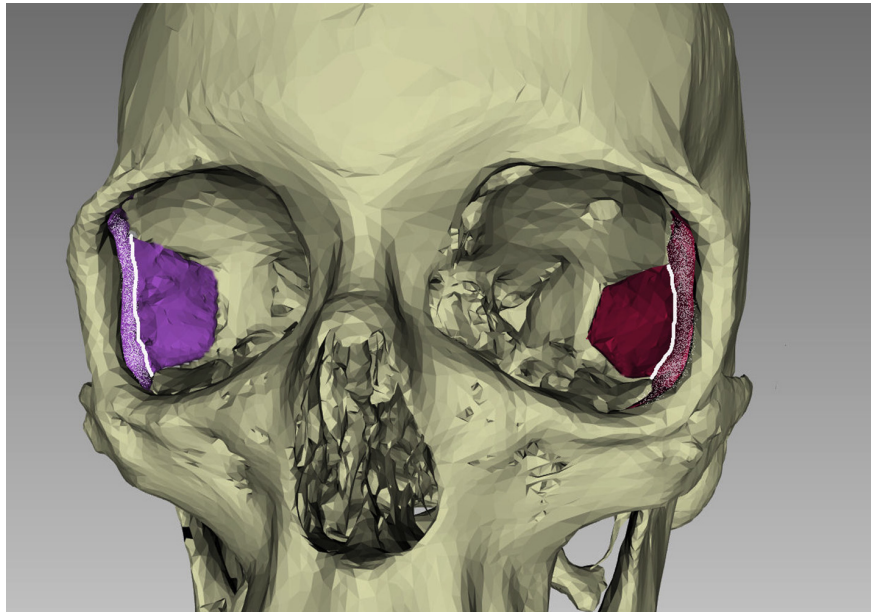


**Fig. 2.** Bilateral lateral orbital wall area (red and purple) with concomitant lateral rim advancement (LARA) displayed in Facial Analysis Tool (FAT) software. The additional anterior area after lateral rim advancement left is highlighted.

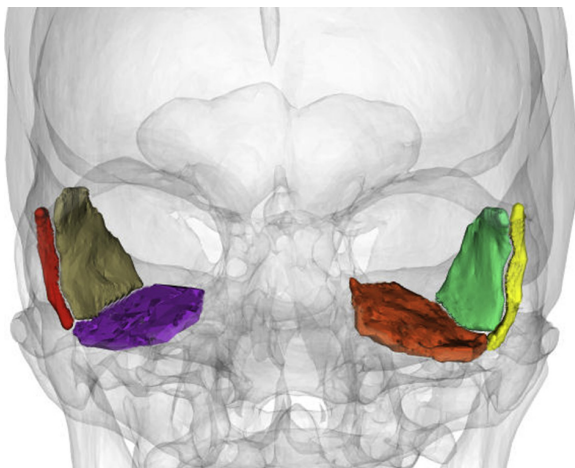


**Fig. 3.** Bilateral two-wall decompression with lateral rim advancement (LARA) in Facial Analysis Tool (FAT) software. The segmented, removed lateral orbital wall (brown, light green) and the inferior orbital wall (red, purple) on both sides are shown. The additional area after lateral rim advancement is marked in yellow on the left side and in red on the right side.

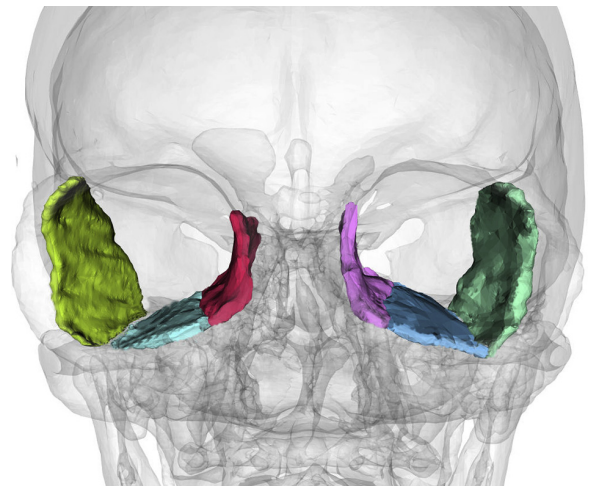


**Fig. 4.** Bilateral three wall decompression displayed in Facial Analysis Tool (FAT) software. The areas of lateral rim advancement (LARA) are not depicted for better vision of the lateral walls. This shows the large area of the orbital cavity removed in this procedure.

an important part regarding the postsurgical effects. Therefore this knowledge would be a necessary prerequisite for numerical simulations in orbital decompression surgery. [Luboz et al., \(2004\)](#) were the first to simulate the effect of decompression surgery via finite element analysis in a single patient. Besides the material parameters of the orbital tissues, the resected orbital wall area was a crucial variable to perform such a simulation. The authors considered a 2.9-cm<sup>2</sup> ostectomy as a large one and a 1.4-cm<sup>2</sup> decompression as a medium one. Compared to our measurements, these values seem quite small, as even the “large” decompression is less than 50% of our average resected area. This shows that quantitative data such as our findings are important and are required to simulate surgical outcome on a realistic basis. In addition to patient-specific

presurgical simulation, a further question is whether the size of the orbital wall removal would be a better variable comparing outcome reports than the statement of how many walls had been removed. For now this remains unclear.

This study can be seen as a basis for further investigations to elucidate the effects of decompression surgery in EO, which could potentially lead to an individualized predictable treatment plan. This, however, will work only if surgery is planned exactly and controlled intraoperatively. Here, intraoperative navigation is considered an ideal tool ([Lee et al., 2009](#); [Millar and Maloof, 2009](#); [Susarla et al., 2015](#); [Hierl et al., 2016](#)).

Even if the mean values for the resected walls are almost identical, the results show a wide spectrum depending on the



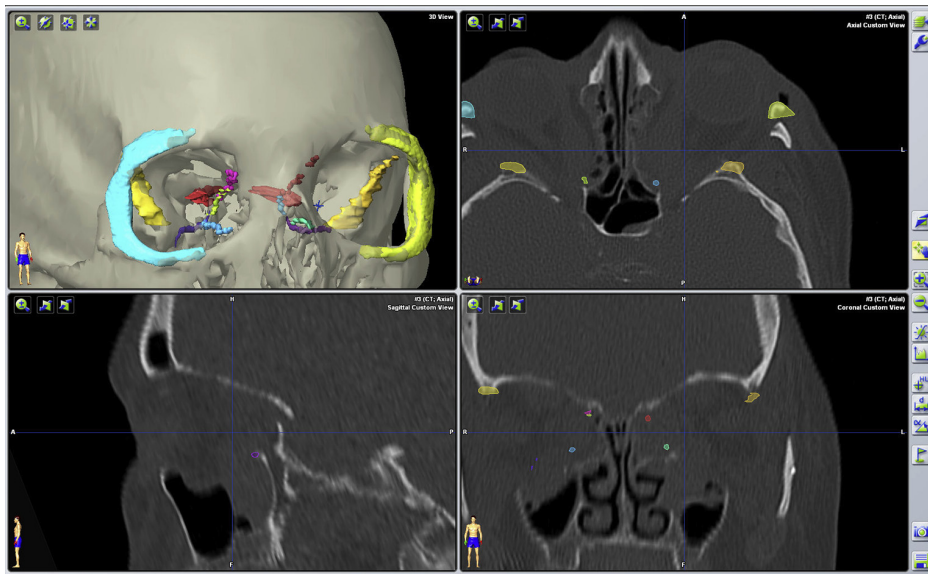


**Fig. 5.** Postoperative computed tomographic scan. The preoperative plan (resection borders and lateral rim advancement [LARA]) are overlaid after registration of pre- and postsurgical data. The examination shows that plan and surgical results match.

**Table 2**  
Results of measurements.

	Removed areas	
Lateral wall	6.9 cm <sup>2</sup> (4.9–11.8 cm <sup>2</sup> ; SD ± 1.8 cm <sup>2</sup> )	n = 70
Inferior wall	6.7 cm <sup>2</sup> (4.5–9.9 cm <sup>2</sup> ; SD ± 1.4 cm <sup>2</sup> )	n = 64
Medial wall	6.2 cm <sup>2</sup> (4.3–8.8 cm <sup>2</sup> ; SD ± 1.4 cm <sup>2</sup> )	n = 16
LARA	1.8 cm <sup>2</sup> (0.8–3.3 cm <sup>2</sup> ; SD ± 0.7 cm <sup>2</sup> )	n = 50

Average, standard deviation, and range for each resected orbital wall are stated. LARA, lateral rim advancement; SD, standard deviation.

individual anatomy. Thus the difference for the lateral wall can be 200% and it seems inappropriate to disregard the individual anatomy in defining the surgical treatment plan. Lateral orbital rim advancement according to Gonzales-Garcia et al. (González et al., 2008) increases lateral expansion area by 25% and is judged by the authors of this paper to be beneficial in anatomically “shallow” orbits.

## 5. Conclusion

This investigation describes, for the first time, the osteotomy size following surgery for endocrine orbitopathy in a larger patient group. These data are viewed by the authors as a valuable prerequisite for future patient-specific surgical simulation and planning. Furthermore, the metric definition of what has been done intra-operatively will be needed to compare outcome studies. Further work in this field will be needed, and should investigate additional variables such as the relation of removed orbital wall area to the total intra-orbital wall area and orbital volume.

## Funding

The development of the 3D analysis software (FAT) is partially funded by German Federal Ministry of Economics and Technology ZIM KF2036708SS0.

## Conflict of interest

The authors declare no conflicts of interest.

## References

- Bartalena L, Lai A, Compri E, Marocci C, Tanda ML: Novel immunomodulating agents for graves orbitopathy. *Ophthal Plast Reconstr Surg* 24(4): 251–256, 2008a
- Bartalena L, Pinchera A, Marocci C: Management of Graves' ophthalmopathy: reality and perspective. *Endocr Rev* 21(2): 168–199, 2000
- Bartalena L, Baldeschi L, Dickinson A, Eckstein A, Kendall-Taylor P, Marocci C, et al: Consensus statement of the European Group on Graves' orbitopathy (EUGOGO) on management of GO. *Eur J Endocrinol* 158: 273–285, 2008b
- Bonara P, Vannucchi G, Campi I, Rossi S, Cantoni F, Frugoni C, et al: Rituximab induces distinct intraorbital and intrathyroidal effects in one patient satisfactorily treated for Graves' ophthalmopathy. *Clin Rev Allergy Immunol* 34(1): 118–123, 2008
- Dollinger J: Die Druckentlastung der Augenhöhle durch Entfernung der äußeren Orbitawand bei hochgradigem Exophthalmos (Morbus Basedowii) und konsekutiver Hauterkrankung. *Dtsch Med Wochenschr* 37: 1888–1890, 1911
- González-García R, Sastre-Pérez J, Rodríguez-Campo FJ, Naval-Gías L, Monje F: C-modified osteotomy for bilateral advancement of the orbital rim in Graves orbitopathy: a technical note. *Int J Oral Maxillofac Surg* 37(9): 853–857, 2008
- Graham SM, Carter KD: Combined-approach orbital decompression for thyroid related orbitopathy. *Clin Otolaryngol Allied Sci* 24(2): 109–113, 1999
- Hierl T, Hümpfner-Hierl H, Kruber D, Gaebler T, Hemprich A, Wollny G: Requirements for a universal image analysis tool in dentistry and oral and maxillofacial surgery. In: Daskalaki A (ed.), *Dental computing and applications. Advanced techniques for clinical dentistry*. Hershey, London: IGI Global, 79–89, 2009
- Hierl T, Huempfner-Hierl H, Sterker I, Krause M: Decompression in endocrine orbitopathy with a navigated piezosurgical bone grinder. *Br J Oral Maxillofac Surg*. <http://dx.doi.org/10.1016/j.bjoms.2016.09.008>, 2016
- Holck DEE, Ng JD: Evaluation and treatment of orbital fractures: a multidisciplinary approach, 1st edn. Philadelphia: Elsevier Saunders, 3–8, 2005
- Kamer L, Noser HR, Schramm A, Hammer B, Kirsch E: A step towards individualized, anatomy-based surgical concepts for orbital decompression in Graves' orbitopathy. *Orbit* 28(4): 237–240, 2009
- Kirsch E, Hammer B, von Arx G: Graves' orbitopathy: current imaging procedures. *Swiss Med Wkly* 139(43–44): 618–623, 2009
- Lee KY, Ang BT, Ng I, Looi A: Stereotaxy for surgical navigation in orbital surgery. *Ophthal Plast Reconstr Surg* 25: 300–302, 2009
- Lee TJ, Kang MH, Hong JP: Three-wall orbital decompression in Graves' ophthalmopathy for improvement of vision. *J Craniofac Surg* 14(4): 500–503, 2003
- Leong SC, White PS: Outcomes following surgical decompression for dysthyroid orbitopathy (Graves' disease). *Curr Opin Otolaryngol Head Neck Surg* 18(1): 37–43, 2010
- Luboz V, Pedrono A, Ambard D, Boutault F, Payan Y, Swider P: Prediction of tissue decompression in orbital surgery. *Clin Biomech* 19: 202–208, 2004
- Millar MJ, Maloof AJ: The application of stereotactic navigation surgery to orbital decompression for thyroid-associated orbitopathy. *Eye* 23: 1565–1571, 2009
- Mourits MP, Bijl H, Altea MA, Baldeschi L, Boboridis K, Curró N, et al: Outcome of orbital decompression for disfiguring proptosis in patients with Graves

- orbitopathy using various surgical procedures. *Br J Ophthalmol* 93(11): 1518–1523, 2009
- Mourits MP, Koornneef L, Wiersinga WM, Prummel MF, Berghout A, van der Gaag R: Orbital decompression for Graves' ophthalmopathy by inferomedial, by inferomedial plus lateral, and by coronal approach. *Ophthalmology* 97(5): 636–641, 1990
- Schaefer SD, Soliemanzadeh P, Della Rocca DA, Yoo GP, Maher EA, Milite JP, et al: Endoscopic and transconjunctival orbital decompression for thyroid-related orbital apex compression. *Laryngoscope* 113(3): 508–513, 2003
- Susarla SM, Duncan K, Mahoney NR, Merbs SL, Grant MP: Virtual surgical planning for orbital reconstruction. *Middle East Afr J Ophthalmol* 22: 442–446, 2015
- Tavassol F, Kokemüller H, Müller-Tavassol C, Schramm A, Rücker M, Gellrich NC: A quantitative approach to orbital decompression in Graves' disease using computer-assisted surgery: a compilation of different techniques and introduction of the "temporal cage". *J Oral Maxillofac Surg* 70(5): 1152–1160, 2012
- Tessier P: [Surgical widening of the orbit. Orbits too small. Basedowexophthalmos. Exorbitisms of cranio-facial dysostosis. Congenital anophthalmia, microphthalmia. Orbital atresia of young enucleated eyes. Orbital tumors (angioma, meningioma, Recklinghausen)]. *Ann Chir Plast* 14(3): 207–214, 1969
- Wolfe SA: Modified three-wall orbital expansion to correct persistent exophthalmos or exorbitism. *Plast Reconstr Surg* 64(4): 448–455, 1979
- Wulc AE, Popp JC, Bartlett SP: Lateral wall advancement in orbital decompression. *Ophthalmology* 97(19): 1358–1369, 1990
- Zielinski CC, Weissel M, Müller C, Till P, Hofer R: Long-term follow-up of patients with Graves' orbitopathy treated by plasmapheresis and immunosuppression. *Dev Ophthalmol* 20: 130–138, 1989



## 2.7 Three-dimensional changes of scleral show after surgical treatment of endocrine orbitopathy

Neben dem Exophthalmus stellt der erweiterte Lidspalt mit dem ausgeprägten „scleral show“ (Zunahme der sichtbaren Sklera) ein Stigma der endokrinen Orbitopathie dar (Abbildung 2.15). Bisher ungeklärt war, inwieweit das durch die Dekompression erreichte Zurücksinken des Augapfels zu einer Verminderung des „scleral shows“ führt. Ziel war eine vollständige dreidimensionale Quantifizierung die in der folgenden Veröffentlichung auf Basis von optischen 3D-Scans erstmalig erfolgte.

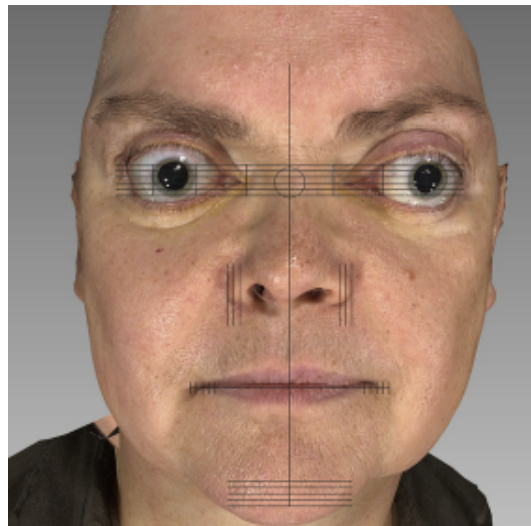


Abbildung 2.15: Darstellung einer an endokriner Orbitopathie leidenden Patientin mit Symmetrie-Schablone in FAT

Bei der folgenden Veröffentlichung wurde die dreidimensionale Oberfläche der sichtbaren Sklera prä- und postoperativ untersucht. Es wurde dabei ermittelt wie stark die Veränderungen der sichtbaren Fläche nach chirurgischer Dekompression bei Patienten mit endokriner Orbitopathie sind.

FAT wurde dabei wie folgt eingesetzt:

Markieren der Sklera im optischen 3D-Scan über Landmarken, nach Feinkorrektur Ausschneiden der Sklerafächen, Glätten der Oberfläche und Berechnung des Meßfehlers auf Grund der Einziehung im Bereich der Pupille

## Kapitel 2. FAT-Anwendungen

### Vergleich und Analyse komplexer Flächen

---

(die Pupille ist optisch durchsichtig und reflektiert Licht kaum, die übrige Sklera ist feucht was eine leichte Oberflächenunregelmäßigkeit im optischen Scan hervorruft).

In der nachfolgenden Abbildung 2.16 wird lediglich die Registrierung der Datensätze mit anschließender Analyse-Auswertung vereinfacht dargestellt. Die zusätzlich oben erwähnten Bearbeitungsschritte wurden nicht mit in der Darstellung berücksichtigt.

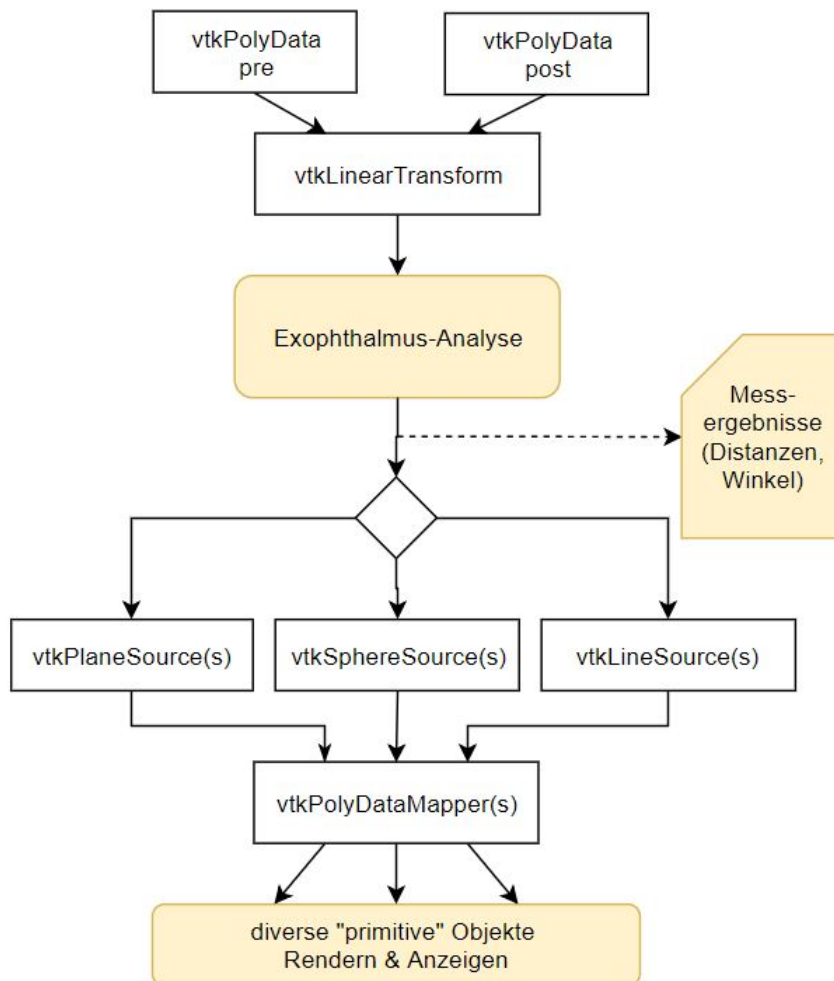
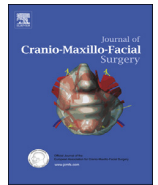


Abbildung 2.16: Workflow der Exophthalmus-Analyse mit Ausgabe der konstruierten Hilfsobjekte und Ergebnisse



Contents lists available at ScienceDirect

## Journal of Cranio-Maxillo-Facial Surgery

journal homepage: [www.jcmfs.com](http://www.jcmfs.com)

## Three-dimensional changes of scleral show after surgical treatment of endocrine orbitopathy



Matthias Krause<sup>a</sup>, Daniel Kruber<sup>a</sup>, Heike Hümpfner-Hierl<sup>a</sup>, Ina Sterker<sup>b</sup>,  
Thomas Hierl<sup>a,\*</sup>

<sup>a</sup> Department of Oral & Maxillofacial Plastic Surgery (Head: Alexander Hemprich MD DDS PhD), Leipzig University, Liebigstr. 12, 04103, Leipzig, Germany

<sup>b</sup> Department of Ophthalmology, Leipzig University, Liebigstr. 12, 04103, Leipzig, Germany

### ARTICLE INFO

#### Article history:

Paper received 13 June 2017

Accepted 24 October 2017

Available online 31 October 2017

#### Keywords:

Endocrine orbitopathy

Decompression

Scleral show

### ABSTRACT

**Purpose:** Surgery in endocrine orbitopathy should address exophthalmos and adjunct stigmata such as increased lid aperture and scleral show. Secondary to decompression, rehabilitative surgical treatment such as blepharoplasty is routinely used to achieve this goal. Until now, however, there has been no investigation to measure the effect of decompression surgery on scleral show and lid aperture 3-dimensionally.

**Materials and methods:** Ocular surface area (OSA) and lid aperture of 34 patients (67 orbits) were measured pre and post decompression surgery in a retrospective investigation using 3-dimensional (3D) stereophotogrammetry. The mean follow-up after decompression was  $6 \pm 4$  months.

**Results:** Mean OSA ranged between  $3.1 \pm 1.5$  cm<sup>2</sup> (pre orbital decompression) and  $2.5 \pm 0.6$  cm<sup>2</sup> (post orbital decompression). Orbital decompression caused a statistically significant reduction of the surface area of about 19.4% ( $p < 0.001$ ). Lid apertures showed average values between  $12.7 \pm 3.3$  mm (pre orbital decompression) and  $11.3 \pm 2.2$  mm (post orbital decompression). Thus orbital decompression led to a statistically significant reduction of the palpebral fissure of about 11% ( $p < 0.001$ ). OSA correlated with lid aperture pre and post surgery ( $p < 0.001$ ). The extent of OSA reduction showed no correlation with the amount of exophthalmos reduction.

**Conclusion:** Our results show that surgical decompression, besides correcting exophthalmos, leads to a significant reduction of scleral show and lid aperture. However, it is not possible to estimate its effect on an individual basis.

© 2017 European Association for Cranio-Maxillo-Facial Surgery. Published by Elsevier Ltd. All rights reserved.

### 1. Introduction

Endocrine orbitopathy (EO) is a complex inflammatory disorder and the main extrathyroidal manifestation of Graves' disease. Surgical rehabilitative treatment such as orbital decompression surgery, squint surgery or eyelid surgery is needed in the majority of patients when EO has been conservatively managed and inactivated by immunosuppressive treatment (Bartalena et al., 2016). This treatment follows the algorithm: orbital decompression is first addressed because of its influence on ocular motility and lid

position, followed by strabismus surgery, and, last, eyelid surgery. Upper and/or lower eyelid blepharoplasty is frequently needed as the last step for functional and esthetic rehabilitation (Barrio-Barrio et al., 2015).

The prediction of surgical outcome, however, is difficult (Kang et al., 2015). To prevent under- or overcorrection in eyelid surgery, it is important to analyze the eyelid contour and the scleral shape and area.

With the development of digital photography technology and software, the eyelid position can be analyzed more accurately. By now several studies have utilized a two-dimensional (2D) approach to measure lid contour and scleral show (Cruz et al., 1998, 2003; Cruz and Lucchezi, 1999; Koushan et al., 2008; Flynn et al., 2011; Milbratz et al., 2012; Nishihira et al., 2014; Prado et al., 2012; Lee et al., 2014; Kang et al., 2015; Tsai et al., 2012; Ahn et al., 2016; Zheng et al., 2016). 2D measurements, however, suffer from

\* Corresponding author. Department of Oral & Maxillofacial Plastic Surgery, Leipzig University, Liebigstr. 12, 04103, Leipzig, Germany.

E-mail addresses: [KrauseMa@medizin.uni-leipzig.de](mailto:KrauseMa@medizin.uni-leipzig.de) (M. Krause), [danielkruber@gmx.de](mailto:danielkruber@gmx.de) (D. Kruber), [heike.huempfer-hierl@gmx.de](mailto:heike.huempfer-hierl@gmx.de) (H. Hümpfner-Hierl), [Ina.Sterker@medizin.uni-leipzig.de](mailto:Ina.Sterker@medizin.uni-leipzig.de) (I. Sterker), [hiet@medizin.uni-leipzig.de](mailto:hiet@medizin.uni-leipzig.de) (T. Hierl).

inherent shortcomings such as changing camera positions, which cause distortions, and metrical calibration can be difficult. Furthermore, it is not possible to calculate spatial changes between two time points.

Therefore the purpose of this study was to measure the real 3-dimensional (3D) ocular surface area (OSA) (the OSA or palpebral fissure is defined as the area between the eyelids) in the treatment of patients with EO for the first time. Here 3D stereophotogrammetry provides an ideal, novel, non-invasive method which can be used for measuring and comparing surgery results (Nkenke et al., 2003; Hontscharuk et al., 2012; Mailey et al., 2016). Besides the absolute changes in OSA, 3D scanning would also allow investigation of whether OSA values would correlate with proptosis and its reduction.

## 2. Materials and methods

From 2010 to 2015, a total of 34 patients (67 orbits) with endocrine orbitopathy underwent surgery and were retrospectively evaluated by using the routinely acquired data. All patients who underwent surgery in this period were included. Surgical bony orbital decompression was planned and timed according to the recommendations of guidelines for the management of endocrine orbitopathy (Bartalena et al., 2016).

Surgery ranged from 1-wall to 3-wall decompression including lateral rim advancement in 61 orbits (1-wall decompression: 6 orbits, 2 walls: 47 orbits, 3 walls: 14 orbits) according to the procedure described earlier (Krause et al., 2017). Lateral rim advancement was performed in all bilateral decompression cases (González-García et al., 2008). In this procedure, the lateral, superolateral and infralateral orbital rim portions are detached during surgery, refixed with microplates at the superolateral and infralateral osteotomies, while the lateral rim pivots anteriorly (González-García et al., 2008; Krause et al., 2017). Thus the orbital depth is increased laterally. During surgery, the attachments of the lower lid were freed from the infraorbital rim, and no kanthopexy was performed. Instead, upper and lower lid were allowed to redrape freely after the transconjunctival suturing. Subcutaneous sutures were used only in the region of the lateral kanthotomy (not in the infraorbital region). After surgery, adhesive strips were fixed to the upper and lower lids for 1 week.

Criteria for decompression surgery were.

- Optic neuropathy with vision impairment (these were the cases with “non-pathologic presurgical exophthalmos values due to a non-existing auto-decompression by way of increased exophthalmos).
- Marked asymmetry in unilateral EO.
- Failed previous therapy and persisting proptosis. All patients had presurgical corticosteroid medication and thyroid surgery, 40% retrobulbar radiation therapy.

Surgery was performed according to the following standards: In all cases except unilateral exophthalmos, lateral rim advancement was performed. The criteria for 1- to 3-wall decompression were:

- 3-wall decompression in acute optic neuropathy with imminent vision loss.
- 1- to 2-wall decompression (lateral or lateral and inferior decompression) according to the amount of proptosis and the patient anatomy. If a proptosis reduction of more than 3–4 mm was needed, 2-wall surgery was chosen.
- All surgeries were planned in iPlan software (Brainlab Co.) with presurgical marking of the resection borders and utilizing intraoperative navigation.

All patients had optical facial 3D images taken with the Vectra M3 passive stereophotogrammetric system (Canfield Scientific Inc., Fairfield, NJ), which were used for this analysis. These scans were used for all measurements of exophthalmos and sclera replacing conventional Hertel or Naugle exophthalmometers. The system consists of 3 acquisition pods taking 9 images simultaneously. Scanning was performed with the patients sitting in repose on a motor-driven, height-adjustable stool. Natural head position was gained by looking in a mirror and at a fixation point marked between the pods. Patients were scanned before orbital decompression, after orbital decompression, and prior to further surgery which was used as the endpoint scan. To measure OSA and lid aperture, the following workflow was used: 3D stereophotogrammetry data were exported into OBJ-format from the Vectra system. Then they were imported into Facial Analyses Tool (FAT) software (Hierl et al. 2009). After import into FAT software, the ocular surface area (OSA) and the height between the two eyelids, i.e., the lid aperture, were measured (Figs. 1 and 2).

Measurement of OSA was performed by placing landmarks on the scleral–eyelid junction at a 1- to 2-mm distance. These were then connected to define the 3D area as a new object. FAT software allows different ways of area measurement such as marking the polygons of the palpebral fissure or encircling the area with a “lasso” function. Comparing these with the landmark-based procedure showed that this was the best method. Using landmarks, the polygons of the original surface mesh were cut according to the landmark position and the respective connecting line.

To define lid aperture, the optical scan was registered to a template (Fig. 3) to guarantee proper orientation. Then a grid template was created in FAT software which was projected parallel to the frontal plane (Fig. 2). By changing grid spacing, parallel vertical lines were created which allowed exact vertical landmark placing on the upper and lower eyelid borders. Next the distances between these landmarks were calculated.

Regarding optical scanning of the orbital fissure, 2 problems arise. First, liquid-covered surfaces such as the sclera cause light scattering which results in a non-smooth surface. Therefore single-use lenses could be used to create an even surface. As this could change the upper and lower lid positions, however, lenses were not inserted and the resulting slightly uneven surface was automatically smoothed in FAT software instead. The second problem is caused by the transparency of the lens, which creates a slight inward bulging of the central ocular surface. Again, this could be prevented by using non-transparent lenses with the problem of potential irritation and incorrect lid margins, or by software-based surface correction. When the original surface area was compared to the corrected surface, a uniform 0.1- to 0.09-cm<sup>2</sup> difference was seen. In relation with our measurements, this would account for a constant 3% area difference. In this study, the original (uncorrected) values were used.

In addition to the measurement of absolute OSA and lid aperture values, we studied pre- and postsurgical symmetry. Therefore the larger value of both eyes was divided by the smaller one before and after decompression to generate an asymmetry score. Values ranging between 1 and 1.1 were classified as score 1, 1.2 as score 2, and larger than 1.2 as 3.

Finally, we wanted to correlate OSA and lid aperture to the extent of pre-surgical exophthalmos and potential OSA changes to proptosis reduction. Correlating OSA and lid aperture changes to surgical procedures would not have been possible due to the small number of each procedure. Therefore the reduction of proptosis was taken as the relevant variable, as it is reasonable to suppose that the change in globe position would affect lid position and not bony changes within the bony orbital cavity.

To define pre-existing exophthalmos and its decrease, the optical 3D scans were used instead of manual devices. As lateral rim



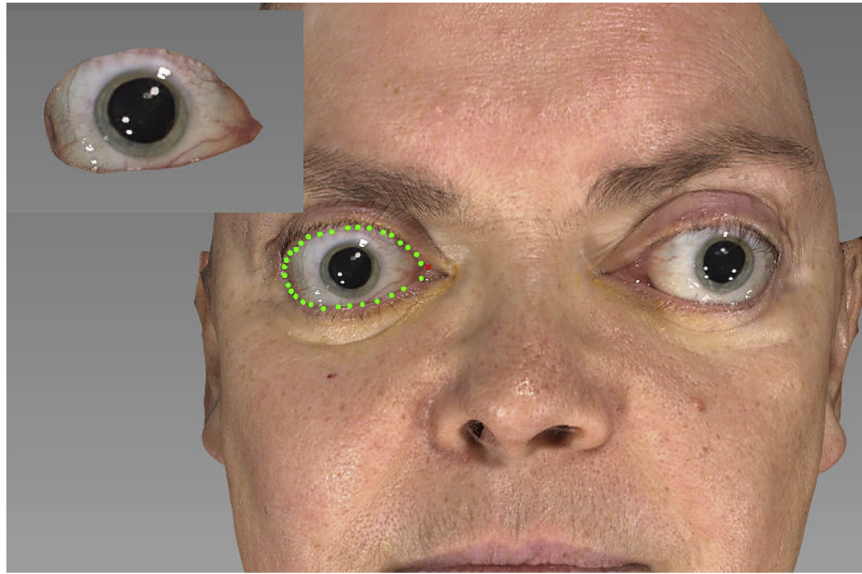


**Fig. 1.** Measurement of ocular surface area (OSA) using FAT software. The scleral area has been digitized by placing landmarks. The inset shows the cut scleral area.

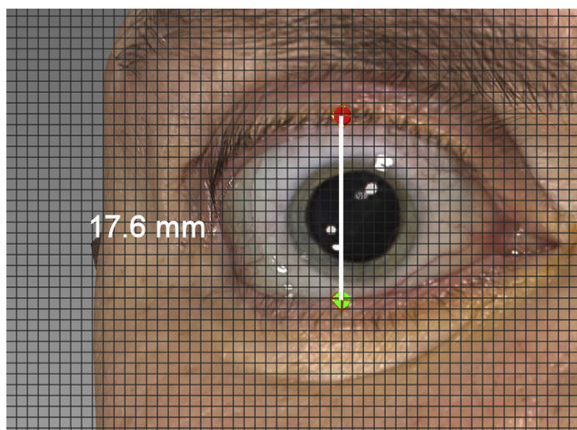


**Fig. 2.** Measurement of lid aperture. A metric grid is projected on the 3D scan after registration; thus the landmarks can be properly placed.

advancement was performed in most orbits, postsurgical values using a Hertel exophthalmometer would have been misleading, as the lateral orbital rim position was changed during surgery. Therefore a 3D cephalometric analysis was implemented in FAT software, which exactly matched the definition of the Hertel exophthalmos value to permit comparison with previous studies. The results of this 3D analysis served as the preoperative exophthalmos evaluation. Next the pre-to postsurgical changes in proptosis were calculated without referring to the changing lateral rim position (Fig. 4). This was achieved by registration and superimposition of the pre- and postsurgical optical scans. Here non-changing surfaces such as the forehead and nose were utilized. After superimposition, the presurgical reference was used on the postsurgical scans to measure the new value of proptosis and subsequently its decrease.

Statistical analysis was performed with SPSS 14.0 (Statistic Package for the Social Sciences; SPSS Inc., Chicago, IL, USA). Concerning statistical evaluation, we decided not to combine the left and right sides to achieve higher numbers, but to evaluate both sides individually.

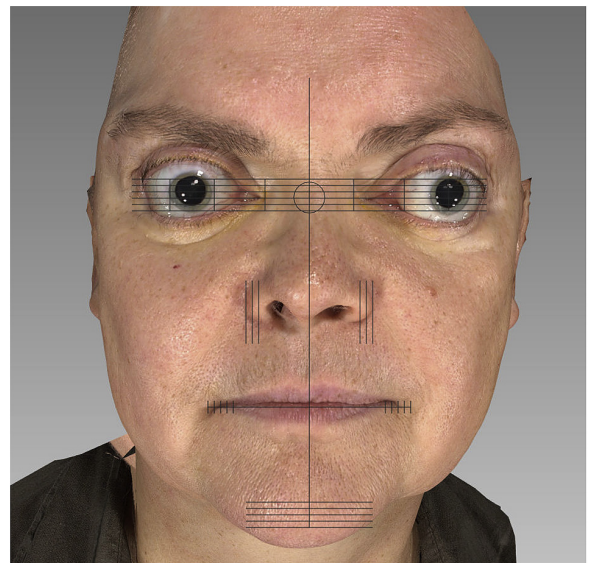


**Fig. 3.** Scan registration prior to measuring lid aperture. A registration template ensures proper orientation to permit exact lid measurements.

This retrospective study was approved by the Local Ethic Committee and followed the Declaration of Helsinki on medical protocol and ethics.

### 3. Results

OSA and lid apertures of 67 orbits (33 right orbits, 34 left orbits) were analyzed pre and post orbital decompression according to the above-mentioned workflow.

The mean patient age was 51.0 years (range 31–76,  $51.0 \pm 8.6$ ) and the group consisted of 24 women (71%) and 10 men (29%). Eight patients (23.5 %) had dysthyroid optic neuropathy.

The mean follow up was  $6.2 \pm 3.9$  months after surgical decompression. A longer follow-up period would have been





**Table 2**

Asymmetry evaluation concerning ocular surface area (OSA) and lid aperture (LA).

	OSA AS mean	OSA AS 1 (1.0-1.1)	OAS AS 2 (1.2)	OSA AS 3 ( $\geq 1.3$ )
pre-surgery	1.1 $\pm$ 0.2	23	4	6
postsurgery	1.1 $\pm$ 0.2	27	2	4
	LA AS mean	LA AS 1 (1.0-1.1)	LA AS 2 (1.2)	LA AS 3 ( $\geq 1.3$ )
pre-surgery	1.1 $\pm$ 0.1	25	7	1
postsurgery	1.1 $\pm$ 0.1	25	7	1

An asymmetry score (AS) was created by dividing the larger value of both eyes by the smaller one. Although the number of more pronounced asymmetry in OSA decreased, no statistical significant changes were seen.

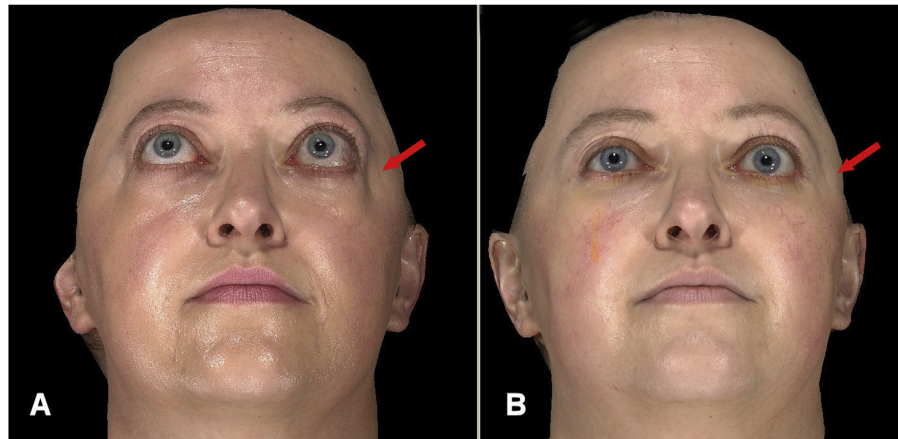


**Fig. 5.** Comparison of presurgical (A) and postsurgical (B) optical scans in a patient. After a bilateral 2-wall decompression including the lateral and inferior walls, a distinct reduction in proptosis and ocular surface area (OSA) is seen. On the left side, which presented with a larger OSA preoperatively, adjunct lid surgery is still needed. Red arrows highlight the effect of lateral rim advancement, as the presurgical skin retraction is leveled due to the forward rotation of the lateral rim.

**Table 3**

Statistical results in study patients.

		LA pre	Pro pre	Test
OSA pre	R	p < 0.001; r = 0.942	p = 0.02; r = 0.396	2
	L	p < 0.001; r = 0.905	p = 0.02; r = 0.396	2
OSA post	R	<b>LA post</b> p < 0.001; r = 0.952	<b>Pro post</b> p = 0.15; r = 0.253	2
	L	p < 0.001; r = 0.930	p = 0.04; r = 0.352	2
OSA change	R	<b>Pro change</b> p = 0.79; r = -0.46	<b>OSA change L</b> p < 0.001; r = 0.631	2
	L	p = 0.82; r = -0.4		2
Pro change R		<b>Pro change L</b> p < 0.001; r = 0.867		2
OSA pre	R	<b>OSA post</b> p < 0.001		1
	L	p < 0.001		1
LA pre	R	<b>LA post</b> p < 0.001		1
	L	p < 0.001		1

OSA: ocular surface area; LA: lid aperture; pre: before decompression surgery; post: after surgery; R: right side; L: left side; r: Pearson correlation coefficient. Tests: 1: paired Student test; 2: Pearson correlation analysis.

OSA values in 3D using stereophotogrammetry, and it is the first such study regarding EO patients.

The results show that decompression surgery is an effective means to reduce scleral show in EO in most of our patients. Furthermore, our results indicate that increased scleral show accompanies increased exophthalmos preoperatively. Interestingly, the amount of OSA reduction did not correlate with the extent of proptosis reduction. Possible causes relating to the surgical procedure were that the soft tissue was allowed to redrape freely and no fixation sutures were used. Our surgical procedure, which includes an anterior swiveling of the total lateral orbital rim (Krause

et al., 2017), may further contribute to the measured effect of OSA decrease, as the more anteriorly positioned mediolateral infraorbital and lateral orbital rim could provide better support for the soft tissues of the lower lid. As our patient group without lateral rim advancement is small, a statistical analysis was not possible.

Regarding asymmetry of scleral show, a tendency toward increased asymmetry was seen. Pre-existing marked asymmetry was reduced in some cases but tended to persist as OSA was reduced in both sides. This is demonstrated in the patient example in Fig. 5. Concerning lid aperture, no changes in symmetry were seen. One explanation is that OSA is most pronounced in the lateral

scleral aspect (lateral flaring) and not in the central aspect where lid aperture is measured.

The study results suggest an individualized staged procedure as proposed within the known guidelines (Bartalena et al., 2016). Thus patients can be informed that there is a strong possibility that scleral show will decrease due to decompression surgery, but that, as the exact outcome cannot be foreseen, ancillary surgery might still be needed. As no values of “normal” OSA are known to the authors at this point, only lid aperture values can be used to define the patient group, in which “normal” scleral values were reached after EO surgery (i.e. the group that benefited not only regarding proptosis but changed from pathological scleral show to non-pathological values). Here almost 19% of all orbits (34 orbits pre surgery, 46 orbits post surgery) showed this improvement if the 12-mm threshold is used. Although Hontscharuk et al. suggested optical 3D scanning to measure OSA and lid aperture and reported on a study on 26 patients, they did not state any absolute values; only differences between both sides were given and correlated with a disfigurement questionnaire. Furthermore, their values regarding OSA asymmetry are difficult to understand, as the authors stated an absolute asymmetry of OSA area in a control group to be 0.22 mm, which relates to a distance and not an area. Thus our findings cannot be compared with theirs.

OSA and lid aperture showed a high correlation, which was not surprising. Although lid aperture is easier to calculate, we think that OSA is an important variable for future investigations, as OSA includes features such as lateral scleral show, which is missed in singular lid aperture measurements.

3D measurements appear to be a noninvasive, easy-to-perform means to investigate OSA and lid changes. Calibration is not needed; errors due to improper photography techniques are nonexistent and pre and postsurgical 3D scans can be registered, allowing even more detailed investigations. With our proposed steps to minimize the inherent problems of optical 3D measurements of the sclera and lens, technical errors are small. Our results can be seen as a first step toward exact data acquisition concerning upper and lower lid position and contour and potential changes caused by different surgical procedures in EO. Future investigations will deal with the effects of blepharoplasty and lid procedures and will compare the results to values in non-EO patients. Furthermore our workflow permits the analysis of changes in lid contour 3-dimensionally. This will show to which extent upper and lower lid changes contribute to OSA changes, and the results may influence our surgical procedures.

## 5. Conclusion

The results of this investigation demonstrate that most patients benefit not only from proptosis reduction but also from OSA improvement after EO decompression surgery. As a prediction on the amount of improvement was not possible, a staged procedure in rehabilitative surgery in EO seems adequate. Optical 3D scanning proved to be an effective means in data acquisition, as it allowed exact proptosis measurement and comparison even in cases in which the bony orbit was changed.

## Conflict of interest

The authors declare no conflicts of interest.

## Acknowledgements

The development of the 3D analysis software (FAT) is partially funded by German Federal Ministry of Economics and Technology ZIM KF2036708SS0.

## References

- Ahn S, Lee H, Lee J, Park J, Park M, Baek S: Analysis of surgical outcome after levator advancement by assessing changes in eyelid contour. *J Craniofac Surg* 27: 1147–1150, 2016
- Barrio-Barrio J, Sabater AL, Bonet-Farriol E, Velázquez-Villoria A, Galofré JC: Graves Ophthalmopathy: VISA versus EUGOGO classification, assessment, and management. *J Ophthalmol* 16: 1–16, 2015
- Bartalena L, Baldeschi L, Borborides K, Eckstein A, Kahaly GJ, Marcocci C, et al: European Group on Graves Orbitopathy (EUGOGO). The 2016 European Thyroid Association/European Group on Graves Orbitopathy guidelines for the management of Graves' orbitopathy. *Eur Thyroid J* 5: 9–26, 2016
- Cruz AA, Lucchezi MC: Quantification of palpebral fissure shape in severe congenital blepharoptosis. *Ophthal Plast Reconstr Surg* 15: 232–235, 1999
- Cruz AA, Coelho RP, Baccaga A, Lucchezi MC, Souza ADA, Ruiz EESI: Digital image processing measurement of the upper eyelid contour in Graves disease and congenital blepharoptosis. *Ophthalmology* 105: 913–918, 1998
- Cruz AA, Akaishi PM, Coelho RP: Quantitative comparison between upper eyelid retraction induced voluntarily and by Graves orbitopathy. *Ophthal Plast Reconstr Surg* 19: 212–215, 2003
- Farkas LG: Anthropometry of the head and face. New York, NY: Raven Press, 1994
- Flynn TH, Rose GE, Shah-Desai SD: Digital image analysis to characterize the upper lid marginal peak after levator aponeurosis repair. *Ophthal Plast Reconstr Surg* 27: 12–14, 2011
- González-García R, Sastre-Pérez J, Rodríguez-Campo FJ, Naval-Gías L, Monje F: C-modified osteotomy for bilateral advancement of the orbital rim in Graves orbitopathy: a technical note. *Int J Oral Maxillofac Surg* 37: 853–857, 2008
- Hierl Th, Hümpfner-Hierl H, Kruber D, Gäbler Th, Hemprich A, Wolny G: Requirements for a universal image analysis tool in dentistry and oral and maxillofacial surgery. In: Daskalaki A (ed.), *Dental computing and applications. Advanced techniques for clinical dentistry*. Hershey, London: IGI Global, 79–89, 2009
- Hontscharuk R, Fialkov JA, Binhammer PA, McMillan CR, Antonyshyn O: Primary orbital fracture repair: development and validation of tools for morphologic and functional analysis. *J Craniofac Surg* 23: 1044–1049, 2012
- Kang D, Lee J, Park J, Lee H, Park M, Baek S: Analysis of lid contour in thyroid eye disease with upper and lower eyelid retraction using multiple radial midpupil lid distances. *J Craniofac Surg* 27: 134–136, 2015
- Koushan K, Skibell BC, Harvey JT, Jankowski HK, Deangelis DD, Oestreicher JH: Digital photography as a novel technique of measuring ocular surface dimensions. *Orbit* 27: 259–265, 2008
- Krause M, Hümpfner-Hierl H, Kruber D, Sterker I, Hierl T: Calculation of resected orbital wall areas in the treatment of endocrine orbitopathy. *J Craniomaxillofac Surg* 45: 485–490, 2017
- Lee H, Lee JS, Chang M, Park M, Baek S: Analysis of lid contour change with aging in Asians by measuring midpupil lid distance. *Plast Reconstr Surg* 134: 521e–529e, 2014
- Mailey B, Baker JL, Hosseini A, Collins J, Suliman A, Wallace AM, et al: Evaluation of facial volume changes after rejuvenation surgery using a 3-dimensional camera. *Aesthet Surg J* 36: 379–387, 2016
- Milbratz GH, Garcia DM, Guimarães FC, Cruz AA: Multiple radial midpupil lid distances: a simple method for lid contour analysis. *Ophthalmology* 119: 625–628, 2012
- Nishihira T, Ohjimi H, Eto A: A new digital image analysis system for measuring blepharoptosis patients' upper eyelid and eyebrow positions. *Ann Plast Surg* 72: 209–213, 2014
- Nkenke E, Benz M, Maier T, Wiltfang J, Holbach LM, Kramer M, et al: Relative end- and exophthalmometry in zygomatic fractures comparing optical non-contact, non-ionizing 3D imaging to the Hertel instrument and computed tomography. *J Craniomaxillofac Surg* 31: 362–368, 2003
- Prado RB, Silva-Junior DE, Padovani CR, Schellini SA: Assessment of eyebrow position before and after upper eyelid blepharoplasty. *Orbit* 31: 222–226, 2012
- Tsai PY, Wu YC, Lai CH, Huang SH, Lai YW, Lai CS: Ocular surface area changes after double eyelid-plasty. *J Plast Reconstr Aesthet Surg* 65: e141–e145, 2012
- Zheng X, Kakizaki H, Goto T, Shiraishi A: Digital analysis of eyelid features and eyebrow position following CO<sub>2</sub> laser-assisted blepharoptosis surgery. *Plast Reconstr Surg Glob Open* 4: 1–6, 2016

## 2.8 Weitere Einsatzgebiete

Weitere Anwendungsbereiche von FAT sind in Abbildung 2.17 zu sehen. Die dort farbkodierte Darstellung zeigt eine beispielhafte automatische Weichteildicken-Messung eines männlichen Probanden, was z. B. für die plastische Chirurgie oder biomechanische Fragestellungen von Bedeutung ist.

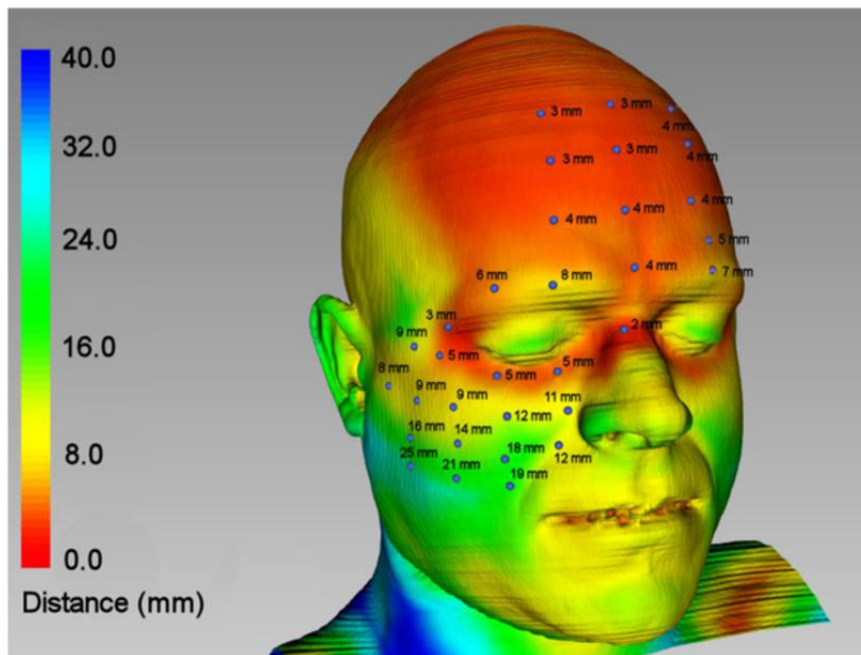


Abbildung 2.17: farbkodierte Weichteildicken-Messung

Ein weiteres Einsatzgebiet liegt in der Konstruktion von Pilotschablonen auf der Basis medizinischer Bilddaten, die dann im Rapid Prototyping Verfahren hergestellt werden können. Beispielhaft wird das am ersten Einsatz einer Pilotschablone für die Kiefergelenkarthroskopie dargestellt. Hierfür wurde ein optischer 3D-Gesichtsscan mit einer Cone-Beam CT-Aufnahme registriert und anschließend die Trajektorien für den oberen und unteren Gelenkspalt berechnet. Hiernach wurde eine auf nicht verschieblichen Hautarealen verankerte Schablone generiert. [KKD<sup>+</sup>18]



## Einsatz einer digital erstellten Pilotschablone für die minimalinvasive Chirurgie des Kiefergelenkes

Matthias Krause<sup>1</sup>, Daniel Kruber<sup>1</sup>, Hans-Martin Dörfler<sup>2</sup>, Alexander Hemprich<sup>1</sup>, Heike Hümpfner-Hierl<sup>1</sup>, Thomas Hierl<sup>3</sup>

<sup>1</sup>Klinik und Poliklinik für Mund-, Kiefer- und Plastische Gesichtschirurgie, UKL Leipzig AöR

<sup>2</sup>Hochschule für Technik, Wirtschaft und Kultur, Leipzig

<sup>3</sup>Klinik und Poliklinik für Mund-, Kiefer-, Gesichtschirurgie/Plastische Operationen, Helios Vogtland-Klinikum Plauen

### Fragestellung

• Die minimalinvasive Chirurgie des Kiefergelenkes hat sich als erfolgversicheres Verfahren in der Behandlung von Kiefergelenkerkrankungen etabliert und wurden erstmals von Onishi [1] und Murakami [2] beschrieben.

• Anspruchsvoll ist die komplexe Anatomie (Abb.1), eine kleine, obere Gelenkhöhle und Indikationen, die sich bei nur 10% der Patienten mit Kiefergelenksbeschwerden stellen [3].

• Aus diesen Gründen werden in der Literatur navigierte Vorgehensweisen gefordert [4].

• Ziel dieser Studie war es zu prüfen, ob eine schienengeführte Navigation, in Form einer digital erstellten Pilotschablone, die minimalinvasiven Zugänge zum Kiefergelenk erleichtert.

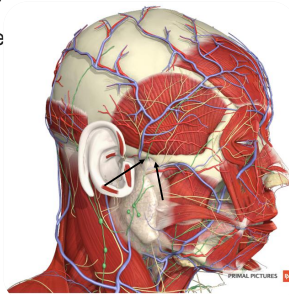


Abb.1: Anatomie des Kiefergelenkes mit Zugangswegen (schwarze Pfeile)

### Methoden

• Die Erstellung ist ein rein digitaler Workflow. Es werden die aus der Diagnostik vorhandenen digitalen Volumentomographien (DVT) – Datensätze des Patientenschädels (Kodak 9500 3D, Carestream Health, Toulouse, France) mit optischen Oberflächenscans der Gesichtsregion incl. des Ohres (Vectra® M3, Canfield Scientific Inc., Fairfield, USA) benutzt um eine digitale Schablone mit Führungshülsen im STL - Format im Facial Analyses Tool [5] zu erstellen (Abb. 2).

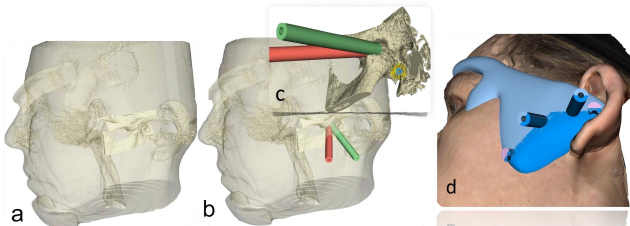


Abb. 2: Überlagerung der Datensätze (a), Platzierung der Hülsen (b), in der Vergrößerung (c) und die druckfähige, geteilte Schablone (d) im FAT

• Es folgt der 3D – Druck (Formlab 2 Drucker, Formlabs Inc., Somerville, USA) mit einem CE-zertifizierten Kunststoff.

### Ergebnisse

• Vom März 2017 – April 2018 wurden 3 Patienten mit chronischen Kiefergelenksbeschwerden, nach erfolgloser konservativer Vorbehandlung, insgesamt 3x arthroskopisch - chirurgisch und 3x durch Arthrozentese mit Hilfe der digital erstellten Pilotschablone behandelt (Tab. 1).

Tabelle 1: Tabellarische Darstellung der behandelten Patienten (n=3)

Nr.	Geschl.	Alter	Diagnose	OP-Datum	Therapie	Komplikationen
1	w	53	ID, Ws V, KG L	27.03.2017 13.10.2017	ASK, Lavage, Shaving, 10 mg TrimaHEXAL® (HEXAL AG) ASK, Lavage, Shaving, 10 mg TriamHEXAL® (HEXAL AG)	keine keine
2	w	44	ID, Ws V, KG R	27.04.2018	ASK, Lavage, Shaving, 10 mg TriamHEXAL® (HEXAL AG)	keine
3	m	75	ID, Ws IV, KG R	27.04.2017	AZ, Lavage, 1,5ml Hya Ject® (ORMED GmbH)	keine
				11.05.2017	AZ, Lavage, 1,5ml Hya Ject® (ORMED GmbH)	keine
				12.06.2017	AZ, Lavage, 1,5ml Hya Ject® (ORMED GmbH)	keine
		57,3				

ID - internal derangement n. Wilkes [6], Ws - Wilkes Stadium I - V, KG - Kiefergelenk, ASK - Arthroskopie, AZ – Arthrozentese

• Um jederzeit ein Umsteigen von der schablonengeführten Endoskopie zur konventionellen Vorgehensweise zu garantieren, hat sich die Teilung der Schablone bewährt, so dass sie intraoperativ entfernt werden kann. Abb.3,4 zeigen diese Schablone.

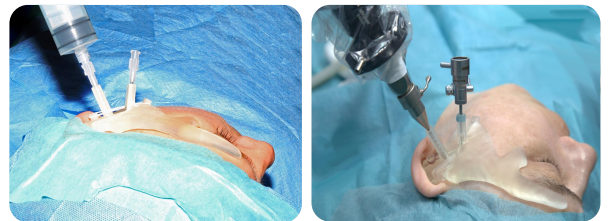


Abb.3: Intraoperative Darstellung der Pilotschablone mit AZ (links), ASK (rechts)

### Zusammenfassung

• Die digital erstellte, geteilte Pilotschablone (Abb. 4) ist als eine Form der schienengeführten Navigation anzusehen.

• Sie erleichtert bei Arthroskopie oder Arthrozentese minimalinvasive Zugänge zum Kiefergelenk.

• Die Teilung der Schablone hat sich bewährt.



Abb. 4: Die geteilte Pilotschablone

### Literatur

- [1] Onishi M. (1975) Arthroscopy of the temporomandibular joint. Kokubyo Gakkai Zasshi 42: 207–13
- [2] Murakami K, Ono T. (1986) TMJ arthroscopy by inferolateral approach. Int J Oral Maxillofac Surg 15: 410–7.
- [3] Smolka W. (2008) Efficiency of arthroscopic lysis and lavage for internal derangement of the temporomandibular joint correlated with Wilkes classification. Oral Surg Oral Med Oral Pathol 106: 317-23
- [4] González-García R. (2015) The Current Role and the Future of Minimally Invasive Temporomandibular Joint Surgery. Oral Maxillofacial Surg Clin N Am 27: 69–84
- [5] Hierl Th, Hümpfner-Hierl H, Kruber D, Gäbler Th, Hemprich A, Wollny G. (2009) Requirements for a universal image analysis tool in dentistry and oral and maxillofacial surgery. In: Daskalaki A.: Dental Computing and Applications. Advanced techniques for clinical dentistry. Hershey, London, IGI Global, pp 79-89
- [6] Wilkes CH. (1989) Internal derangements of the temporomandibular joint. Pathological variations. Arch Otolaryngol Head and Neck Surg 115: 469-47

Kontakt: KrauseMa@medizin.uni-leipzig.de



### 3. Ausblick

Anhand der oben aufgeführten Möglichkeiten, die FAT bisher bietet, können zukünftige Fragestellungen betrachtet werden. Hierbei wäre es denkbar den Ansatz der statistisch-anatomischen Modelle aufzugreifen, um beispielsweise schon präoperativ zu entscheiden, welches präformierte Implantatmaterial für einen bestimmten Eingriff am besten geeignet sein könnte.

Weiterhin stellen sich im Bereich der Operationssimulation eine Vielzahl interessanter Ansätze, die z. Zt. in Entwicklung sind. Darunter zählt beispielhaft die in Abbildung 3.1 und Abbildung 3.2 veranschaulichte OP-Simulation zur ästhetischen Gesichtskorrektur.

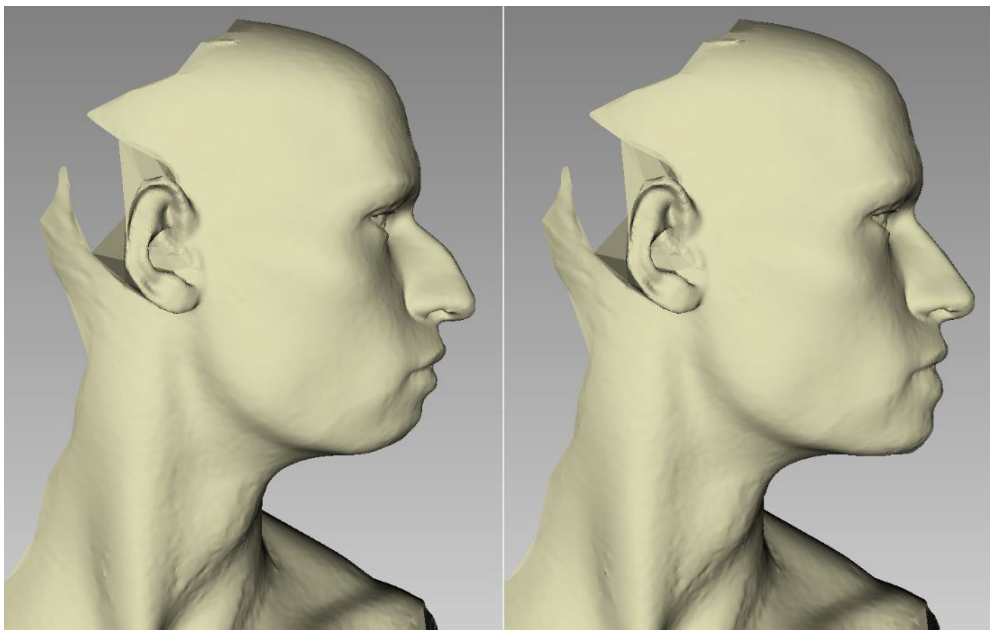


Abbildung 3.1: Exemplarische OP-Simulation – Prä - Post

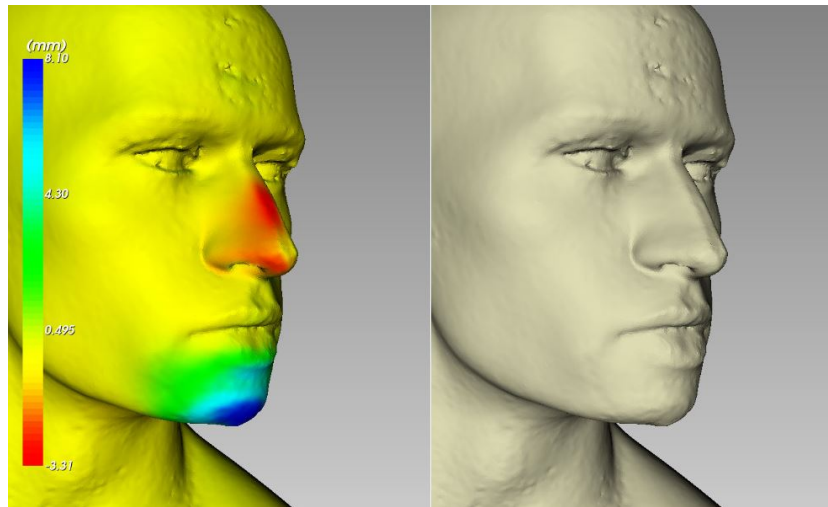


Abbildung 3.2: Visuelle und metrische Darstellung der veränderten Bereiche

In diesem Zusammenhang stellt auch die Option, Osteosynthesmaterialien virtuell an die jeweilige Knochenoberfläche anzupassen (Abbildung 3.3) eine interessante Neuentwicklung dar, die zum Zeitpunkt ebenfalls in FAT implementiert wird.

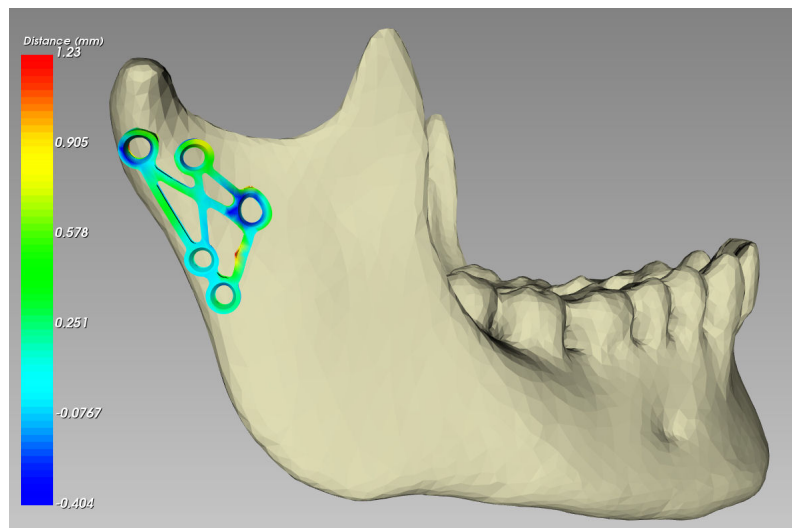


Abbildung 3.3: das Osteosynthese-Implantat wird automatisch an die knöcherne Unterlage angepasst – die Farbwerte zeigen die Verformung metrisch an

# 4. Zusammenfassung der Arbeit

Dissertation zur Erlangung des akademischen Grades  
Dr. rer. med.

## **Eine auf VTK basierende Analyse-Software zur Untersuchung der Orbita und des Mittelgesichts**

ingereicht von:  
Daniel Kruber, Dipl. Inf. (FH)

angefertigt an der:  
Klinik und Poliklinik für Mund-, Kiefer- und Plastische Gesichtschirurgie;  
Universitätsklinikum Leipzig AöR

betreut von:  
Prof. Dr. med. Dr. med. dent. Thomas Hierl  
Prof. Dr. med. Dr. med. dent. Alexander Hemprich

Juni 2018

Die bisher kommerziell erhältlichen Programme zur Analyse von medizinischen Bilddaten werben mit vielfältigen Messfunktionen, verfügen jedoch häufig nur über vordefinierte Strecken-, Symmetrie-, Winkel- und Flächenmessungen. Dies bedeutet, dass sie für viele neue Fragestellungen nur bedingt lösungstauglich sind. Die hier vorgestellte, modular erweiterbare Softwareumgebung FAT erlaubt die exakte Bemaßung und Bearbeitung dreidimensionaler medizinischer Bilddaten und beinhaltet zudem Konstruktionswerkzeuge aus dem CAD-Bereich. Wie anhand der in dieser Arbeit präsentierten Fragestellungen und deren Lösung gezeigt werden konnte, stellt FAT eine wertvolle Bereicherung der medizinischen Bildbearbeitungssoftware dar und wurde in verschiedenen Projekten erfolgreich eingesetzt.

Beginnend mit einer intraoperativen Hilfsschablone konnte gezeigt werden, wie die kephalometrische Analyse im FAT den Anwender zielführend Unterstützung liefert. Darauf aufbauend konnten weitere Behandlungsmöglichkeiten betrachtet und realisiert werden. Neben der umfangreichen dreidimensionalen Analyse-Funktion trugen auch Registrieralgorithmen und Vergleichsmethoden dazu bei, die in den Studien vorgestellten Probleme zu lösen. Bei der Versorgung von Orbitawandfrakturen wurde die Entwicklung eines statistisch-anatomischen Modells in Form eines Stempels vorgestellt. Dieser ermöglicht eine kostengünstige Versorgung ohne sich dabei auf ein entsprechendes Implantatmaterial festlegen zu müssen.

Durch die daraus neu entwickelte Stempelform führten Experimente mit PDS-Folien zu neuen Erkenntnissen und erleichterten das Anbiegen an die komplexe Geometrie des Orbitabodens. Im weiteren Verlauf wurden der Exophthalmus, die Größe der Orbitawände und der erweiterte Lidspalt bei der endokrinen Orbitopathie mittels FAT analysiert. Es konnte gezeigt werden, welche Einflussgrößen relevant sind und wie die Veränderungen nach dem operativen Eingriff ausfallen. Weiterhin werden aktuelle Entwicklungen und deren mögliche klinische Nutzung aufgezeigt.

Auf Grund der Verwendung des auf VTK beruhenden „Baukastensystems“ ist eine kurzfristige Anpassung an aktuelle Fragestellungen jederzeit umsetzbar, was als Vorteil der gewählten Softwarekonzeption angesehen wird. Da zur Zeit noch keine Zertifizierung als Medizinprodukt vorliegt, ist ein breiter klinischer Einsatz außerhalb von Studien jedoch noch nicht möglich.

# Literaturverzeichnis

- [Bla92] BLAUSTEIN D.I., HEFFEZ L. B.: Arthroscopic atlas of the temporomandibular joint. In: *Journal of Oral and Maxillofacial Surgery* 50 (1992), Nr. 6, S. 657. [http://dx.doi.org/10.1016/0278-2391\(92\)90466-D](http://dx.doi.org/10.1016/0278-2391(92)90466-D). – DOI 10.1016/0278-2391(92)90466-D. – ISSN 02782391
- [Bri] BRINKMEYER, Heiko: *Optische 3D-Analyse an Gesichtern von Patienten mit Lippen-, Kiefer-, Gaumenspalte*. Leipzig, (Dissertation)
- [Das09] DASKALAKI, Andriani (Hrsg.): *Dental computing and applications: Advanced techniques for clinical dentistry*. Hershey, Pa : IGI Global (701 E. Chocolate Avenue Hershey Pennsylvania 17033 USA), 2009. <http://dx.doi.org/10.4018/978-1-60566-292-3>. <http://dx.doi.org/10.4018/978-1-60566-292-3>. – ISBN 978-1-60566-292-3
- [HBKZ95] HAUSAMEN, Jarg-Erich (Hrsg.) ; BIER, Jürgen (Hrsg.) ; KIRSCHNER, Martin (Hrsg.) ; ZENKER, Rudolf (Hrsg.): *Allgemeine und spezielle Operationslehre*. Bd. / begr. von Martin Kirschner. Fortgef. und hrsg. von R. Zenker ... ; Bd. 2: *Mund-, Kiefer- und Gesichtschirurgie*. 3., völlig neubearb. Aufl. Heidelberg : Springer, 1995. – ISBN 3540538658
- [Hie11] HIERL THOMAS, KRUBER DANIEL, BORASCH HENRY, HÜMPFNER-HIERL HEIKE: Neu entwickelte 3D-Analysesoftware für Zahnheilkunde und MKG-Chirurgie. In: *Digital Dental News* 5 (2011), 6–10. <http://www.ddn-online.net>, Abruf: 25.05.2018 - nicht mehr abrufbar
- [HKHH10] HIERL, Thomas ; KRUBER, Daniel ; HÜMPFNER-HIERL, Heike: Die dreidimensionale Bildgebung: Analyse und Manipulation von Bilddaten: Digitale Zahnheilkunde. In: *teamwork SPECIAL* 13 (2010), 86–90. <https://www.teamwork-media.de/journal/tw/>, Abruf: 25.05.2018
- [Kit] KITWARE INC.: *Visualization Tool Kit (VTK)*. <https://www.vtk.org/>, Abruf: 25.05.2018
- [Kit06] KITWARE: *The Visualization Toolkit*. (4th ed.). 2006. – ISBN 978-1-930934-19-1
- [KKD<sup>+</sup>18] KRAUSE, Matthias ; KRUBER, Daniel ; DÖRFLER, Hans-Martin ; HEMPRICH, Alexander ; HÜMPFNER-HIERL, Heike ; HIERL, Thomas: *Ein-satz einer digital erstellten Pilotschablone für die minimalinvasive Chirurgie des Kiefergelenkes*. Dresden, 06.-08.06.2018 (Postervortrag)



- [Kru] KRUBER, Daniel: *Entwicklung einer Kephalometrie-Software für 3D-Berechnungen und Auswertungen von medizinischen Bilddaten mittels anatomischer Landmarken*. Leipzig, (Diplomarbeit)
- [ML94] MERTEN, H. A. ; LUHR, H. G.: Resorbierbare Kunststoffe (PDS-Folien) zur Überbrückung ausgedehnter Orbitawanddefekte im tierexperimentellen Vergleich. In: *Fortschritte der Kiefer- und Gesichtschirurgie* 39 (1994), S. 186–190. – ISSN 0071–7916
- [NAF32] NAFFZIGER, HOWARD C.: THE SURGICAL TREATMENT OF PROGRESSIVE EXOPHTHALMOS FOLLOWING THYROIDECTOMY. In: *Journal of the American Medical Association* 99 (1932), Nr. 8, S. 638. <http://dx.doi.org/10.1001/jama.1932.02740600030008>. – DOI 10.1001/jama.1932.02740600030008. – ISSN 0002–9955
- [Nat03] NATIONAL INSTITUTE OF HEALTH AND US NATIONAL LIBRARY OF MEDICINE: “*The visible human project*”. [http://www.nlm.nih.gov/research/visible/visible\\_human.html](http://www.nlm.nih.gov/research/visible/visible_human.html). Version: 2003, Abruf: 25.05.2018
- [SEW36] SEWALL, E. C.: OPERATIVE CONTROL OF PROGRESSIVE EXOPHTHALMOS. In: *Archives of Otolaryngology - Head and Neck Surgery* 24 (1936), Nr. 5, S. 621–624. <http://dx.doi.org/10.1001/archotol.1936.00640050634010>. – DOI 10.1001/archotol.1936.00640050634010. – ISSN 0886–4470

## Darstellung des eigenen Beitrags

**Titel der Veröffentlichung:**

Preforming of polydioxanone sheets for orbital wall fractures –  
A technical note

**Erstautor:**

Daniel Kruber

**Mitautoren:**

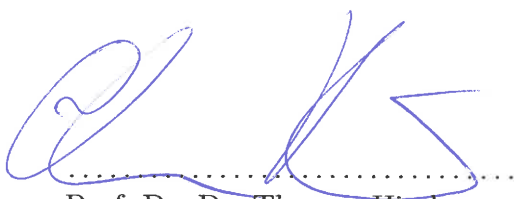
Thomas Hierl, Hans-Martin Dörfler, Heike Hümpfner-Hierl, Matthias Krause

**Darlegung des eigenen wissenschaftlichen Anteils:**

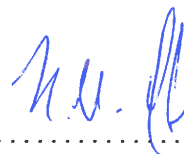
Die Programmierung der Softwarewerkzeuge für diese Arbeit wurde vollständig von mir übernommen. Des Weiteren war ich an der Studienkonzeption, der Versuchsdurchführung und dem Abfassen des Artikels beteiligt.

Die unten aufgeführten Koautoren waren neben mir an der Ergebnisauswertung und dem Abfassen der Veröffentlichung beteiligt.

Ich bestätige die von Herrn Kruber, Daniel oben abgegebene Erklärung:



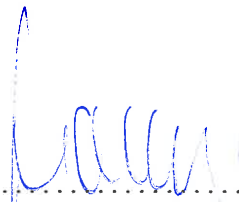
Prof. Dr. Dr. Thomas Hierl



M.Eng. Hans-Martin Dörfler



PD Dr. Dr. Heike Hümpfner-Hierl



Dr. Dr. Matthias Krause M.Sc

## **Erklärung über die eigenständige Abfassung der Arbeit**

Hiermit erkläre ich, dass ich die vorliegende Arbeit selbstständig und ohne unzulässige Hilfe oder Benutzung anderer als der angegebenen Hilfsmittel angefertigt habe. Ich versichere, dass Dritte von mir weder unmittelbar noch mittelbar eine Vergütung oder geldwerte Leistungen für Arbeiten erhalten haben, die im Zusammenhang mit dem Inhalt der vorgelegten Dissertation stehen, und dass die vorgelegte Arbeit weder im Inland noch im Ausland in gleicher oder ähnlicher Form einer anderen Prüfungsbehörde zum Zweck einer Promotion oder eines anderen Prüfungsverfahrens vorgelegt wurde. Alles aus anderen Quellen und von anderen Personen übernommene Material, das in der Arbeit verwendet wurde oder auf das direkt Bezug genommen wird, wurde als solches kenntlich gemacht. Insbesondere wurden alle Personen genannt, die direkt an der Entstehung der vorliegenden Arbeit beteiligt waren. Die aktuellen gesetzlichen Vorgaben in Bezug auf die Zulassung der klinischen Studien, die Bestimmungen des Tierschutzgesetzes, die Bestimmungen des Gentechnikgesetzes und die allgemeinen Datenschutzbestimmungen wurden eingehalten. Ich versichere, dass ich die Regelungen der Satzung der Universität Leipzig zur Sicherung guter wissenschaftlicher Praxis kenne und eingehalten habe.

.....  
Datum

.....  
Unterschrift

# Curriculum Vitæ

## Eigene Publikationen

2008

Kruber, D.; Gäbler, Th.; Jaeger F.; Hemprich, A.; Hierl, Th.:  
*Facial Analysis Tool - eine neuentwickelte Software zur Analyse  
medizinischer Bilddaten.*  
Poster - 7th Leipzig Research Festival for Life Sciences 2008.  
Abstract Book, S.119, ISBN 3-9810760-4-4.

2009

Hierl, Th.; Hümpfner-Hierl, H.; Kruber, D.; Gäbler, Th.; Hem-  
prich, A.; Wollny, G.:  
*Requirements for a universal image analysis tool in dentistry and  
oral and maxillofacial surgery*  
In: Daskalaki, A.: Dental Computing and Applications. Advanced  
Techniques for Clinical Dentistry.  
IGI Global Hershey, London, 2009, S.79-89, ISBN 978-1-60566-  
292-3.

2012

Raschpichler, M.C.; Sorge, I.; Hirsch, W.; Mende, M.; Sergeyev,  
E.; Kruber, D.; Koerner, A.; Schick, F.:  
*Evaluating childhood obesity: magnetic resonance-based quantifi-  
cation of abdominal adipose tissue and liver fat in children.*  
In: Rofo. 2012 Apr;184(4):324-32.

2013

Hierl, T.; Arnold, S.; Kruber, D.; Schulze, F.P.; Hümpfner-Hierl,  
H.:  
*CAD-CAM-assisted esthetic facial surgery.*  
In: J Oral Maxillofac Surg. 2013 Jan;71(1):e15-23.



Hierl, T.; Krause, M.; Kruber, D.; Hümpfner-Hierl, H.:  
*Positioning of bone segments during navigated surgery.*  
In: J Oral Maxillofac Surg. 2013 Feb;71(2):376-81.

2015

Huempfner-Hierl, H.; Doerfler, H.M.; Kruber, D.; Hierl, T.:  
*Morphologic comparison of preformed orbital meshes.*  
In: J Oral Maxillofac Surg. 2015 Jun;73(6):1119-23.

2017

Krause, M.; Hümpfner-Hierl, H.; Kruber, D.; Sterker, I.; Hierl, T.:  
*Calculation of resected orbital wall areas in the treatment of endocrine orbitopathy.*  
In: J Craniomaxillofac Surg. 2017 Apr;45(4):485-490.

Doerfler, H.M.; Huempfner-Hierl, H.; Kruber, D.; Schulze, P.; Hierl, T.:  
*Template-Based Orbital Wall Fracture Treatment Using Statistical Shape Analysis.*  
In: J Oral Maxillofac Surg. 2017 Jul;75(7):1475.e1-1475.e8.

2018

Krause, M.; Kruber, D.; Hümpfner-Hierl, H.; Sterker, I.; Hierl, T.:  
*Three-dimensional changes of scleral show after surgical treatment of endocrine orbitopathy.*  
In: J Craniomaxillofac Surg. 2018 Jan;46(1):44-49.

Krause, M.; Kruber, D.; Dörfler, H.-M.; Hemprich, A.; Hümpfner-Hierl, H.; Hierl T.:  
*Einsatz einer digital erstellten Pilotschablone für die minimalinvasive Chirurgie des Kiefergelenkes.*  
Poster präsentiert auf dem 68. Kongress der Deutschen Gesellschaft für Mund-, Kiefer- und Gesichtschirurgie (2018, Juni)

Kruber, D.; Hierl T.; Dörfler, H.-M.; Hümpfner-Hierl, H., Krause, M.; :  
*Preforming of polydioxanone sheets for orbital wall fractures – A technical note*  
In: J Craniomaxillofac Surg. 46(2018):1159-1161.

## Danksagung

Nachfolgend möchte ich mich bei den Personen bedanken, die es mir möglich machten diese Promotion zu schreiben, mich unterstützten und mir mit wertvollen Ratschlägen zur Seite standen.

Mein herzlichster Dank gilt Herrn Prof. Dr. Dr. Alexander Hemprich, der mir ermöglichte an seiner Klinik diese Promotionsarbeit zu realisieren und mir als Betreuer beistand.

Besonders möchte ich auch Herrn Prof. Dr. Dr. Thomas Hierl für die jahrelange Zusammenarbeit, seiner ansteckenden Motivation und seinem Engagement danken. Seine Denkanstöße und Erfahrung waren eine große Hilfe bei der Umsetzung dieser Arbeit.

Und nicht zuletzt danke ich meiner Familie und meiner Partnerin Caroline, die mich in allen Situationen unterstützen und mir stets den Rücken stärken.